UNIVERSITÉ DE NANTES

Ecole polytechnique de l'université de Nantes

———

ÉCOLE DOCTORALE

SCIENCES ET TECHNOLOGIES DE L'INFORMATION ET MATHEMATIQUES

N° attribué par la bibliothèque

Année 2010

EFFICACITÉ ÉNERGÉTIQUE, SYNCHRONISATION ET CONTRÔLE DE PUISSANCE POUR L'IMPLÉMENTATION DES COMMUNICATIONS COOPÉRATIVES DANS LES RÉSEAUX DE CAPTEURS SANS FIL

———

THÈSE DE DOCTORAT

Discipline - Spécialité : Electronique

Présentée
et soutenue publiquement par

Haitao WAN

le 9 décembre 2010, devant le jury ci-dessous

Président	Jean-François HELARD, Professeur, IETR, INSA Rennes
Rapporteurs	Jean-Marie GORCE, Professeur, CITI, INSA Lyon
	Olivier SENTIEYS, Professeur, IRISA, ENSSAT Lannion
Examinateurs	Guillaume ANDRIEUX, Maître de Conférences, IREENA, IUT La Roche s/Yon
	Jean-François DIOURIS, Professeur, IREENA, Polytech'Nantes
	Gang WEI, Professeur, South China University of Technology, Guangzhou, Chine

Directeur de thèse : Jean-François DIOURIS
Encadrant : Guillaume ANDRIEUX
Laboratoire IREENA EA1770

ED 503-113

To my parents

Acknowledgements

Have a lot of wonderful memories, I went through four years' journey in Nantes. The people I met here is really unbelievable. A few words mentioned here cannot capture all my appreciation to your supports and the pleasure you brought to me.

First of all, I would like to express my great, great ... thanks to my advisor, Professor Jean-François Diouris. It has been a pleasant experience of working with him. I want to thank him for his gentleness, encouragement and inspiration. I have benefited tremendously from that, not only at the academic research but also on the personal growth. This impact will go along with me throughout my life.

I would also like to thank Guillaume Andrieux, Assistant Professor with Polytech'Nantes, for many contributions of his broad perspective to refine the works of my thesis and for his countless help during the writing of my dissertation.

Grateful acknowledgements are also given to Professor Jean-Marie Gorce and Professor Olivier Sentieys, the reviewers of my dissertation, for their acceptance of being the reviewer of my dissertation and their careful reviewing works. I would also like to thank the other members of the jury, Professor Jean-François Helard and Professor Gang Wei, for their valuable suggestions.

The IREENA lab has provided a great collegial environment for academic research. I thank Professor Yide Wang, for his tremendous supports and also good care for my daily life. Grateful thanks are also given to Professor Joseph Saillard and Professor Serge Toutain, for their encouragement. The works in IREENA cannot be so efficient without help from Sandrine Charlier, secretary of IREENA, and Marc Brunet, engineer of IREENA. They deserve many thanks.

Last, of my friends and colleagues, I want to thank Hongyang, Yuehua, Siamak, Atef, Ahmad, Max, Janic, Nicolas and Gildas. We have a great time on the cafe break and sharing our works. Especially, great thanks are given to Jiazi, Bangge, Happy, Zhujie, Baobao, Chuanlin, Kunshu and Guoxian. We have shared many wonderful experiences on traveling and cuisine...

Contents

List of Figures

List of Tables

General Introduction

In the history of computing hardware, the Moore's law guides a long-term evolution. It indicates that the number of transistors, which can be placed inexpensively on an integrated circuit, doubles approximately every two years. These trends of miniaturization and increasing computing capacity allow researchers to manufacture inexpensive, low-power communication devices. Wireless sensor networks interconnected by these tiny devices (known as sensor nodes) can be used for environmental monitoring, target tracking and industrial controlling, etc. They can be deployed from small to large range scale. Wireless sensor networks are becoming a class of distinguished wireless networks and attracting more attentions and research works.

Wireless sensor networks are usually deployed in rigorous environment where the communication channels suffer from shadowing and multipath fading. Multi-antenna systems perform great in the fading channel by exploring the channel diversity. However, due to the size limitation, implementing multiple antennas in these tiny nodes is impractical. Considering the broadcast nature of radio signal, the message transmitted by one node is listened by the other nodes. They can forward the same version of the source message by the form of relaying cooperation or space-time coding cooperation. We refer to them as cooperative relaying scheme and virtual Multi-Input-Single-Output (MISO) cooperative scheme. These cooperative communication schemes can achieve the performance similar to a multi-antenna system. They are more energy efficient than the Single-Input-Single-Output (SISO) communication in long distance fading channel.

The sensor nodes are usually resource constrained, such as limited with power supply, processing capability and communication bandwidth. The power constraint and simple architecture of the sensor nodes should be taken into account when considering the implementation of cooperative communication schemes in wireless sensor networks. This is the main motivation of our works. Considering

the virtual MISO cooperative communication, we focus on the Alamouti coding scheme. The simple implementation of this scheme requires that the sensor nodes can be well synchronized by signal arrival time. So we propose a synchronization scheme that can achieve the precision requirement while introduces low complexity to the system design. By applying the synchronization scheme, we suppose that the time synchronization problem can be properly solved. The power control schemes are investigated for cooperative relaying scheme and virtual MISO cooperative scheme to further improve the energy efficiency of cooperative communications. Furthermore, the energy efficient implementation of error control schemes is proposed for cooperative communications to provide reliable link between the sensor nodes.

The outline of the dissertation is summarized as follows:

In Chapter 1, we present some background materials and the related concepts that will be considered in the later analysis.

In Chapter 2, we introduce three cooperative communication schemes that could be applied at the network layer and physical layer in wireless sensor networks. The network coding scheme can improve the network throughput by taking several packets and combining them together for further transmission. The cooperative relaying scheme and virtual MISO cooperative scheme provide a reliable communication link in fading channel by exploiting the channel diversity. We present the system models for these cooperative schemes and analyse the requirements on the implementation of these schemes.

In Chapter 3, we introduce the needs of network clock and signal arrival time synchronization in wireless sensor networks. Since signal arrival time synchronization is usually required in the virtual MISO cooperative communication, we explore the effect of synchronization error on the cooperative communication utilizing distributed Alamouti code. The analysis and simulation results show that a small synchronization error has negligible effect on Bit Error Rate (BER) performance. In order to synchronize the distributed sensor nodes within an acceptable error, we propose a physical layer synchronization scheme. This scheme is composed of an initial synchronization of the cooperative transmitters, the synchronization error estimation at the cooperative receiver and finally a feedback phase. A maximum likelihood method is proposed to make the synchronization error estimation. It achieves better performance than the matched filter method at the price of moder-

ate increase in computational complexity and memory space. Two strategies after synchronization error estimation have been analysed. They provide better BER performance in the existence of an initial synchronization error. They are practical to be implemented in the sensor nodes before the Alamouti decoding.

In Chapter 4, supposing the synchronization problem can be properly solved, we consider power allocation strategies for cooperative relaying scheme and virtual MISO cooperative scheme. The power allocation strategies aim at minimizing the total transmit power with a constraint on the average BER performance. They help to reduce the energy consumption for long distance data transmission. The optimal transmit power can be approximated in analytical way and matches well with the precise results. Furthermore, for the case without direct link between the source and destination nodes, we propose two cooperative strategies where the optimal power allocation is applied at different stages. The proposed solutions are more energy efficient and achieve fair allocation of the transmit power among the sensor nodes. According to different topology structures, we derive a heuristic policy to select the optimal cooperative nodes for the corresponding cooperative strategies.

In Chapter 5, we consider three kinds of error control protocols: Basic ARQ, Hybrid ARQ-I and Hybrid ARQ-II, to be incorporated in the SISO system and MISO cooperative system. To analyse their energy efficiency, we consider that the total energy consumption accounts for the transmission energy and the energy consumption on coding and decoding processing and the involved analog circuitry. Since stronger codes provide more coding gain but at a cost of longer coded redundancy and more complex coding/decoding process, the choice of error correction codes would have an influence on the energy efficiency of the error control protocols. According to different channel conditions, we investigate the requirement on the error correction codes and their energy efficient implementation in error control protocols.

Finally, Chapter 6 presents conclusions and discusses the perspective of the research works in this area.

Chapter 1

Related Concepts

1.1 Wireless Sensor Network

A *wireless sensor network* consists of a number of spatially distributed sensor nodes connected in wireless way to help people perceiving the world. It is becoming a distinguished wireless network with the trend of *Internet of Things*. Wireless sensor networks can be deployed in a range from small to large scale, such as body sensor networks in body area and environmental monitoring sensor networks in city area or even larger. All the sensor nodes are normally autonomous and organized in wireless connection requiring little or no planning. They showed the benefits and also the challenges when sensor networks are extended to be wireless. The information gathered by wireless sensor networks is different in accordance with the interests of people. It can be accessed from a special node working as the gateway.

The unique feature of wireless sensor networks is their ability of perceiving the world. As we extend this ability to be ubiquitous and pervasive, more characteristics exist in wireless sensor networks, such as:

- Long term operation with limited power supply or battery storage
- Ability to work in unattended way and flexibility to node failures
- Ability to withstand harsh environmental and communication conditions
- Feasible integration of heterogeneous nodes
- Large scale deployment and dynamic networking topology

The applications of wireless sensor networks are various [2, 3, 4] and have been implemented for environmental monitoring, target tracking or industrial controlling. They are going to make a great impact on modern life. Depending on the application requirements, wireless sensor networks may operate in either of two basic topologies, or a combination of both. Figure 1.1 shows these two basic topologies: the star topology and the peer-to-peer topology [5]. In the star topology, the head node is the primary controller. All the other nodes are associated nodes that are normally controlled by the head node. The associated nodes only communicate with the head node, which can route the messages between the head nodes around the network. Unlike the star topology, all nodes in the peer-to-peer topology are self-organized and operate in ad hoc mode. A node could directly communicate with any other nodes as long as they are within the radio range. Multi-hops are allowed to route messages between the nodes which are not in one hop range. The expandability of peer-to-peer topology is better than star topology. Peer-to-peer topology allows to be implemented in larger scale networks, but at the cost of more complex maintenance.

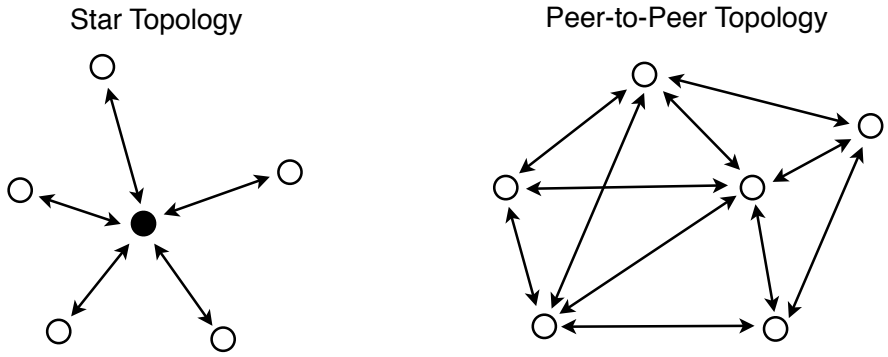

Figure 1.1: Star topology and Peer-to-Peer topology

Cluster topology which operates with a combination of star topology and peer-to-peer topology could be a good choice to lower the maintenance complexity while keeping the expandability of the network. In cluster topology, each cluster is considered as a local star topology. The head node in each cluster, designated as the cluster head, is responsible for information collection in the local region. All the cluster heads in the network could implement peer-to-peer communication. Messages are routed among these head nodes around the network. In addition, the cluster heads could also be organized in clusters. This gives rise to hierarchical

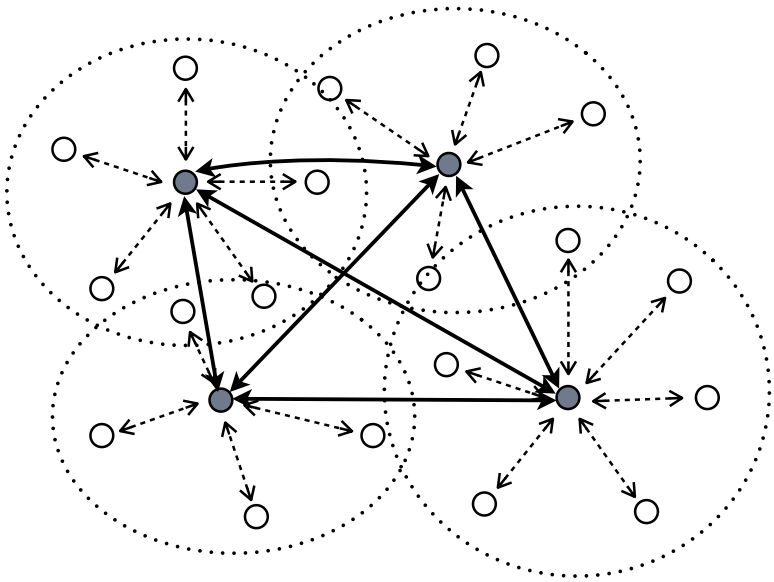

Figure 1.2: One-tier cluster topology

cluster topology. Figure 1.2 shows a one-tier cluster topology where the cluster heads operate in the way of peer-to-peer.

Along with the development of Micro-Electro-Mechanical Systems (MEMS) and Nano-Electro-Mechanical Systems (NEMS), sensor nodes would progress towards miniaturization, low cost and low power. The sensor nodes normally have four basic components: a sensing unit, a processing unit, a transceiver unit and a power supply unit [6]. Some complementary components may also be used on the sensor nodes according to the requirements of applications. In order to facilitate the communication in wireless sensor networks, protocol stacks consisting of physical, data link, network, transport and application layers are also applied to sensor nodes. Nowadays, IEEE 802.15.4-2006 standard, which specifies the physical layer and media access control in data link layer, is the most used underlying radio standard on wireless sensor networks. Some upper layer protocols are specified as ZigBee, 6LoWPAN and ISA100 standards for different requirements.

1.2 Wireless Channel Models

Wireless communication channel has a large impact on the operation of wireless sensor networks. The design of the protocol stacks should take wireless channel

condition into account. A rigorous channel condition requires some compensative or mitigated schemes to be applied at different protocol layers. As the environment could be indoor or outdoor for various applications, the characteristics of wireless channel would be different. The classical additive white Gaussian noise (AWGN) channel is usually considered as basic performance degradation of communication systems. The primary source of AWGN comes from the thermal noise generated in the receiver. In addition, the signal propagated in wireless channel may suffer from two fading effects: large-scale fading and small-scale fading. These fading effects would have greater impact on the receiver performance. In the following discussion, we present some details regarding the mechanisms and mathematical representations of the channel characteristics that we consider in this dissertation.

1.2.1 AWGN Channel

In communication systems, the AWGN is modelled as an additive noise with a constant power spectral density and a Gaussian amplitude distribution. The power spectral density N_0 is commonly determined by the temperature value T_0 of the transceiver and the Boltzmann constant $k_B = 1.38 \times 10^{-23} W \cdot s/K$ as:

$$N_0 = k_B T_0 \tag{1.1}$$

It is a simple and tractable mathematical models, which gives useful insight into the underlying behaviour of a system before taking other phenomena into account. The AWGN channel is a good model for satellites and deep space communication links. However, it is not a sufficient model for terrestrial links due to the existences of multipath propagation, blocking obstacle, interference, etc. Anyway, for terrestrial channel modelling, AWGN is commonly simulated as a background noise to the channel in addition to other channel fading effects.

1.2.2 Large-Scale Fading

Large-scale fading represents path-loss effect and average power attenuation on the propagated signal. On radio channel, the path-loss effect expresses that the attenuation on signal power is proportional to propagation distance. In the ideal assumption of free space model, the space between the transmitter and receiver is

supposed to be in far-field region and be free of objects that could absorb or reflect the signal. It also assumes that the atmosphere within this region behaves as a uniform medium. So in the idealized free space model, the attenuation of signal power conforms to an inverse-square law. The received signal power is given by [7]:

$$P_r = P_t \left(\frac{\lambda}{4\pi d} \right)^2 G_t G_r \tag{1.2}$$

where P_t and P_r are the transmitted and received powers respectively, λ is the wavelength, d is the separation distance, G_t and G_r are the power gains of the transmit and receive antennas respectively.

Recall that a far-field region is supposed between the transmit and receive antennas. In wireless sensor networks, this assumption could be satisfied, as the far-field region is commonly recognized to exist if the distance d between the antennas is larger than a threshold distance $d_{ff} = 2D^2/\lambda$, where D is the maximum dimension of the antenna. Typically, carrier frequencies used in sensor nodes are 868 MHz, 915 MHz and 2.45 GHz [5]. The corresponding wavelengths are about 34.6 cm, 32.8 cm and 12.2 cm. For a normal sensor node with an antenna size not larger than a few centimetres, the threshold distance is less than a meter. Hence, the far-filed assumption is justified for most wireless sensor network deployments.

The assumption that the propagation path is free of objects is far from the real case. In reality, the deploying environments of wireless sensor networks are complex. Various objects, like the ceilings and walls in indoor environments or forests and buildings in outdoor environments, are encumbering the radio propagation path. Thus, the statistics of large-scale fading should consider not only the path loss effect, but also the macroscopic fading effect that can be represented by a log-normally distributed variation as described in [8]. It has the probability density function (pdf) of:

$$f(x) = \frac{1}{\sqrt{2\pi}\sigma_x} e^{-\frac{(x-\mu_x)^2}{2\sigma_x^2}} \tag{1.3}$$

where x is a random variable in decibel representing the long term signal power fluctuation. The parameters μ_x and σ_x, also expressed in decibel, are respectively the mean and standard variance of x. A more comprehensive representation of

large scale fading attenuation could therefore be [9]:

$$L_P(d)_{(dB)} = L_S(d_0)_{(dB)} + 10n\log_{10}(\frac{d}{d_0}) + X_{\sigma(dB)} \tag{1.4}$$

where d_0 corresponds to a reference distance of the far-field region from the antenna. We consider it as $1m$ for wireless sensor networks scenario. $L_S(d_0)$ has the form of $L_S(d_0) = \frac{P_t}{P_r} = \left(\frac{4\pi d_0}{\lambda}\right)^2$ by considering equation (1.2) and assuming the transmit and receive antennas to be isotropic ($G_t = G_r = 1$). The path loss factor n depends mainly on the deploying environment. In free space, $n = 2$ as in equation (1.2). In real deployment, n can vary from 2 to 4 according to a wide variety of channel conditions. $X_{\sigma(dB)}$ represents a margin that captures the long term signal power fluctuation, which is related to σ_x described in equation (1.3). We note that this long term fluctuation is different from the short term fading effect that will be discussed in the following part. Moreover, as the long term fluctuation $X_{\sigma(dB)}$ is supposed to change more slowly than short term fading, we will take $X_{\sigma(dB)}$ as a link margin [7] to be compensated before each message transmission. It would be a constant, which upper bounds the real long term fluctuation, for a relative long time.

1.2.3 Small-Scale Fading

In addition to path loss effect and long term fluctuation, the received signal on radio channel may exhibit fast fluctuation in signal level. The fluctuation is due to any or both of two mechanisms: time variation of the channel and time spreading of the signal. A time variant behaviour of the channel is normally caused by the motion of antennas or by the movements of objects within the channel. Thus, for a continuous signal transmitted in the channel, the receiver detects variations in the signal amplitude and phase. These variations come from the time-variant channel response. The coherent time T_c is a measurement of the expected time duration over which the channel response is essentially invariant. According to the fading speed of the channel, this time-variant nature can be categorized as fast fading and slow fading.

Time spreading of the signal arises when the propagated signal goes through different propagation paths and arrives at the receiver at different time. This phenomenon is very normal for the communication between sensor nodes. The objects

in deployment regions of wireless sensor networks cause the radio wave to be reflected in different paths. These multipath received signals result in constructive or destructive combinations at the receiver. According to different relations between the maximum time delay and transmitted symbol duration, time spreading of the signal has flat fading effect or frequency selective fading effect. They will be examined in the following.

Flat Fading Effect

In multipath delaying, the maximum delay time T_m refers to a maximum delay for which the delay profile is above a threshold power. If T_m is smaller than a symbol interval T_s, the degradation channel is said to exhibit flat fading. The received signal is made up of multiple reflective components arriving within the symbol time interval. Since no significant overlap among neighbouring symbols is generated, the channel does not induce Inter-Symbol-Interferences (ISI) distortion in this case.

According to the contribution of different kinds of multipath components, the flat fading effect can be mainly characterized as Rician fading or Rayleigh fading. For the Rician fading channel, there is a significant line-of-sight component besides a multiple of reflective components. The envelope amplitude has a Rician pdf. As the line-of-sight component approaches zeros, the Rician pdf tends to Rayleigh pdf which can be expressed as:

$$p(r) = \frac{r}{\sigma^2} e^{-\frac{r^2}{2\sigma^2}} \tag{1.5}$$

where r is the random variable representing the envelope amplitude of the received signal, $2\sigma^2$ is the mean power of the multipath signals. For simplicity, Rayleigh fading channel can be modelled as a complex variable $a \cdot e^{j\theta}$ showing the gain and phase elements. In this case, Rayleigh fading channel is exhibited by the assumption that the real and imaginary parts are modelled by independent and identically zero-mean Gaussian distributions with variance of σ^2.

In our work, we consider the case where line-of-sight propagation is lacked for the rigorous deployment environment of wireless sensor networks. Therefore, when we consider the flat fading effect, Rayleigh fading channel is almost assumed. It is a reasonable model when many objects exist in the environment scattering the

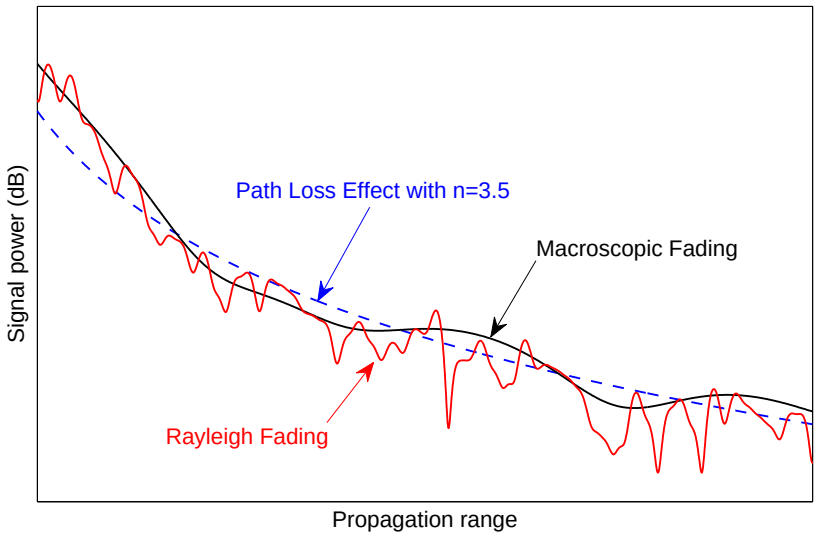

Figure 1.3: Channel exhibitions: path loss effect with $n = 3.5$, Macroscopic fading with $\sigma_x^2 = 8dB$ and Rayleigh fading

radio signal before it arrives at the receiver. In addition, the propagation radio over a large area on far-field region experiences both types of small and large scale fading. It is shown as an example in Figure 1.3 where small-scale fading of Rayleigh fading effect is superimposed on large-scale fading of path loss and macroscopic fading effects.

Frequency Selective Fading Effect

A channel is said to be frequency selective if $T_m > T_s$. In this case, all multipath components of the received signal arrive during an extending duration beyond the symbol time. It causes channel induced ISI to the signal. An intuitive characterization of frequency selective fading can be expressed in frequency domain by using the terminology of coherent bandwidth f_0, which is a statical measurement of the range of frequencies over which channel responses to the signal components have approximately equal gain and phase rotation. Thus, within the range of a coherent bandwidth, signal spectral components exhibit flat fading effect as described in the previous subsection. A signal suffering from frequency selective fading is said to have a range of spectral components larger than the coherence bandwidth of the

channel. Note that f_0 and T_m are reciprocally related by the approximation of $f_0 \approx 1/T_m$. In our works, without especially statement, we assume that the sensor nodes are stationary and multipath delays of the signal are within the symbol time interval. Thus, frequency selective fading will not be considered.

1.3 Capacity and Performances

1.3.1 Channel Capacity

In wireless communication, channel capacity provides a theoretical view on the performance limit that a system can achieve. Shannon defined the channel capacity as the maximum mutual information over all possible input distributions. Specifically, it provides a tightest upper bound on the amount of information that can be reliably transmitted through the channel. Given a band-limited wireless channel with a capacity of C, it is theoretically possible to achieve reliable or error free transmission with information rate R less than C. On the other hand, if $R > C$, reliable transmission is not possible regardless of any signal processing technology or error control code. Approaching this theoretical bound is practically difficult for wireless sensor networks where sensor nodes work on lower power level and have limited signal processing capability. However, it provides a hint on the design of cooperative protocols and communication frameworks among the nodes.

The Shannon-Hartley theorem states that the channel interfered by AWGN has a channel capacity C given by [7]:

$$C = \log_2(1 + \tfrac{S}{N}) \quad bps/\text{Hz} \tag{1.6}$$

where S is the average transmit power of the signal, N is the average power of the noise. Equation (1.6) shows that the available channel capacity of AWGN channel is in a logarithmic increase with the received signal to noise ratio (SNR).

In contrast to AWGN channel, large-scale fading and small-scale fading are more common in wireless sensor networks. The fading effects will decrease the received SNR and therefore reduce the available channel capacity. Cooperative space time coding and cooperative relaying schemes, which will be investigated in details in the following chapters, are promising solutions to overcome these fading effects. The construction of the cooperative scheme means that a choice of Single-Input-

Multi-Output (SIMO), Multi-Input-Single-Output (MISO) and Multi-Input-Multi-Output (MIMO) channels will be established among the sensor nodes.

In more general case, we consider the capacity of MIMO channel that are spanned by M_T transmit antennas and M_R receive antennas. The $M_R \times M_T$ channel matrix is denoted as:

$$H = \begin{bmatrix} h_{11} & h_{12} & \cdots & h_{1,M_T} \\ h_{21} & h_{22} & \cdots & h_{2,M_T} \\ \vdots & \vdots & \ddots & \vdots \\ h_{M_R,1} & h_{M_R,2} & \cdots & h_{M_R,M_T} \end{bmatrix} \tag{1.7}$$

where each component $h_{i,j}$ for the transmit and receive antenna pair is assumed to be a zero mean complex Gaussian random variable (i.e. $|h_{i,j}|$ has a Rayleigh distribution). Then, the baseband received signal y ($M_R \times 1$ vector) can be modelled as:

$$y = Hx + n \tag{1.8}$$

where $x \in \mathbb{C}^{M_T \times 1}$ is the transmit signal vector, $n \in \mathbb{C}^{M_R \times 1}$ is the Zero Mean Circularly Symmetric Complex Gaussian (ZMCSCG) noise with covariance matrix $E\left[nn^H\right] = NI_{M_R}$.

Considering a fixed channel matrix H, the MIMO channel capacity can be derived to be:

$$C = \log_2 \det(I_{M_R} + \frac{HA_sH^H}{N}) \tag{1.9}$$

where $A_s = E\left[xx^H\right]$ is a diagonal matrix representing the codeword covariance. For a communication system with available total transmit power as $tr(A_s) = S$ (where $tr(\cdot)$ denotes the trace operator) and the fraction of the total transmit power allocated to the i^{th} transmit antenna as ε_i, the channel capacity in equation (1.9) can be rewritten as:

$$C = \sum_{i=1}^{M_T} \log_2(1 + \varepsilon_i \lambda_i \frac{S}{N}) \tag{1.10}$$

where λ_i is a positive eigenvalue of $H^H H$. We note that the capacity expressed in equations (1.9) and (1.10) refers to the instantaneous capacity in the fading channel. They have no meaning in the Shannon sense where the codeword has infinite duration.

If λ_i varies over a transmitted codeword with infinite duration but all its moments are constant, then the channel is referred to as an ergodic channel. Supposing the transmitted codeword is ZMCSCG distributed, the capacity of the ergodic MIMO channel can be maximized as:

$$C = E\left[\log_2 \det\left(I_{M_R} + \frac{HH^H}{M_T}\frac{S}{N}\right)\right] \tag{1.11}$$

With the defined parameters $m \triangleq \min\{M_T, M_R\}$ and $n \triangleq \max\{M_T, M_R\}$, the expression in equation (1.11) can also be evaluated as [10]:

$$C = E_{\vec{\lambda}}[\sum_{i=1}^{m} \log_2(1 + \frac{\lambda_i}{M_T}\frac{S}{N})] \tag{1.12}$$

where $\vec{\lambda} = (\lambda_1, \lambda_2 \cdots \lambda_m)$ is the ordered eigenvalues with the joint pdf to be known as [11]:

$$pdf_\lambda(\vec{\lambda}) = \frac{1}{K_{mn}} \prod_i e^{-\lambda_i} \lambda_i^{n-m} \prod_{j>i} (\lambda_i - \lambda_j)^2 \tag{1.13}$$

where K_{mn} is a normalizing factor. Therefore, equation (1.12) turns into:

$$C = \int \cdots \int_{\vec{\lambda}} \sum_{i=1}^{m} \log_2\left(1 + \frac{\lambda_i}{M_T}\frac{S}{N}\right) \cdot pdf_\lambda(\vec{\lambda}) d\vec{\lambda} \tag{1.14}$$

After some algebraic manipulations as shown in [10], a landmark of the ergodic MIMO capacity can be expressed as:

$$C = \int_0^\infty m \log_2(1 + \frac{\lambda}{M_T}\frac{S}{N}) \cdot \frac{1}{m} \sum_{k=0}^{m-1} \frac{k!}{(k+n-m)!} \left[L_k^{n-m}(\lambda)\right]^2 \lambda^{n-m} e^{-\lambda} d\lambda \tag{1.15}$$

where $L_k^{n-m}(\lambda)$ is the associated Laguerre polynomial of order k. This integral

form of the capacity has been extended to an explicit closed form as [12]:

$$C = \sum_{k=0}^{m-1} \frac{k!}{(k+d)!} \left[\sum_{l=0}^{k} A_l^2(k,d) \hat{C}_{2l+d}(a) + \sum_{l_1=0}^{k} \sum_{\substack{l_2=0, \\ l_2 \neq l_1}}^{k} (-1)^{l_1+l_2} A_{l_1}(k,d) A_{l_2}(k,d) \hat{C}_{l_1+l_2+d}(a) \right] \tag{1.16}$$

where $a \triangleq \frac{1}{M_T} \frac{S}{N}$, $d \triangleq n-m$, $A_l(k,d) \triangleq \frac{(k+d)!}{(k-l)!(d+l)!l!}$ and $\hat{C}_\eta(a)$ can be expressed as:

$$\hat{C}_\eta(a) = \frac{1}{\log(2)} \sum_{\mu=0}^{\eta} \frac{\eta!}{(\eta-\mu)!} \left[(-1)^{\eta-\mu-1} (1/a)^{\eta-\mu} e^{1/a} Ei(-1/a) + \sum_{k=1}^{\eta-\mu} (k-1)! (-1/a)^{\eta-\mu-k} \right] \tag{1.17}$$

with $Ei(\zeta) \triangleq \int_{-\infty}^{\zeta} \frac{e^t}{t} dt$ is a typical exponential integral. Considering the MISO system with $M_R = 1$, the capacity in equation (1.16) can be expressed in a simple form as:

$$C = \hat{C}_{M_T-1}(\frac{1}{M_T} \frac{S}{N}) / \Gamma(M_T) \tag{1.18}$$

While for the SIMO system with $M_T = 1$, the capacity can be expressed as:

$$C = \hat{C}_{M_R-1}(\frac{S}{N}) / \Gamma(M_R) \tag{1.19}$$

where $\Gamma(n) = (n-1)!$ of n is an integer. We present the capacity of Rayleigh fading channel for various systems as shown in Figure 1.4. It is interesting to compare the 2*2, 1*4 and 4*1 systems. For each of these cases, four independent Rayleigh fading links exist. The 2*2 system shows higher capacity at the SNR larger than 8dB, whereas the 1*4 system obtains better capacity gain in the low SNR region. Furthermore, increasing the number of receive antennas in SIMO system achieves more capacity gain than increasing the transmit antennas in MISO system. This can be shown more clearly in Figure 1.5. The capacity saturates the most rapidly in the MISO system. It seems that more than two transmit antennas is not necessary

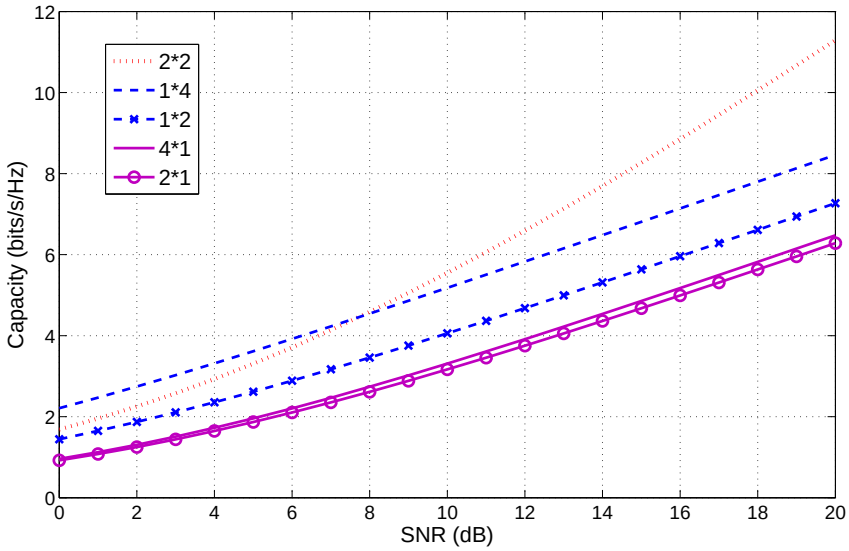

Figure 1.4: Capacity Vs SNR for various systems in Rayleigh fading channel

on the perspective of obtaining capacity gain in ergodic Rayleigh fading channel. If the available total transmit power for the MISO system is constrained, employing more transmit antennas seems a waste of resources on the perspective of obtaining larger channel capacity. Therefore, communication system with multiple receive antennas achieves more capacity gain than with multiple transmit antennas. But we have to mention that, in these comparisons, the transmit power at each antenna in MISO system (M transmit antennas) is divided by M with respect to the corresponding SIMO system (M receive antennas).

Although multiple receive antennas will further increase the capacity as shown by the 1*4 and 2*2 systems, they increases the transceiver complexity. In this thesis, we consider the scenario of wireless sensor networks, where each node is normally equipped with one antenna and supplied with low power battery. In addition, energy efficiency and simple implementation are more important than capacity achievement. Hence, MISO system will be investigated in this thesis.

1.3.2 Outage Probability

The ergodic fading channel means that all channel states are realized over an infinite sequence. Practically, it is more reasonable to assume that channel realization

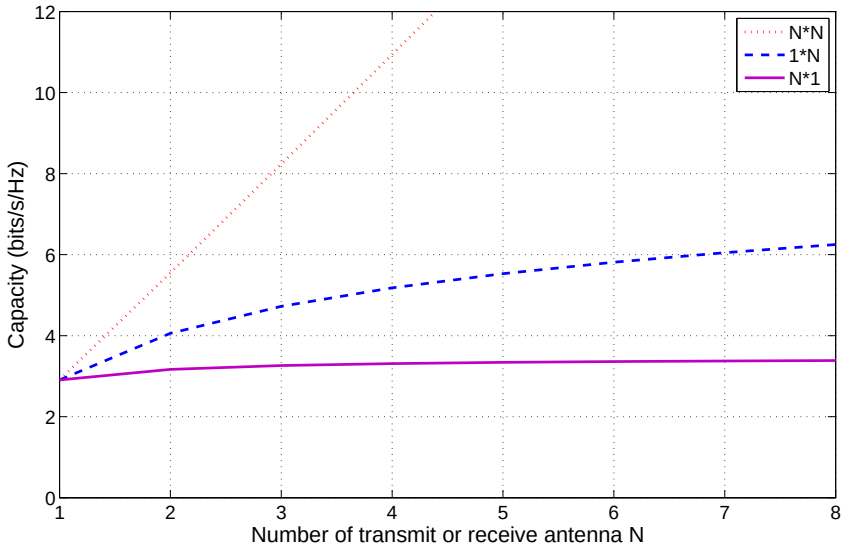

Figure 1.5: Capacity Vs Number of transmit or receive antenna for various systems in Rayleigh fading channel; SNR=10dB

is randomly fixed for a finite sequence and changes its states for the other finite sequences. In this case, it is determinant, for each channel realization, whether this transmission can be supported by a given communication rate. The outage probability is utilized to indicate the probability that a certain communication rate can be supported by the channel realizations. For a given communication rate R, the expression of outage probability can be given as [12]:

$$P_{out}(R) = \Pr\left(\log_2 \det\left(I_{M_T} + \frac{HH^H}{M_T}\frac{S}{N}\right) < R\right) \tag{1.20}$$

which can also be written as:

$$P_{out}(R) = \Pr\left(\sum_{i=1}^{m} \log_2\left(1 + \frac{\lambda_i}{M_T}\frac{S}{N}\right) < R\right) \tag{1.21}$$

This requires the calculation of an m-fold integral over the random λ_i with the probability distribution function given by equation (1.13). For the special case of MISO Rayleigh fading channel, the solution can be expressed as [12]:

$$P_{out,M_T\times 1}(R) = \gamma\left(M_T, \frac{M_T(2^R-1)}{S/N}\right)/\Gamma(M_T) \tag{1.22}$$

where $\gamma(\cdot)$ is the lower incomplete Gamma function defined as:

$$\gamma(a,x) \triangleq \int_0^x u^{a-1}e^{-u}du \tag{1.23}$$

In Figure 1.6 and Figure 1.7, we show the performance of outage probability in MISO system. Considering the cases of the desired communication rate to be 1 bit/s/Hz and 2 bits/s/Hz respectively, it is interesting to note that the intersection points in the two cases are at around the SNR of 0dB and 5dB respectively. As shown in Figure 1.4, these regions also coincide with the channel capacity at about 1 bit/s/Hz and 2 bits/s/Hz. Therefore, at a specific SNR, more engaged transmit antennas can not noticeably increase the channel capacity but can decrease the outage probability when the communication rate is lower than the achievable channel capacity. This is shown in Figure 1.7. We constrain the SNR to be 5dB. When the desired communication rate is lower than about 2 bits/s/Hz, more engaged transmit antennas decrease the outage probability greatly. The discussion of the diversity and the multiplexing gains in the next subsection can further strengthen these statements.

1.3.3 Diversity and Multiplexing

Wireless links are impaired by the random fluctuations across space, time and frequency known as fading. Diversity provides the receiver with multiple looks at the same transmitted signal so as to improve the reliability of the wireless links. It is based on the principle that, the receiver receives multiple independently faded replicas of the same information signal, so the probability that all the signal components are simultaneously faded is reduced. Thus diversity techniques stabilize the wireless links and lead to an improvement on reliability.

As an example, we consider the uncoded binary phase-shift keying (BPSK) signals over Rayleigh fading channel. In the case of SISO communication, the received bit error probability (BER) at high SNR is well known [7] as:

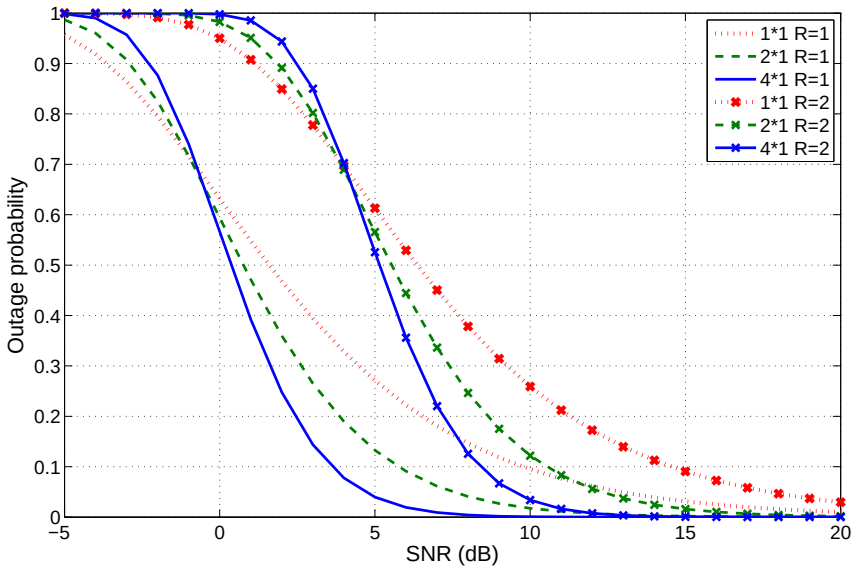

Figure 1.6: Outage probability vs SNR in MISO system, the desired communication rates are R=1bit/s/Hz and R=2bits/s/Hz respectively

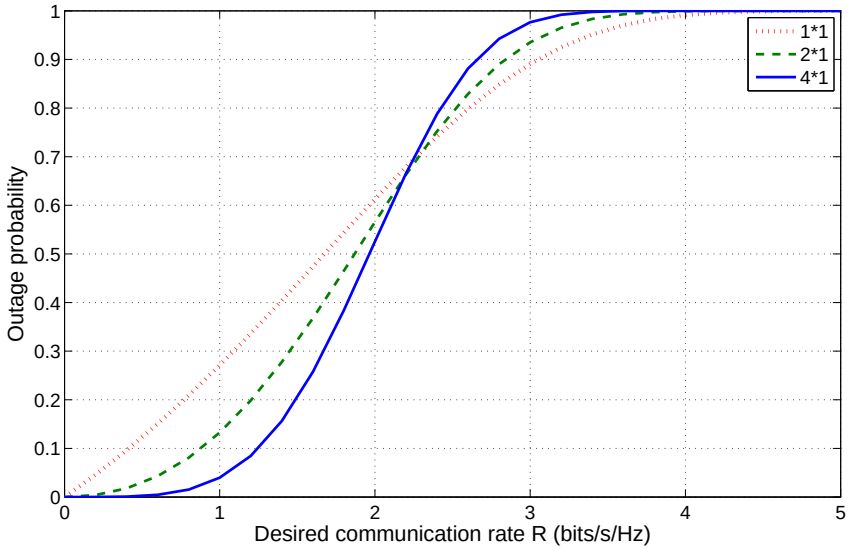

Figure 1.7: Outage probability vs desired communication rate in MISO system, SNR=5dB

$$P_e(SNR) \approx \frac{1}{4} SNR^{-1} \tag{1.24}$$

In contrast, supposing two replicas of the independently faded signal are received and properly combined (e.g. maximum ratio combination), the error probability at high SNR region is:

$$P_e(SNR) \approx \frac{3}{16} SNR^{-2} \tag{1.25}$$

We observe that, by having the extra receive antenna, the error probability decreases with SNR at a faster speed of SNR^{-2}. Similar results can be obtained if we change the BPSK signals to other constellations. Since the performance gain at high SNR region is indicated by the SNR exponent as shown in equations (1.24) and (1.25), this exponent is called the diversity gain. Thus, the definition of the *diversity gain* d can be represented as [13]:

$$d = -\lim_{SNR \to \infty} \frac{\log P_e(SNR)}{\log SNR} \tag{1.26}$$

Intuitively, it corresponds to the number of independently fading paths that the signal passes through. In a general system with M_T transmit antennas and M_R receive antennas, there are in total $M_T \times M_R$ random fading coefficients. Hence, the maximal (full) diversity gain provided by the channel is $M_T \times M_R$. As we will discuss in the next chapter, cooperative schemes exploring the spatial diversity of the channel can be used to improve the reliability of wireless link.

Besides providing diversity to improve reliability, multiple antennas system also supports a higher data rate than single antenna system. Considering an ergodic flat fading channel, where the channel matrix is i.i.d. across blocks of message, the capacity in equation (1.11) can be approximated as [13]:

$$C(SNR) = \min\{M_T, M_R\} \log \frac{SNR}{M_T} + \sum_{i=|M_T - M_R|+1}^{\max\{M_T, M_R\}} \varepsilon[\log \chi^2_{2i}] + o(1) \tag{1.27}$$

where χ^2_{2i} is chi-square distributed with $2i$ degrees of freedom. Thus, at high SNR

region, the number of the degrees of freedom is the minimum of M_T and M_R. It suggests that the MIMO channel can be viewed as $\min\{M_T, M_R\}$ parallel spatial channels. Notice that channel capacity increases with SNR as shown in equation (1.27). We consider a family of codes which have the communication rate of $R(SNR)$ (bps/Hz) also increasing with the SNR level. The spatial multiplexing gain r can be defined as:

$$r = \lim_{SNR\to\infty} \frac{R(SNR)}{\log_2 SNR} \tag{1.28}$$

It means that independent information symbols could be simultaneously transmitted in these r parallel channels. So the multiplexing gain provides a higher communication rate. However, in our works, we consider the reliable communication is more important than the higher data rate requirement in wireless sensor networks. Thus multiplexing gain will not be investigated through this dissertation.

1.4 Narrow-Band and Wide-Band Communication

In the previous discussion of wireless channels, we mentioned that the signal will suffer from frequency selective fading if its bandwidth exceeds the channel coherent bandwidth. In wireless sensor networks, the communication data rate (maximum of 250 kbps in [5]) is nowadays lower than other wireless network using Wi-Fi technology. So the bandwidth in wireless sensor networks are typically in a narrowband situation. Meanwhile, the delay spread of wireless channels are normally at the nano scale. It implies that, for wireless sensor networks, the communication suffers from flat fading in most case.

Although narrow-band communication can avoid the effect of frequency selective fading in most channel, some communication links deliberately use a wider bandwidth than necessary in order to gain other advantages. The spread spectrum system is a typical example. On one hand, by spreading the original message with a wider spectrum, the interference to other communication can be lowered. On the other hand, a CDMA system employing spread-spectrum technology allows multiple users to be multiplexed over the same physical channel. OFDM is also becoming

a popular scheme for wide-band communication. The primary advantage of OFDM is its ability to overcome narrowband interference and frequency-selective fading due to multipath propagation. So wide-band communication might sometimes be interesting for wireless sensor networks.

In this dissertation, we focus on exploiting cooperative communication to make wireless sensor networks operate more energy efficiently. Using the narrow-band communication or exploring a wider band, like spread spectrum system and OFDM system, can facilitate the cooperative communication. From this point of view, we notice that, narrow-band communication has the advantage of lower complexity for the implementation, while it is vulnerable to time synchronization errors among the cooperative nodes. On the other hand, exploring the previous mentioned wider band systems has the advantage to tolerate multipath delay or time synchronization error. But they require higher complexity at the baseband signal processing. Furthermore, frequency synchronization problem should not be ignored for OFDM system. These issues will exist when we discuss the implementation of cooperative communications, especially the virtual MISO cooperative communication, in wireless sensor networks. Here, we just mention that, the synchronization problem is an obstacle to implementation of cooperative communication in wireless sensor networks, whereas, narrow-band and wide-band systems have their respective advantage and disadvantage to cope with cooperative communications.

1.5 Summary

In this chapter, the characteristics of wireless sensor networks and their possible network topologies are presented. Then, the channel models incorporating the large-scale fading and small-scale fading are investigated. These models will be utilized throughout this dissertation for the analysis of cooperative communications in wireless sensor networks. In order to reveal the benefits of cooperative communication, the capacity of Rayleigh fading channel and the outage probability for block Rayleigh fading channel are evaluated. Furthermore, the idea of exploring diversity and multiplexing in MIMO channel is discussed. On the view of facilitating cooperative communications, the advantage and disadvantage of narrow-band and wide-band communications are also analysed briefly.

In wireless sensor networks, energy efficiency is the most important designing factor. The purpose of this thesis work is to investigate energy efficient commu-

nication schemes for wireless sensor networks. Cooperative communications could provide good performance on energy efficiency and resist to hostile channel fading effect. So in the next chapter, some cooperative communication schemes that could be employed in wireless sensor networks will be introduced.

Chapter 2

Cooperative Communication in Wireless Sensor Networks

2.1 Introduction

Wireless sensor networks are usually deployed in rigorous environment where communication channels suffer from shadowing and multipath fading. As sensor nodes are typically power constrained and size limited, multi-antenna systems are impractical to be implemented in these tiny nodes. Cooperative communications exploiting the diversity of the fading channels could be interesting for wireless sensor networks. It helps to guarantee reliable communication and maintain a good connectivity of the network. Furthermore, channel diversity can be explored in space and frequency domains. Experimental results in [14] show that significant benefits could be found when the separation between the carrier frequencies or the space between the antennas is sufficient. Meanwhile, cooperative schemes could be applied to different protocol layers, such as network layer and physical layer.

For cooperative scheme in network layer, network coding scheme is an active research area in recent years. It was first introduced in [15]. By employing network coding scheme, the transmitted packet should have additional information to indicate source nodes or source messages from which it was combined. Physical layer implementation of network coding scheme is possible, but more complex processing on the baseband signal is required [16, 17]. For wireless sensor networks, low requirements on signal processing capability are more appreciated.

In physical layer, two other kinds of cooperative schemes are mostly used.

The first cooperative scheme, which we call *cooperative relaying scheme*, utilizes the assisting radio of relays to compensate the bad fading effect as presented in [18, 19, 20]. Using the scheme of decode-and-forward or the scheme of amplify-and-forward, the relay node retransmits the received signal from source node to destination node. At the destination, based on maximum-likelihood or maximum signal-to-noise ratio criteria, the node combines the received signals from the source and the relay. The second diversity scheme [1, 21, 22], called *virtual MISO* (*multi-input multi-output*) *cooperative scheme*, benefits from the employment of orthogonal space time code. The transmission message will firstly be encoded by one kind of space time codes at each cooperative node. Redundant copies of the data stream, transmitted to the receiver, are in the hope that at least some of them may survive to the faded paths between the transmitters and the receiver. The *virtual MISO cooperative scheme* can be integrated with OFDM modulation scheme to overcome time synchronization problem for the distributed sensor nodes. We refer it as *OFDM-based cooperative scheme*.

In this chapter, we will discuss the cooperative schemes that could be implemented in wireless sensor networks. System models for these cooperative schemes will be presented. The analysis on the requirements of these schemes will be evaluated briefly.

2.2 Network Coding Scheme

When using network coding during data communication, instead of simply forwarding original packets, nodes may recombine several input packets into one or several combined output packets. The combination can be made on bit streams or on analog modulated symbols. We refer to them as digital network coding scheme and analog network coding scheme respectively.

A simple example with two wireless nodes (A and B) exchanging messages via a router node (R), as shown in Figure 2.1, can be used to explain the basic principle of network coding. Considering that only one channel is utilized, signal interference should be avoided in the traditional method. So the message exchange between the two nodes A and B requires four time slots, where the first two time slots are allocated for the message collection and the last two time slots are for the message distribution. Similar to the traditional method, two time slots are necessary for the message collection in digital network coding scheme. In the contrary, digital

network coding scheme only broadcasts the combination of [a *xor* b], so only one time slot is required for message distribution. Since the nodes A and B already know the messages a and b respectively, they can obtain message b from [a *xor* (a *xor* b)] and message a from [b *xor* (a *xor* b)]. It should be mentioned that, for any node who want to recover the original message, it should be capable of receiving enough independent combined messages.

The works in [16, 17] have shown that, instead of implementing network coding on digital bit streams, we can also implement it on analog modulated symbols. Figure 2.1 shows the analog networking coding scheme where $f(a,b)$ refers to the combination of a and b on analog symbol level. The analog network coding scheme could obtain more network throughput gain as illustrated in Figure 2.1 where only two time slots are required for the message exchange.

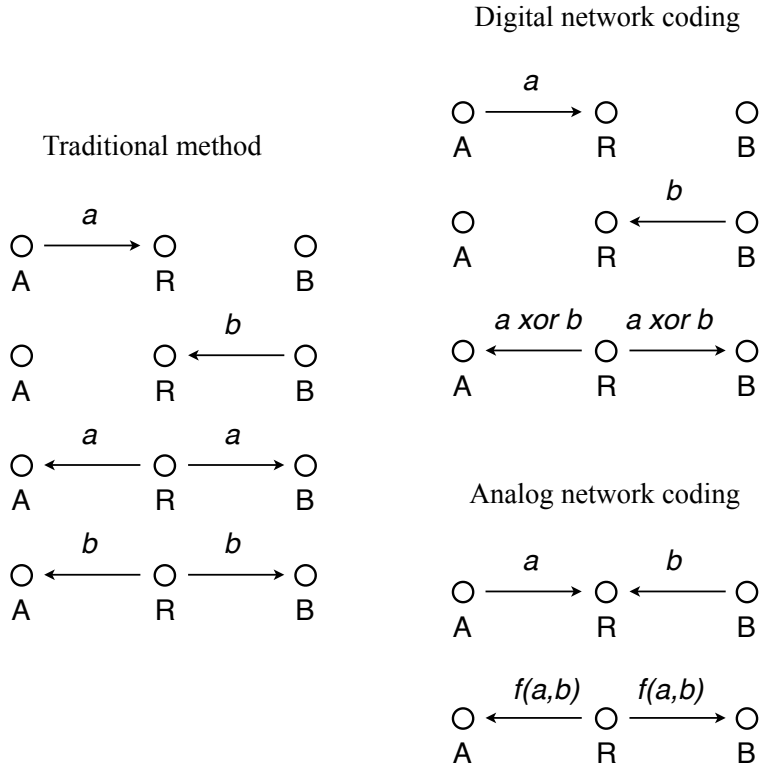

Figure 2.1: Examples of message exchange using traditional method, digital network coding scheme and analog network coding scheme

The algorithm in [16] assumes that symbol-level time synchronization, carrier

Modulation mapping at A and B				Demodulation mapping at R		
				input	output	
input		output			Modulation mapping at R	
					input	output
1	1	1	1	2	0	-1
0	1	-1	1	0	1	1
1	0	1	-1	0	1	1
0	0	-1	-1	2	0	-1

Figure 2.2: Modulation and demodulation mapping

phase synchronization and power control among the nodes are perfect. Therefore, the signals simultaneously transmitted from A and B arrive at R with the same phase and amplitude. Then the combined baseband signals will be passed through a special demodulation/modulation mapping to obtain a bit stream equivalent to the combination using in the digital network coding scheme. Considering BPSK modulation, the mapping table can be shown in Figure 2.2. The modulation mappings at A and B in the first time slot and at R in the second time slot are the same as BPSK modulation, while the demodulation mapping at R is performed similar to *xor* operation, with the difference that it is estimated on the soft decision. The decoding processes at A and B are the same as the digital network coding scheme. However, the synchronization requirement will add more constraints on the deployment or introduce more energy consumption.

In [17], the authors have presented a more general algorithm that makes no synchronization assumption. In fact, a random delay of the transmission in the first time slot at A and B has intentionally been introduced. The relay node R makes no decision on the receive signals, it just amplify-and-forwards the signals. Due to the additive intentional delay, signals received at the node A and B will have interference-free symbols at the head and the tail of the frame. In the second time slot, these interference-free symbols are used to estimate the wireless channels. Using the channel information and self-cancelling with the already known signals, the received frame could be properly decoded. We note that the requirement on signal processing capability should be considered when the analog network coding scheme is implemented in physical layer.

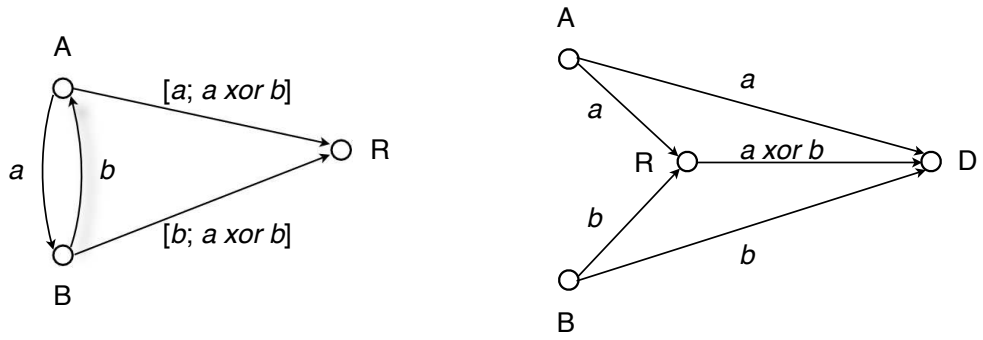

Figure 2.3: Two simple cooperative paradigms utilizing network coding scheme

In addition to message exchange, network coding scheme can also be incorporated with cooperative schemes in physical layer. Two simple cooperative paradigms implementing digital network coding, where the combination operation is also defined as *xor*, are shown in Figure 2.3. The cooperative paradigms comprise the virtual MISO cooperative process and cooperative relaying process that will be illustrated in the following sections. In these paradigms, the additional digital combined message (a *xor* b), instead of only the message a or b, will be transmitted. In that case, cooperative diversity gain could also be obtained. The work in [23] has presented that network coding scheme could improve the outage performance of cooperative communication. Furthermore, as the benefits of network coding scheme is to increase the network throughput on the network layer, network throughput gain is also reasonable to be obtained by incorporating the cooperative communication with network coding scheme.

2.3 Cooperative Relaying Scheme

Multi-hop transmission is a traditional scheme for long distance communication in wireless networks. Based on this traditional scheme and exploiting the broadcast nature of wireless medium, several cooperative relaying schemes have been discussed in [18, 24]. In general, they can be classified into fixed relaying schemes exploring decode-and-forward relaying or amplify-and-forward relaying and optional relaying schemes utilizing selective relaying or incremental relaying [18].

Decode-and-forward

The decode-and-forward process is also employed in traditional multi-hop scheme. While the difference in cooperative relaying scheme is that the source node S attempts to transmit a message to destination node D with the cooperation of relay node R, other that only by the relay hopping of the node R. As shown in Figure 2.4, the transmission is divided into two time slots. At the first time slot, message is broadcasted by the source node. The destination and relay node receive this message by the nature of wireless broadcast. The signal received at the relay node and destination node can be written as:

$$r_1 = h_{sd}\sqrt{P_s}s_0 + n_1 \tag{2.1}$$

$$r_2 = h_{sr}\sqrt{P_s}s_0 + n_2 \tag{2.2}$$

where s_0 is the transmitted signal by the source node with power P_s, r_1 and r_2 are the received signals at the relay and destination node, h_{sd} and h_{sr} are the channel coefficients, n_1 and n_2 capture the effect of AWGN.

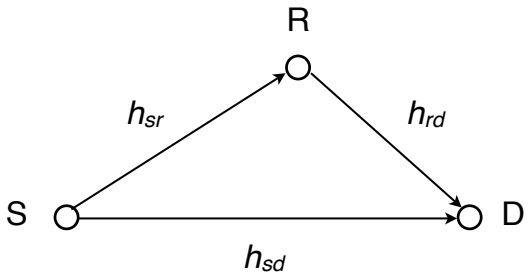

Figure 2.4: Fixed cooperative relaying

Due to the different channel conditions, the relay and destination nodes detect the message differently. It is reasonable that, in most case, the relay node can receive this message with less error probability than the destination node does. So at the second time slot, the relay node will retransmit the decoded message. The retransmitted signal is expressed as:

$$r_3 = h_{rd}\sqrt{P_r}s_r + n_3 \tag{2.3}$$

where s_r is the retransmitted signal by the relay node with power P_r, h_{rd} is the

channel coefficient between the relay and destination nodes, n_3 captures the effect of AWGN. Based on the two received signals shown in equations (2.1) and (2.3), the destination node using maximum ratio combination (MRC) can detect the source signal with less error probability.

Amplify-and-forward

The amplify-and-forward scheme also consists of three nodes as shown in Figure 2.4. However, in amplify-and-forward scheme, the relay node just amplifies the received signal without decoding it. So in the first time slot, the received signals at the relay node and destination node are the same as in decode-and-forward scheme shown in equations (2.1) and (2.2). In the second time slot, the destination node receives the amplified signal from the relay path as:

$$r_3 = \alpha_r h_{rd} r_2 + n_3 \tag{2.4}$$

Note that, in order to remain within its power constrain, the relay node uses the amplifying factor α_r. It is determined by the allocated transmit power and instantaneous channel gain as shown in the follows:

$$\alpha_r = \sqrt{\frac{P_r}{|h_{sr}|^2 P_s + N_0 B}} \tag{2.5}$$

where N_0 is the power spectral density of AWGN and B is the bandwidth of baseband signals. Based on the received signals in the two time slots shown in equations (2.1) and (2.4), the destination node decodes the source message. Considering the MRC of the received signals at the destination node, the received SNR after combination is:

$$\gamma_{AF} = \gamma_{sd} + \frac{\gamma_{sr}\gamma_{rd}}{1 + \gamma_{sr} + \gamma_{rd}} \tag{2.6}$$

$$with \quad \gamma_{sd} = \frac{|h_{sd}|^2 P_s}{N_0 B}, \quad \gamma_{sr} = \frac{|h_{sr}|^2 P_s}{N_0 B}, \quad and \quad \gamma_{rd} = \frac{|h_{rd}|^2 P_r}{N_0 B}$$

Selective relaying

Fixed relaying schemes as described before are usually considered when the relay node was assigned in advance. However, in most case, the signal broadcasted by the source node is overheard by several nodes, while the assigned cooperative node may not be the best node that can correctly receive this signal. So in selective relaying scheme, the node which can better receive the signal will be selected as the cooperative node. This can be realized by the strategy that among the relay nodes between the source node and destination node, if the measured $|h_{sr}|^2$ falls below a certain threshold, the source node simply continues its transmission to the destination node in the form of repetition or in allocating more transmit power. If the measured $|h_{sr}|^2$ lies above the threshold, the best node which has the highest $|h_{sr}|^2$ will be selected as the relay. The effective process of selecting the relay node can be performed similarly as described in [25], where each relay node uses a timer related to the channel condition. The timer of the relay node with the best channel condition will expire first. Then it transmits a short flag, announcing its presence, and stops the timer of the other nodes. The channel models of this scheme are similar to those employed in decode-and-forward relaying scheme or amplify-and-forward relaying scheme.

Incremental relaying

In the above relaying schemes, the relay node performs cooperative relaying all the time. In some case, it might be inefficient to utilize the degrees of freedom of the channels. Occasionally, if the channel between the source and destination nodes is good enough, it is not necessary for the relay node to retransmit or amplify the received signal to the destination node. Otherwise, the destination node might indicate a failure of the direct transmission from the source. By exploiting this feedback from the destination, relaying process is required to be performed. It can alternatively use the fixed relaying or selective relaying. On the other hand, in addition to relaying the whole sequence of the source information, an incremental redundancy might also be necessary. It could be achieved by implementing stronger error control code in the relaying process.

How to select the relay node?

At the beginning of fixed relaying schemes, we should consider the strategy to choose the best candidate relay node. Meanwhile, in the optional relaying schemes, selecting a set of candidate relay nodes in advance would sometimes be

more efficient.

Several strategies could be used to choose the optimal relay. The *minimal transmit power* (P_t) *strategy* is more straightforward to minimize the energy consumption for cooperative relaying schemes. In this strategy, a predefined bit error probability is supposed to be met. The optimal relay is chosen in order to make the total required transmit power at the source and relay to be minimal. The *minimal outage probability strategy* chooses the relay by minimizing the outage probability under the constraint of available total transmit power. For cooperative communication schemes, outage probability is usually easier to be expressed analytically than bit error rate probability. Without the knowledge of channel condition, the *maximal residual energy* (E_i) *strategy* can be performed more efficiently sometimes. Furthermore, it is helpful to achieve the balance of energy consumption among the cooperative nodes. An integration strategy can be represented as the *maximal energy efficiency* (E_i/P_t) *strategy*, which takes both channel condition and residual energy into account. Then, the choice of the relay is to exploit more diversity degree of the channel and achieve more balance on energy consumption.

2.4 Virtual MISO Cooperative Scheme

Space-time block codes introduced in [26] can be employed on multiple transmit antennas to exploit full diversity of Rayleigh fading channel. The coding scheme can be defined as a $m \times n$ coding matrix as follows:

$$C_2 = \begin{bmatrix} s_1 & s_2 \\ -s_2^* & s_1^* \end{bmatrix} \qquad C_3 = \begin{bmatrix} s_1 & s_2 & s_3 \\ -s_2 & s_1 & s_4 \\ -s_3 & s_4 & s_1 \\ -s_4 & -s_3 & s_2 \\ s_1^* & s_2^* & s_3^* \\ -s_2^* & s_1^* & s_4^* \\ -s_3^* & s_4^* & s_1^* \\ -s_4^* & -s_3^* & s_2^* \end{bmatrix} \tag{2.7}$$

These two matrices can be used in two transmit antennas and three transmit antennas systems respectively. The message will first be encoded using these matrices and then be transmitted simultaneously from multiple antennas. In wireless sensor networks, due to the small physical size of sensor nodes, direct implemen-

tation of a multi-antenna system on the sensor node is impractical. *Virtual MISO cooperative scheme* has been proposed in [27] to provide a comparable performance to a multi-antenna system. It can be performed by selecting m cooperative nodes from a set of potential relaying nodes to constitute a virtual multi-antenna system. Data are encoded by a $m \times n$ space time coding matrix and split into m data streams which are simultaneously transmitted by the m cooperative nodes. In order to explore more details of employing space-time block codes in distributed way, we will explain the simplest implementation of this scheme using the code described by C_2 in (2.7), which is generally referred as Alamouti code [28].

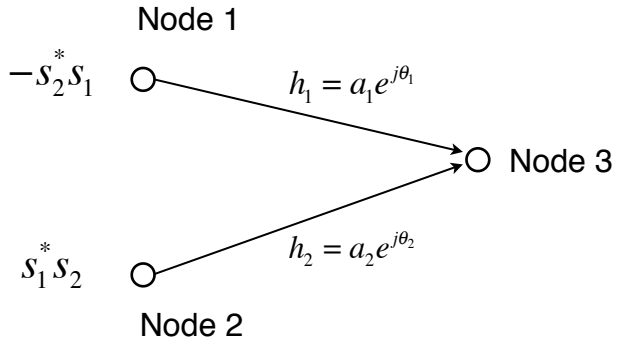

Figure 2.5: Virtual MISO cooperative communication using Alamouti code

As shown in Figure 2.5, there are two transmit nodes and one receive node. We suppose that both of the two transmit nodes already got the same original message. The transmission at the baseband could employ a signal constellation with 2^b elements. At the first time slot, $2b$ bits arrive at the encoder which selects the constellation signals s_1 and s_2. These two signals are transmitted simultaneously from $Node1$ and $Node2$. At the second time slot, the signals $-s_2^*$ and s_1^* are transmitted simultaneously from $Node1$ and $Node2$. The operator * refers to the complex conjugation. If the channel is static during these two time slots, the received signals r_1 and r_2 at $Node3$ will be:

$$\begin{aligned} r_1 &= h_1\sqrt{P_{T1}}s_1 + h_2\sqrt{P_{T2}}s_2 + n_1 \\ r_2 &= -h_1\sqrt{P_{T1}}s_2^* + h_2\sqrt{P_{T2}}s_1^* + n_2 \end{aligned} \tag{2.8}$$

where P_{T1} and P_{T2} are the transmit powers at $Node1$ and $Node2$, h_1 and h_2 are

the channel coefficients of the respective channels defined as $a_1 e^{j\theta_1}$ and $a_2 e^{j\theta_2}$, n_1 and n_2 capture the effect of AWGN. Then, as discussed in [29], the maximum likelihood detection is utilized to minimize the decision metric:

$$\left[\left|r_1 - h_1\sqrt{P_{T1}}s_1 - h_2\sqrt{P_{T2}}s_2\right|^2 + \left|r_2 + h_1\sqrt{P_{T1}}s_2^* - h_2\sqrt{P_{T2}}s_1^*\right|^2\right] \tag{2.9}$$

This in turn is equivalent to minimizing the decision metric for detection s_1 as:

$$\left|(r_1 h_1^*\sqrt{P_{T1}} + r_2^* h_2\sqrt{P_{T2}}) - s_1\right|^2 + (-1 + \sum\nolimits_{i=1}^{2} |h_i|^2 P_{Ti}) \cdot |s_1|^2 \tag{2.10}$$

and for detection s_2 as:

$$\left|(r_1 h_2^*\sqrt{P_{T2}} - r_2^* h_1\sqrt{P_{T1}}) - s_2\right|^2 + (-1 + \sum\nolimits_{i=1}^{2} |h_i|^2 P_{Ti}) \cdot |s_2|^2 \tag{2.11}$$

So the combined signals sent to the maximum likelihood detector are:

$$\begin{aligned}\tilde{s}_1 &= r_1 h_1^*\sqrt{P_{T1}} + r_2^* h_2\sqrt{P_{T2}} = (a_1^2 P_{T1} + a_2^2 P_{T2})s_1 + h_1^*\sqrt{P_{T1}}n_1 + h_2\sqrt{P_{T2}}n_2^* \\ \tilde{s}_2 &= r_1 h_2^*\sqrt{P_{T2}} - r_2^* h_1\sqrt{P_{T1}} = (a_1^2 P_{T1} + a_2^2 P_{T2})s_2 - h_1\sqrt{P_{T1}}n_2^* + h_2^*\sqrt{P_{T2}}n_1\end{aligned} \tag{2.12}$$

This kind of cooperative scheme, utilizing Alamouti coding, can achieve a diversity with two degrees of freedom. However, when applying *virtual MISO cooperative scheme* to wireless sensor networks, there are still some practical issues that should be considered. In the previous analysis, we assume that the frequency and time are perfectly synchronized. While in reality, due to the inconsistency on the oscillator and distributed deployment of the nodes, the problem of synchronization should not be ignored. For the carrier synchronization, we can assume that a reference carrier is transmitted and all nodes can lock to this reference carrier using a phase locked loop, or it can be estimated using some pilot symbols at the beginning of the packet as presented in [30]. Other than carrier synchronization, arrival time synchronization of the received signal would be more significant for

the implementation of virtual MISO cooperative scheme. As in the receiver side, the received signal from multiple transmitters should be coherently combined; it requires the nodes to be well synchronized. The effect of synchronization problem will be discussed in more detail in Chapter 3.

2.5 Summary

In this chapter, various cooperative communication schemes, which are implemented either in physical layer or in network layer, are presented. They could be used to exploit cooperative diversity in fading channel. In this dissertation, we focus on physical layer cooperative communication schemes. But we note that, network layer cooperative scheme, such as network coding scheme, can be implemented in parallel with physical layer cooperative schemes.

Considering the practical implementation of cooperative communication in physical layer, the synchronization requirements are different. For cooperative relaying scheme and OFDM-based cooperative scheme, the requirement on time synchronization is low. While virtual MISO cooperative scheme requires stringent arrival time synchronization of the signals from the distributed cooperative nodes. On the other hand, frequency synchronization should not be ignored for OFDM-based cooperative scheme. In the next chapter, we will analysis the effect of the synchronization problem in more detail and propose a synchronization strategy accordingly.

Chapter 3

Synchronization for Cooperative Communication

3.1 Introduction

Time synchronization is crucial for the implementation of cooperative communication in wireless sensor networks. Previous work by Jagannathan [31] has investigated the effect of time synchronization error on maximum ratio combining diversity techniques and Alamouti coding system. Mei [32] has also analysed this asynchronous effect on time-reverse space-time coding system and space-time OFDM system. All these works have shown that a cooperative system has a good tolerance for small synchronization error. But they didn't propose any synchronization scheme that can constrain the synchronization error into an acceptable range. Some synchronization algorithms have been proposed for wireless sensor networks, but they aimed at the network synchronization. They cannot attain the precision requirement for coherent combining of the distributed space-time codes during decoding procedure.

Our works do not assume a perfect synchronization among the nodes. We explore the effect of synchronization error on cooperative communication utilizing distributed Alamouti code. The analytical and simulated results show that a small synchronization error has negligible effect on bit error rate (BER) performance. In order to synchronize the distributed sensor nodes within this acceptable error, we propose a physical layer synchronization scheme. This scheme consists of an initial synchronization of the cooperative transmitters, synchronization error estimation

at the cooperative receiver and finally a feedback phase. A maximum likelihood method is proposed to make the synchronization error estimation. It achieves better performance than the matched filter method at the price of moderate increase in computational complexity and memory space. After synchronization error estimation, two strategies have been analysed. They provide better BER performance in the existence of initial synchronization error. They are practical to be implemented in the sensor nodes before the Alamouti decoding.

The remainder of this chapter is organized as follows. In section 3.2, we present the needs for time synchronization in wireless sensor works. In section 3.3, system models including the cooperative scheme and the synchronization scheme are presented. The Alamouti scheme in the presence of synchronization error is analysed. In section 3.4, the strategy of time synchronization is discussed in details and the simulated results are presented. In section 3.5, two other candidate solutions that could cope with time synchronization problem are discussed.

3.2 The Needs for Time Synchronization

Time synchronization is always a problem that should be tackled for networks organized in a distributed way. Clock synchronization for the computers connected through Internet is a well studied problem [33]. However, the ad hoc characteristic and the unique system architecture in wireless sensor networks make the time synchronization problem to have more challenges. Furthermore, the synchronization needs and the corresponding precision requirements are various according to different applications and network deployments. In this dissertation, we classify the time synchronization problems in wireless sensor networks into network clock synchronization and signal arrival time synchronization.

3.2.1 Network Clock Synchronization

Normally, network clock synchronization is on the view of the whole network or some local region of the network. Its object is to maintain the network with a global clock. A unique clock time is an important factor to make sure that wireless sensor networks could function properly. Since everything happens over time, most applications require the data collected by the sensor nodes to have a consistent time-stamp. These data related to a time sequence are essential to information

processing [34]. In addition, some deployments of wireless sensor networks arrange the communication among the nodes utilizing TDMA technology [35, 36, 37]. The allocation of communication time slots makes a demand on the clock synchronization. Without a good synchronization, more communication interferences will be introduced or channel access will be delayed.

Various network clock synchronization protocols [38, 39, 40, 41, 42] have already been proposed for wireless sensor networks. A great contribution on the network clock synchronization can be found in the dissertation work by Jeremy Elson [43]. The surveys in [44, 45] summarize the existing clock synchronization protocols for wireless sensor networks. Two synchronization protocols, Reference Broadcast Synchronization (RBS) [38] and Timing-synchronization Protocol for Sensor Network (TPSN) [39], reported relative high precisions which are on the order of few microseconds. For example, RSB has been tested on Berkeley Motes and reported a precision of 11 μs [38]. On the same hardware platform of Mica sensor architecture, TPSN reported a precision of 16.9 μs, while RBS was 29.13 μs [39]. The synchronization precisions of these protocols show that they could be suitable for most needs of wireless sensor network applications.

3.2.2 Signal Arrival Time Synchronization

For the implementation of distributed cooperative communication in wireless sensor networks, higher precision on time synchronization is required. For example, in the distributed beamforming scheme [46], the slave nodes in the cluster should synchronize their clock according to the arriving time of the trigger sequence. The performance gain is obtained by suitably weighting the transmitted signals and directing a beam coherently in the desired direction. So the precision requirement for time synchronization is on the order of symbol time duration. Whereas, a transmit symbol rate of only 50k symbols/second will result in a symbol duration of 20 μs, which is around the precision level of the synchronization protocols RBS and TPSN. So the precisions of the network clock synchronization protocols are not sufficient for high data rate communication. Similarly, in order to form an Opportunistic Large Array (OLA) for cooperative communication [47], symbol synchronization is required for the cooperative nodes. Otherwise, the aggregate transmission could not be enhanced by the accumulation of transmit power from the cooperative nodes. Although, in the analog network coding scheme proposed in [17], asynchronous interval of a few symbols time duration is tolerable, the pre-

cision of the network clock synchronization can only support low transmit data rate.

Cooperative space-time codes have been shown to provide great performance for wireless communications [27]. Forming a virtual MIMO system by employing distributed space-time codes is energy efficient for long distance communications in wireless sensor networks [1]. Most works [20, 48] considering distributed cooperative communications assume that distributed sensor nodes can be perfectly synchronized. We note that this assumption requires elaborate consideration on the protocol design and hardware implementation. The synchronization algorithms on network clock synchronization cannot attain the precision requirement for coherent combining of the distributed space-time codes during decoding procedure. Therefore, signal arrival time synchronization is required for the space-time coded cooperative communication. In the next section, we will analyse the effect of synchronization error on virtual MISO cooperative communications.

3.3 Effect of Synchronization Error on Virtual MISO Scheme

3.3.1 System Model

We consider the deployment of wireless sensor networks where sensor nodes are grouped into clusters. As shown in Figure 3.1, we assume that the distance between two clusters is long and the channel suffers from Rayleigh fading effect, whereas the distance between any two nodes within a cluster is small and the channel is an Additive White Gaussian Noise (AWGN) channel. So the communication between clusters (inter-cluster) is more energy consuming than the communication within the cluster (intra-cluster). In order to improve the energy efficiency for long distance inter-cluster communications, distributed cooperative communication schemes can be employed by sensor nodes.

Alamouti code [28] is well known as one kind of space time codes. It can be used in the distributed cooperative communication. This cooperative scheme can be implemented by two Cooperative Transmit Nodes (*CTN1* and *CTN2*) and one Cooperative Receive Node (*CRN1*) to form a virtual multi-input-single-output (MISO) system. Data are encoded by the Alamouti coding matrix and split into two streams which are simultaneously transmitted by the two cooperative trans-

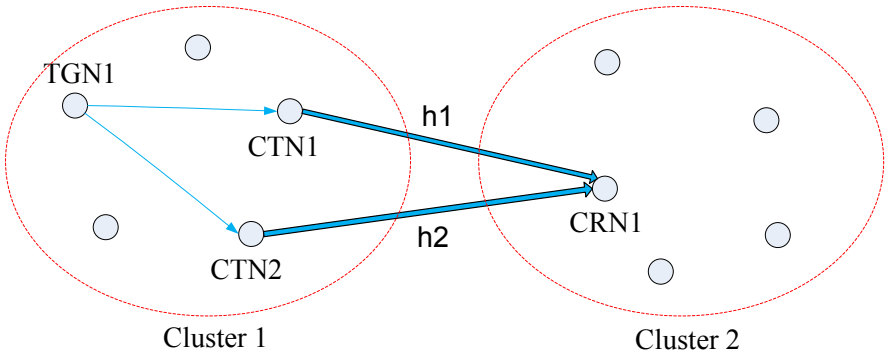

Figure 3.1: Cooperative MISO system in wireless sensor networks

mit nodes. In this study, we limit our analysis to the cooperative scheme utilizing Alamouti code for two reasons. Firstly, since energy consumption of analog circuit is a prominent part of energy depletion, the participation of more nodes in the cooperative transmission may not be more energy efficient [49]. Secondly, this configuration reduces the complexity of clustering coordination between the distributed nodes. However, due to the distributed deployment of sensor nodes, time synchronization in the symbol level could not be assumed to be perfect. So how precise the sensor nodes should be synchronized for cooperative communication is the problem we try to solve in this section.

In order to synchronize the cooperative transmit nodes, we assign a trigger node in each cluster to initiate a first synchronization phase. This trigger node can also perform the role of cluster head as in some scenarios of cluster organized wireless sensor networks [50]. As shown in Figure 3.1, we suppose that the node *TGN1* in the first cluster is the trigger node. It collects monitoring information within the cluster and convergence information from other clusters in the network. All the information enclosed in the trigger packet will be sent to *CTN1* and *CTN2*. In the front of each trigger packet, there is a training and synchronization sequence. Using the synchronization sequence, the arrival time of the packet can be estimated by a predefined matched filter. Therefore, based on the detection of the trigger packet's arrival time, *CTN1* and *CTN2* adjust their clock respectively. So they can be initially synchronized. This initial synchronization phase may not be perfect. Whereas, as the initial synchronization phase is made at the physical layer, its precision can be supposed to be in the level of the symbol time interval. We will explain this in more detail in section 3.4.1.

After the initial synchronization phase, the information sequence will be transmitted cooperatively under the control of the adjusted clock. Although coherent decoding of the cooperative transmitted information needs the two cooperative transmit nodes to be precisely synchronized, we will show that a small synchronization error has little degradation on receiving BER performance. So according to the synchronization error, different strategies stated in section 3.4.2 could be implemented. At the same time, the synchronization error between the two transmit nodes could be fed back to adjust their clock times. Therefore, at the beginning of Alamouti decoding, synchronization error should be estimated to see whether it is in an acceptable range. We proposed a maximum likelihood estimation method to do that. It can estimate the synchronization error in different granularity according to a predefined factor. In order to determine the acceptable range of synchronization error and the granularity for the estimator, we will analyse the effect of synchronization error on the performance of cooperative communication in the next section.

3.3.2 Alamouti Scheme with Synchronization Error

In the distributed deployment of sensor nodes, each node has its local clock circuit. Assumption of perfect clock synchronization in such a distributed setting is not realistic. In order to design a feasible synchronization scheme, it is important to analyse the effect of synchronization error on the communication performance. So in this section, we will investigate the effect of synchronization error on the decoding of Alamouti code.

Due to the synchronization error between the two cooperative transmit nodes (*CTN1* and *CTN2*), the practical combined signals may be different from the perfect ones described in [28]. In our analysis, the clock of *CTN1* is assumed to be the reference clock. In this way, the synchronization error of *CTN2* to *CTN1* can be taken as T_e. So the signals for the Alamouti decoding at *CRN1* will be received in two time slots as:

$$\begin{aligned} r_1(t) = \sum_{k=-L_t}^{L+L_t-1} \big\{ & \sqrt{E_{n1}} s_1(k) h_1(t) p(t - kT_b) \\ & + \sqrt{E_{n2}} s_2(k) h_2(t) p(t - kT_b - T_e) \big\} + n_1(t) \end{aligned} \tag{3.1}$$

$$r_2(t) = \sum_{k=-L_t}^{L+L_t-1} \left\{ -\sqrt{E_{n1}} s_2^*(k) h_1(t) p(t - kT_b) + \sqrt{E_{n2}} s_1^*(k) h_2(t) p(t - kT_b - T_e) \right\} + n_2(t) \tag{3.2}$$

where $s_1(k)$ and $s_2(k)$ are the kth modulated information symbols of the transmit sequences. E_{n1} and E_{n2} are the receive energy per symbol in the path *CTN1* to *CRN1* and the path *CTN2* to *CRN1* respectively. $p(t)$ is the raised cosine pulse shape with $2L_t + 1$ as the approximated effective symbol duration; L is the length of the information sequence. T_b is the symbol duration. $h_1(t)$ and $h_2(t)$ are modelled by independent complex Gaussian random variables of variance 0.5 per real dimension. The coherent time of the fading channel is assumed to be larger than the propagation time of the packet. So the channels are supposed to be constant during the transmission of each packet. $h_1(t)$ and $h_2(t)$ are represented as $a_1 e^{j\theta_1}$ and $a_2 e^{j\theta_2}$ in the following analysis. $n_i(t)$ is the zero mean, circular complex AWGN with variance σ_{ni}^2.

Because of the synchronization error, the overlapped received symbol pulses are not conforming to the Nyquist pulse-shaping criterion and suffer from Inter-Symbol-Interference (ISI). This makes the Alamouti code not perfectly orthogonal. So the estimated symbols after combination are:

$$\begin{aligned} \tilde{s}_1(t) = {} & E_{n1} a_1^2 \sum_{k=-L_t}^{L+L_t-1} s_1(k) p(t - kT_b) + E_{n2} a_2^2 \sum_{k=-L_t}^{L+L_t-1} s_1(k) p(t - kT_b - T_e) \\ & + \sqrt{E_{n1} E_{n2}} h_1^*(t) h_2(t) \sum_{k=-L_t}^{L+L_t-1} s_2(k) \left(p(t - kT_b - T_e) - p(t - kT_b) \right) \\ & + \sqrt{E_{n1}} h_1^*(t) n_1(t) + \sqrt{E_{n2}} h_2(t) n_2^*(t) \end{aligned} \tag{3.3}$$

$$\begin{aligned} \tilde{s}_2(t) = {} & E_{n1} a_1^2 \sum_{k=-L_t}^{L+L_t-1} s_2(k) p(t - kT_b) + E_{n2} a_2^2 \sum_{k=-L_t}^{L+L_t-1} s_2(k) p(t - kT_b - T_e) \\ & + \sqrt{E_{n1} E_{n2}} h_1(t) h_2^*(t) \sum_{k=-L_t}^{L+L_t-1} s_1(k) \left(p(t - kT_b) - p(t - kT_b - T_e) \right) \\ & + \sqrt{E_{n2}} h_2^*(t) n_1(t) - \sqrt{E_{n1}} h_1(t) n_2^*(t) \end{aligned} \tag{3.4}$$

To make the discussion more convenient, we consider the estimation of the symbols transmitted at the lth time (each time is composed of two time slots). They can be decomposed as:

$$\tilde{s}_1(t) = \tilde{s}_1(t)_{desired} + ISI(s_1,t) + ISI'(s_2,t) + ISI''(s_2,t) + N_1 \tag{3.5}$$

$$\tilde{s}_2(t) = \tilde{s}_2(t)_{desired} + ISI(s_2,t) + ISI'(s_1,t) + ISI''(s_1,t) + N_2 \tag{3.6}$$

$$\begin{aligned}
\text{where } \tilde{s}_1(t)_{desired} &= E_{n1}a_1^2 s_1(l)p(t-lT_b) + E_{n2}a_2^2 s_1(l)p(t-lT_b-T_e) \\
ISI(s_1,t) &= E_{n1}a_1^2 \sum_{\substack{k=-L_t \\ k\neq l}}^{L+L_t-1} s_1(k)p(t-kT_b) \\
&\quad + E_{n2}a_2^2 \sum_{\substack{k=-L_t \\ k\neq l}}^{L+L_t-1} s_1(k)p(t-kT_b-T_e) \\
ISI'(s_2,t) &= \sqrt{E_{n1}E_{n2}}h_1^*(t)h_2(t)s_2(l)\left(p(t-lT_b-T_e) - p(t-lT_b)\right) \\
ISI''(s_2,t) &= \sqrt{E_{n1}E_{n2}}h_1^*(t)h_2(t) \\
&\quad \cdot \sum_{\substack{k=-L_t \\ k\neq l}}^{L+L_t-1} s_2(k)\left(p(t-kT_b-T_e) - p(t-kT_b)\right) \\
N_1 &= \sqrt{E_{n1}}h_1^*(t)n_1(t) + \sqrt{E_{n2}}h_2(t)n_2^*(t)
\end{aligned}$$

and the estimated symbol of $\tilde{s}_2(t)$ can be decomposed using the same way. Usually, the tails of the pulse shape $p(t)$ will decay as $1/t^3$ for roll-off factor larger than 0. Consequently, a series of the ISI components from the side lobes converge to a trivial value [7]. In order to simplify the analysis but still maintaining an acceptable precision, we use the similar simplifications as have been done in [31] to restrict the raised cosine pulse to two side lobes on either side (hence, $L_t = 2$ is a reasonable choice) and approximate the pulse with linear pieces as shown in Figure 3.2.

Without loss of generality, we consider the case where packets from *CTN1* arrive first. Before the Alamouti decoding, we use the maximum likelihood estimator to estimate the synchronization error. As the purpose of this section is to analyse the effect of synchronization error on the receiving BER performance, we assume that the estimation of the synchronization error is perfect (that is $\tilde{T}_e = T_e$). Based

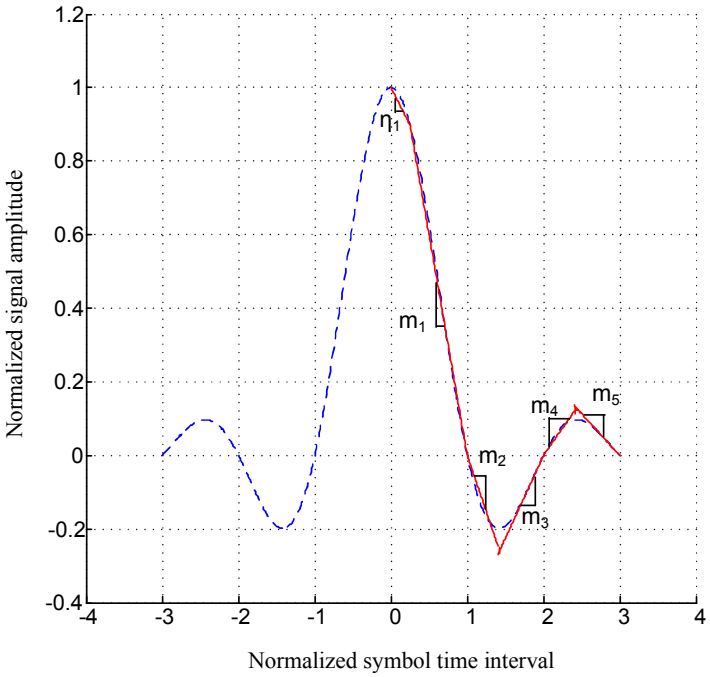

Figure 3.2: Piecewise linear approximation of the raised cosine pulse

on the estimation of the synchronization error, the sampling time for Alamouti decoding can be decided. In [51], the authors use two sampling times locked to the two path sequences respectively. However, as our proposed synchronization scheme can limit the synchronization error within a small range, only one sampling time per symbol interval is chosen to reduce the decoding complexity and therefore the energy consumption. We lock the sampling time to a shift of one half of the estimated synchronization error relative to the reference clock. Then, after the simplification of piecewise linear approximation, the desired sampling signals estimated at the lth time are:

$$\tilde{s}_1\left(lT_b + \tilde{T}_e/2\right)_{desired} = \left(E_{n1}a_1^2 + E_{n2}a_2^2\right)\left(1 + \eta_1\frac{\tilde{T}_e}{2}\right)s_1(l) \tag{3.7}$$

$$\tilde{s}_2\left(lT_b + \tilde{T}_e/2\right)_{desired} = \left(E_{n1}a_1^2 + E_{n2}a_2^2\right)\left(1 + \eta_1\frac{\tilde{T}_e}{2}\right)s_2(l) \tag{3.8}$$

where η_1 is the slope deduced from the linear approximation of the main lobe.

Due to a mutual cancellation as shown in (3.3), the components $ISI'(s_1, lT_b +$

Table 3.1: Coefficients of piecewise linear approximation

k	$l-3$	$l-2$	$l-1$	$l+1$	$l+2$	$l+3$
m_k^+	0	m_4	m_2	$-m_1$	$-m_3$	$-m_5$
m_k^-	$-m_5$	$-m_3$	$-m_1$	m_2	m_4	0

$\tilde{T}_e/2)$ and $ISI'(s_2, lT_b + \tilde{T}_e/2)$ will be zero no matter what estimated synchronization error $\tilde{T}_e$ is. Considering the decoding of signal s_1 after combination, the interference components, after using the linear approximation shown in Table 3.1, are simplified as:

$$\begin{aligned} ISI\left(s_1, lT_b + \tfrac{\tilde{T}_e}{2}\right) &= E_{n2} \sum_{\substack{k=l-3 \\ k\neq l}}^{l+3} s_1(k)(a_1^2 m_k^+ + a_2^2 m_k^-)\tfrac{\tilde{T}_e}{2} \\ ISI''\left(s_2, lT_b + \tfrac{\tilde{T}_e}{2}\right) &= \sqrt{E_{n1}E_{n2}} h_1^* h_2 \sum_{\substack{k=l-3 \\ k\neq l}}^{l+3} s_2(k)(m_k^- - m_k^+)\tfrac{\tilde{T}_e}{2} \end{aligned} \tag{3.9}$$

As a result, for a specific sequence of transmit symbols, the instantaneous signal to noise ratio (SNR) in the presence of ISI due to the side lobes can be expressed as:

$$SNR(a_1, a_2, \theta, state(l)) = \frac{(d+z)^2}{N_0} \tag{3.10}$$

$$\begin{aligned} \text{where } d &= (E_{n1}a_1^2 + E_{n2}a_2^2)(1 + \eta_1 \frac{\tilde{T}_e}{2}) \\ z &= E_{n2} \sum_{\substack{k=l-3 \\ k\neq l}}^{l+3} s_1(k)(a_1^2 m_k^+ + a_2^2 m_k^-)\frac{\tilde{T}_e}{2} \\ &\quad + \sqrt{E_{n1}E_{n2}} a_1 a_2 \cos\theta \sum_{\substack{k=l-3 \\ k\neq l}}^{l+3} s_2(k)(m_k^- - m_k^+)\frac{\tilde{T}_e}{2} \end{aligned}$$

Here N_0 is the noise power spectral density and θ denotes the difference of the phase between the two channels, $state(l)$ refers to the ergodic state of the ISI.

Thus, in order to evaluate the average BER in presence of fading, we will use

the alternative Gaussian Q-function presented in [52]. As the inter-cluster channel suffers from flat Rayleigh fading during each packet transmission, the parameters a_1, a_2 and θ are static within a packet interval. Considering the interferences from the side lobes of the neighbouring symbols and the overlying of the two path signals, the SNR has 2^{12} ergodic states. The receiving BER can be averaged over the ergodic states:

$$P_{e\_static} = \frac{1}{2^{12}} \frac{1}{\pi} \sum_{s_1(l),s_2(l)}^{2^{12}} \int_0^{\frac{\pi}{2}} \exp\left(\frac{-SNR(a_1, a_2, \theta, state(l))}{\sin^2 \phi}\right) d\phi \tag{3.11}$$

When averaging P_{e_static} with Rayleigh distribution $f(a_1)$, $f(a_2)$ and equal distribution of θ, the BER of this MISO system will be:

$$P_e = \frac{1}{2\pi} \int_0^{2\pi} \int_0^{+\infty} \int_0^{+\infty} P_{e\_static} \cdot f(a_1) \cdot f(a_2) da_1 da_2 d\theta \tag{3.12}$$

Simulations of the MISO system using Alamouti code in the presence of synchronization errors are made to verify the analytical results. In the simulations, a raised cosine pulse with roll-off factor of 0.22 is used to shape the signal. The system uses an uncoded binary phase shift keying (BPSK) modulation. We consider independent Rayleigh fading effect on each frame of 100 symbols. The channel estimation is assumed to be perfectly performed. In order to obtain reliable results, at least 10^4 frames have been sent for obtaining a BER of 10^{-3}.

In Figure 3.3, analytical and simulated results of the distributed cooperative MISO scheme using Alamouti code are presented. The synchronization error of $T_e = 0.25T_b$, $0.5T_b$ and $0.6T_b$ are considered. The results show that when the synchronization error is small, for example $T_e = 0.25T_b$, the degradation of BER performance in the cooperative system is negligible. However, when the synchronization error increases to $0.5T_b$, the loss is more than 3dB for the receiver with a required BER of 10^{-2} in comparison with the perfect Alamouti scheme. Moreover, the performance degrades significantly for synchronization error of $0.6T_b$. In this severe desynchronization situation, the MISO system performs even worse than the SISO system. Although different synchronization errors present different BER performances, the acceptable synchronization error for the cooperative scheme is more specific to the design of wireless sensor networks. It depends on many factors like energy efficiency, communication latency and network throughput etc.

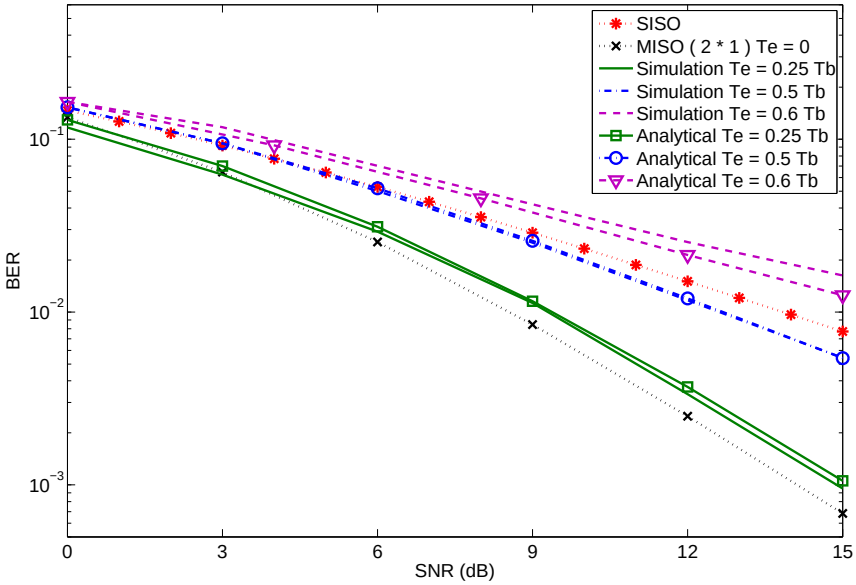

Figure 3.3: Effect of synchronization error in the distributed MISO(2*1) system

And there is a trade-off between the synchronization precision and synchronization complexity. In our works, we assume the acceptable synchronization error as $T_e = 0.25T_b$. The results shown in Figure 3.3 make this assumption reasonable.

3.4 Strategy of Time Synchronization

We consider that the synchronization strategy is implemented in physical layer for distributed cooperative communication. Initially, cooperative transmit nodes can be synchronized by a trigger message. At the cooperative receive node, synchronization error estimation will be performed before the cooperative decoding. We propose a maximum likelihood estimation method to decide whether the synchronization error is in an acceptable range. We show that it obtains better performance than the matched filter method. We suppose the estimated synchronization error can be fed back to cooperative transmit nodes. Then, using trigger sequence from the trigger node and feedbacks from the cooperative receive node, the synchronization error between cooperative transmit nodes can be limited and the distributed cooperative communication is expected to be practical.

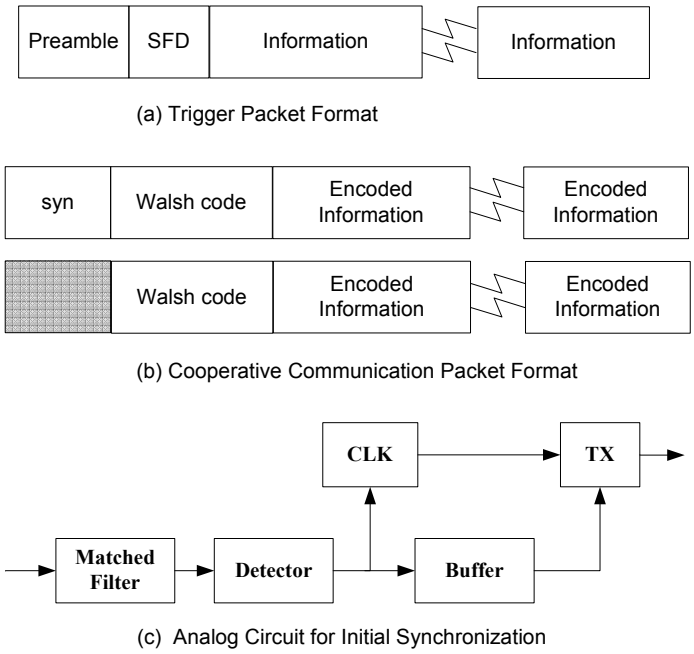

Figure 3.4: Packet format and analog circuit

3.4.1 Time Synchronization and Error Estimation

As is shown in the previous section, a small range of synchronization error (such as $T_e = 0.25T_b$) provides a negligible degradation of the BER performance. So the aim of synchronization scheme is to confine the synchronization error into such a range. Our proposed synchronization scheme is made up of two phases. The initial synchronization phase is defined as follows. The trigger node *TGN1* sends the trigger packet with the format shown in Figure 3.4(a). On receiving this packet, timing acquisition is performed by tracking the preamble sequence on each cooperative transmit node (*CTN1* and *CTN2*). Then, the arrival time of the packet is determined.

Due to different propagation delays and hardware inconsistencies, the arrival times of the packet on the two nodes are different. We assume that, during intra-cluster communication, the received signals are only affected by AWGN. At each cooperative transmit node, the received signal of the trigger packet can be expressed as:

$$x_i(t) = \sqrt{E_{tr}} \sum_{k=-L_t}^{L_0+L_t-1} s_{tr}(k) p(t - kT_b - \sigma_i T_b) + n_{tr}(t) \tag{3.13}$$

where $s_{tr}(k)$ is the symbol in trigger packet; $L_0$is the observation interval. σ_i is the unknown delay normalized to the symbol duration T_b. $n_{tr}(t)$ is modelled as AWGN. This received signal is oversampled at the two nodes by a ratio of Q. And it can be represented as:

$$\begin{aligned} x_i\left[l_i Q + m_i\right] = \sqrt{E_{tr}} \sum_{k=-L_t}^{L_0+L_t-1} & s_{tr}(k) p((l_i Q + m_i) T_b/Q - kT_b - \sigma_i T_b) \\ & + n_{tr}\left[(l_i Q + m_i) T_b/Q\right] \qquad , m_i = 0, 1, ...Q-1 \end{aligned} \tag{3.14}$$

where l_i and m_i are the discrete symbol index and discrete sampling index at the ith node. We assume the sampling instant m_{i_opt}, which is the closest to the optimal instant, is chosen after timing acquisition. Then, the arrival time detection is similar to the start of frame detection (SFD) in IEEE 15.4 standard [5] using a Barker code. However, a little change should be made to the analog circuit in order to achieve the packet arrival time detection. As shown in Figure 3.4(c), the process is done by calculating the cross-correlation between the received signals and the known Barker sequence using the matched filter. Defining the output of cross-correlation as $\Psi_i \triangleq s_{SFD}^H \cdot x_i$, it follows that:

$$\Psi_i\left[\upsilon_i\right] = \frac{1}{N} \sum_{l=0}^{N-1} s_{SFD}\left[l\right] x_i\left[lQ + m_{i\_opt} + \upsilon_i\right] \tag{3.15}$$

where N is the "window size" of the cross-correlation, υ_i is the index of the cross-correlation, s_{SFD} is the symbol sequence of Barker code. The cross-correlation yields to a peak whenever there is an exact alignment between those two sequences. Therefore, the arrival time of the packet can be determined by $\hat{\upsilon}_i$ which is selected as:

$$\hat{\upsilon}_i = \arg\max_{\upsilon_i} \Psi_i\left[\upsilon_i\right] \tag{3.16}$$

As shown in Figure 3.4(c), the clock of the node is synchronized to the arrival

time of the packet. In this initial phase, the synchronization error comes from two parts. The first part is due to the difference of propagation delay. As the trigger node and the two cooperative transmit nodes are in the same cluster, the difference of the distance between them is very small. So the difference of propagation delay is negligible. For example, differences of 30 meters will only introduce a delay of $0.1us$, while the BPSK signal with a bit rate of $250kbps$ (the highest bit rate in IEEE 15.4 standard) has a symbol interval of $4us$. On the other hand, the second part comes from the arrival time estimation error which is comprised of the timing acquisition error and the cross-correlation detection error. The timing acquisition error is assumed to follow a uniform distribution in the range $[-1/2Q, 1/2Q]$ and its mean square error is lower bounded by $1/(12Q^2)$. The mean square error of cross-correlation detection interrupted by AWGN noise is shown in Figure 3.5. It is negligible for most SNR region. As we can see, this initial synchronization phase is made at the physical layer. Its precision can be supposed to be in the level of the symbol time interval.

After this initial synchronization phase, the information sequence is transmitted cooperatively under the control of the adjusted clock. As mentioned before, the initial synchronization phase could not be perfect. So in the second phase of our synchronization scheme, we estimate the synchronization error at the receiver *CRN1* before Alamouti decoding. The estimation granularity is chosen according to the results obtained in the previous section. As a synchronization error of $T_e = 0.25T_b$ introduces negligible effect to the BER performance, we accept this small error for the Alamouti decoding, whereas the packets received with larger synchronization error will be dropped off. The estimation of this synchronization error before the Alamouti decoding can be done by the following methods.

Matched filter Method

Similar to the initial synchronization phase, the synchronization error can be detected by the peaks of the cross-correlation output. However, as the two cooperative transmit nodes are assumed to transmit the packets at the same time, the synchronization sequence can be arranged in the form of orthogonal time slots between the nodes or just arranged in the same time slot. Considering the characteristic of wireless sensor networks, energy efficiency is an important factor. Transmission of a long training sequence may be a waste of the restricted energy consumption. Therefore, we only consider the overlap of synchronization training

sequence in this paper. In the cooperative phase of inter-cluster communication, signals suffering from the Rayleigh fading effect will be received at the destination node as:

$$y(t) = \sum_{i=1}^{2} \sum_{k=-L_t}^{L_0+L_t-1} \sqrt{E_{ni}} s_i(k) h_i(t) p(t - kT_b - \tau_i T_b) + n(t) \tag{3.17}$$

where E_{ni} and $h_i(t)$ refer to the receive energy per symbol and the channel's fading effect as defined before. $s_i(k)$ corresponds only to the synchronization training sequence of Walsh code. $n(t)$ is AWGN. Here, τ_i represents the normalized synchronization error to the symbol interval (so $T_e = \tau_i T_b$). We notice that, due to the synchronization error $\tau_i T_b$, the misalignment of two signals will yield a cross-correlation with more interference. The output of cross-correlator is shown as:

$$\Psi_i \triangleq \mathbf{s}_{walsh\_i}^H \cdot \mathbf{y} \tag{3.18}$$

where $\mathbf{s}_{walsh\_i}$ is the Walsh code used at different nodes. Similar to the initial synchronization phase, the cross-correlation is calculated using the oversampled signal. So using the matched filter method, the precision of the synchronization estimation can be chosen by using different sampling factor Q.

Maximum Likelihood Method

The maximum likelihood estimation has been used for the acquisition of sampling time [53, 54]. In our work, different from the timing acquisition, we use maximum likelihood method to estimate the synchronization error range. As Alamouti code can be decoded by using one sampling time per symbol, we assume the sampling time after timing acquisition is synchronized to one cooperative transmit node. It can be done by adding a *syn* sequence to the packet transmitted by the reference node as shown in Figure 3.4(b). Timing acquisition error can be tracked as described in [55]. But it is out of the range of this work. We also assume that after the initial synchronization phase initiated by the trigger node, the normalized synchronization error τ_i can be limited to the range of [0, 1]. Denoting only the synchronization sequence transmitted by the ith cooperative transmit node as $s_i(k)$, the received signal $y(t)$ can be rewritten as:

$$y(t) = \begin{bmatrix} A_{\tau 1} & A_{\tau 2} \end{bmatrix} \begin{bmatrix} \sqrt{E_{n1}} h_1 s_1 \\ \sqrt{E_{n2}} h_2 s_2 \end{bmatrix} + n(t) \tag{3.19}$$

$$\begin{aligned} \text{where } A_{\tau_i} &= [a_{-L_t}(\tau_i), ..., a_0(\tau_i), ...a_{L_0+L_t-1}(\tau_i)] \\ a_k(\tau_i) &= [p(t - kT_b - \tau_i T_b), p(t - kT_b + T_b - \tau_i T_b), \\ &\quad ..., p(t - kT_b + (L_0 - 1)T_b - \tau_i T_b)]^T \\ s_i &= [s_i(-L_t), ..., s_i(0), ..., s_i(L_0 + L_t - 1)]^T \end{aligned}$$

We use the maximum likelihood estimation to decide whether the synchronization error is in the acceptable range. We assume the normalized synchronization error τ_i in equation (3.19) to be a fraction $(1/M)$ of a symbol time, where M is a predefined factor of the synchronization estimation granularity. It depends on the precision range of the synchronization error we want to estimate. So the likelihood function of the synchronization error and the channel is:

$$\begin{aligned} &ML(y(kT_b/M), n_1/M, n_2/M, \sqrt{E_{n1}} h_1, \sqrt{E_{n2}} h_2) \\ &= (\pi \sigma_w^2)^{-L_0} e^{-\frac{\left\| y(kT_b/M) - \sqrt{E_{n1}} h_1 A_{n_1/M} s_1 - \sqrt{E_{n2}} h_2 A_{n_2/M} s_2 \right\|^2}{\sigma_w^2}} \end{aligned} \tag{3.20}$$

where σ_w^2 is the variance of AWGN $n(t)$. Thus, maximizing the above function is equivalent to minimizing the following function:

$$\begin{aligned} &J(y(kT_b/M), n_1/M, n_2/M, \sqrt{E_{n1}} h_1, \sqrt{E_{n2}} h_2) \\ &= \left\| y(kT_b/M) - \sqrt{E_{n1}} h_1 A_{n_1/M} s_1 - \sqrt{E_{n2}} h_2 A_{n_2/M} s_2 \right\|^2 \end{aligned} \tag{3.21}$$

Considering the partial derivative of equation (3.21), then the ML estimation of the channel coefficient is:

$$\begin{bmatrix} \sqrt{E_{n1}} h_1 \\ \sqrt{E_{n2}} h_2 \end{bmatrix} = \begin{bmatrix} s_1^H A_{n_1/M}^H A_{n_1/M} s_1 & s_1^H A_{n_1/M}^H A_{n_2/M} s_2 \\ s_2^H A_{n_2/M}^H A_{n_1/M} s_1 & s_2^H A_{n_2/M}^H A_{n_2/M} s_2 \end{bmatrix}^{-1} \begin{bmatrix} s_1^H A_{n_1/M}^H y(kT_b/M) \\ s_2^H A_{n_2/M}^H y(kT_b/M) \end{bmatrix} \tag{3.22}$$

After substituting (3.22) into (3.21)

$$
\begin{aligned}
& J(y(kT_b/M), n_1/M, n_2/M, \sqrt{E_{n1}}h_1, \sqrt{E_{n2}}h_2) \\
&= \left\| \left(\mathrm{I} - \left[\begin{array}{cc} A_{n_1/M}s_1 & A_{n_2/M}s_2 \end{array} \right] \cdot R^{-1} \cdot \left[\begin{array}{c} s_1^H A_{n_1/M}^H \\ s_2^H A_{n_2/M}^H \end{array} \right] \right) y(kT_b/M) \right\|^2 \qquad (3.23) \\
&= \left\| \Lambda(n_1/M, n_2/M) y(kT_b/M) \right\|^2
\end{aligned}
$$

$$
\text{where } R = \left[\begin{array}{cc} s_1^H A_{n_1/M}^H A_{n_1/M} s_1 & s_1^H A_{n_1/M}^H A_{n_2/M} s_2 \\ s_2^H A_{n_2/M}^H A_{n_1/M} s_1 & s_2^H A_{n_2/M}^H A_{n_2/M} s_2 \end{array} \right]
$$

Then the decision matrix with parameters n_1/M and n_2/M is:

$$
\Lambda(n_1/M, n_2/M) = \mathrm{I} - \left[\begin{array}{cc} A_{n_1/M}s_1 & A_{n_2/M}s_2 \end{array} \right] \cdot R^{-1} \cdot \left[\begin{array}{c} s_1^H A_{n_1/M}^H \\ s_2^H A_{n_2/M}^H \end{array} \right] \qquad (3.24)
$$

where n_1 and n_2 are integers. The dimension of this matrix depends on the length of the two synchronization sequences (L_0). It can be decided after the synchronization sequences have been chosen. So the decision matrix can be pre-calculated before the synchronization estimation process, or placed in the node memory for a period of time when the same synchronization sequences are used. The space used to store decision matrix depends on the required precision of the synchronization error estimation. It is determined by the factor M. For example, to estimate the synchronization error with a precision of $0.25T_b$, M is set to 4. Then the synchronization error can be estimated according to:

$$
\hat{n} = \arg \min_{n_1, n_2} \left\| \Lambda(n_1/M, n_2/M) y(kT_b/M) \right\|^2 \qquad (3.25)
$$

As we have mentioned, the acquisition of the sampling time can be done by a short training sequence. We need to determine the relative synchronization error between the two cooperative transmit nodes. So, assuming the *CTN1* as the

reference ($n_1 = 0$), only the parameter n_2 must be estimated. For that reason, the sensor nodes need only to store the decision matrix $\Lambda(0, n_2/M)$. Then the estimated synchronization error is $(n_2/M)T_b$. This estimation is only an approximation of the synchronization error. However, as a small range of synchronization error makes little degradation of the reception BER performance, this approximation makes sense for most communication quality requirements.

3.4.2 Performance Evaluation

In this subsection, the performance of the proposed synchronization scheme is demonstrated. Sensor nodes are supposed to be organized in cluster-based topology. For the cooperative communication between two clusters, the trigger node (*TGN1*) and two cooperative transmit nodes (*CTN1* and *CTN2*) are assumed to be located in the same cluster, while the cooperative receive node (*CRN1*) is in another cluster. As we have mentioned, the propagation delay introduces little synchronization error to the initial synchronization phase. For the arrival time estimation, the performances of the cross-correlation detection using a matched filter have been shown in Figures 3.5 and Figure 3.6. In this initial synchronization phase, packets are transmitted through AWGN channel without fading. As shown in Figure 3.5, the MSE of the detection is very low for most SNR region even using the synchronization sequence of 8 symbols. The arrival time can be accurately estimated in most situations. The rate of accurate estimation approaches to 1 with the SNR larger than 6 dB as shown in Figure 3.6. Therefore, the initial synchronization error mainly comes from the timing acquisition error which is assumed to follow a uniform distribution. As a result, the initial synchronization phase could be expected to have a synchronization error smaller than one symbol interval.

We recall that the synchronization error of $0.25T_b$ is assumed to be acceptable for the cooperative scheme. So in all the simulations, the purpose of the synchronization scheme is to restrict the synchronization error to this interval. Then the granularity factor for second phase synchronization error estimation is set to be 4. In order to investigate whether our proposed estimation method is feasible in the cooperative scheme, we define the accurate alarm and the false alarm for the estimation. Assuming a synchronization error of T_e between two cooperative transmit nodes exists, and considering the synchronization error estimation in the cooperative reception node, we consider the estimation output value lower than or equal

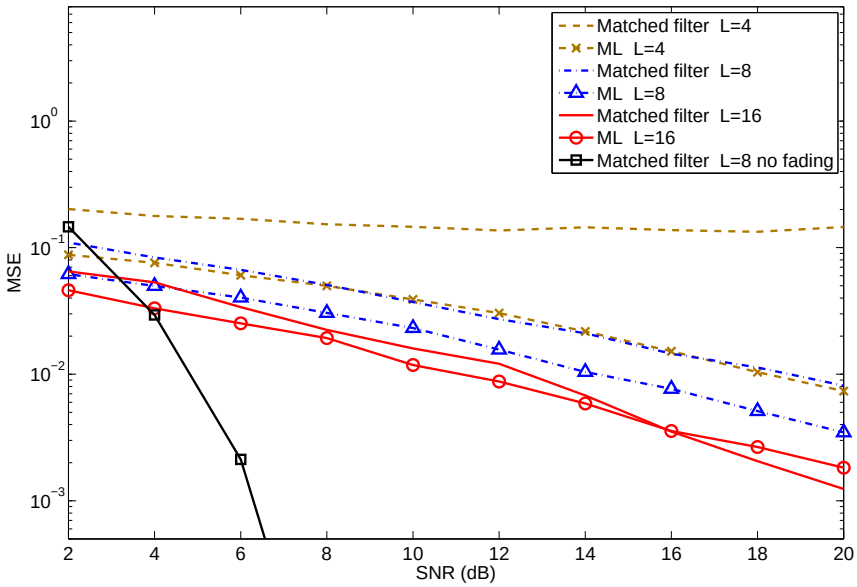

Figure 3.5: MSE performance in the existence of a synchronization error equals to $0.25T_b$

to T_e as an accurate alarm. Otherwise, it is a false alarm. As we will see later, an accurate estimation of the synchronization error will be a useful indication for Alamouti decoding. Based on the estimation, the Alamouti decoder will decide whether to drop the packet or not. Also, the estimated synchronization error could be fed back to the two cooperative transmit nodes. So, false alarm may lead to more dropped packets or larger synchronization error between the two cooperative transmit nodes.

As shown in Figure 3.5, in the existence of a synchronization error equals to $0.25T_b$, the estimation MSE by using the ML method at the cooperative reception node is always better. In the case of using synchronization sequence of 16 symbols, the matched filter method is comparable to the ML method when considering the MSE. On the other hand, the rate of accurate alarm using ML method is much higher than using matched filter method. Even with a synchronization sequence of 4 symbols, the rate of accurate alarm using the ML method is higher than the matched filter method with synchronization sequence of 16 symbols in the high SNR region.

Due to the fact that large synchronization error will degrade the BER per-

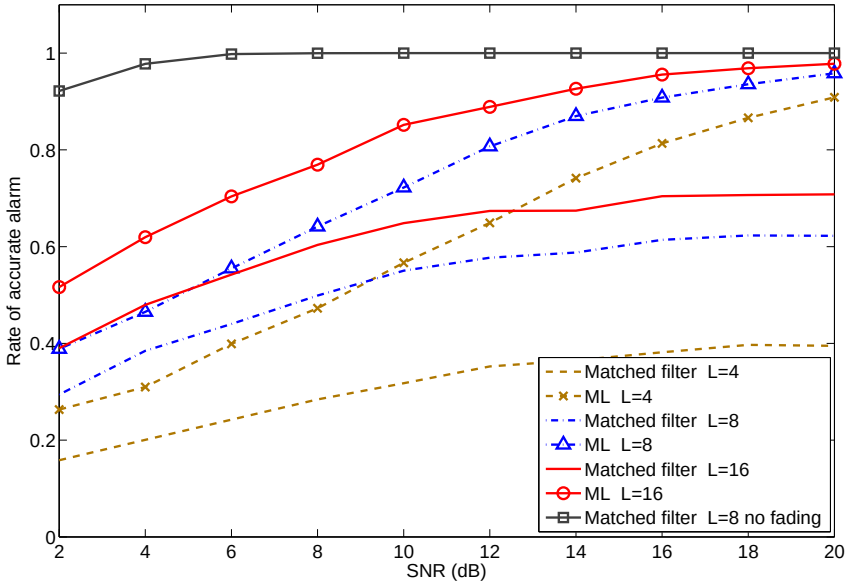

Figure 3.6: Rate of accurate alarm in the existence of a synchronization error equals to $0.25T_b$

formance of Alamouti decoding, we consider two strategies after synchronization error estimation. One is that packets received with an estimated synchronization error larger than $0.25T_b$ will be dropped off. Meanwhile, the estimated synchronization error can be fed back to two cooperative transmit nodes. The second one is that we don't drop the packet, but the estimated synchronization error will be fed back to two cooperative transmit nodes. The first strategy is more suitable for wireless sensor networks which require more stringent accuracy but looser latency constraint, while the adaptability of the second strategy is on the contrary. Since time interval of $0.25T_b$ is used as a threshold of the precision requirement, the estimation granularity factor of 4 will be used. Then the feedback payload of 2 bits will be sufficient. For this kind of short feedback sequence, we assume a rather lower transmit bit rate is utilized as compared to that of the cooperative transmission. The reliability of the feedback link is reasonable to be good enough. Therefore, we assume the erroneous feedback link is negligible .

Considering the implementation of the two strategies, we assume that two cooperative transmit nodes have the initial synchronization error of $0.5T_b$. The performances of the two strategies are shown in Figure 3.7 and Figure 3.8. As

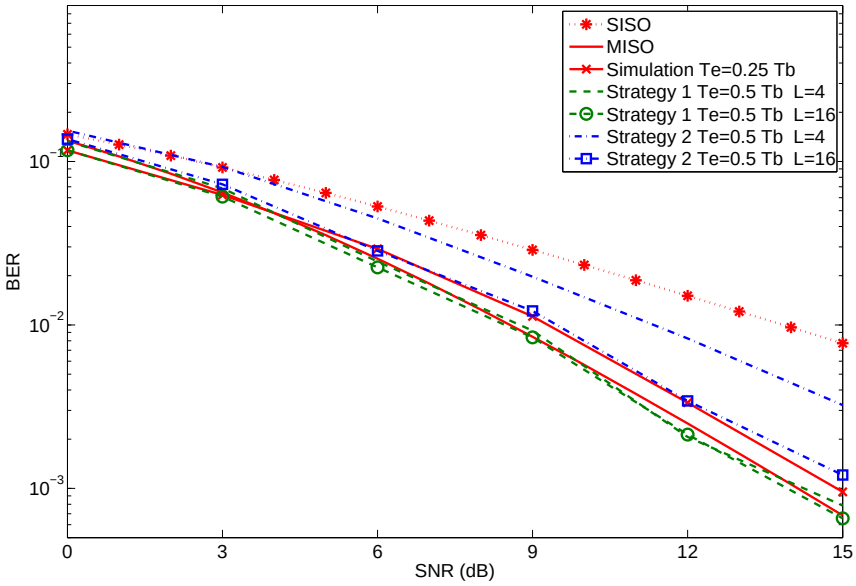

Figure 3.7: BER performance for the two strategies using ML method for synchronization estimation

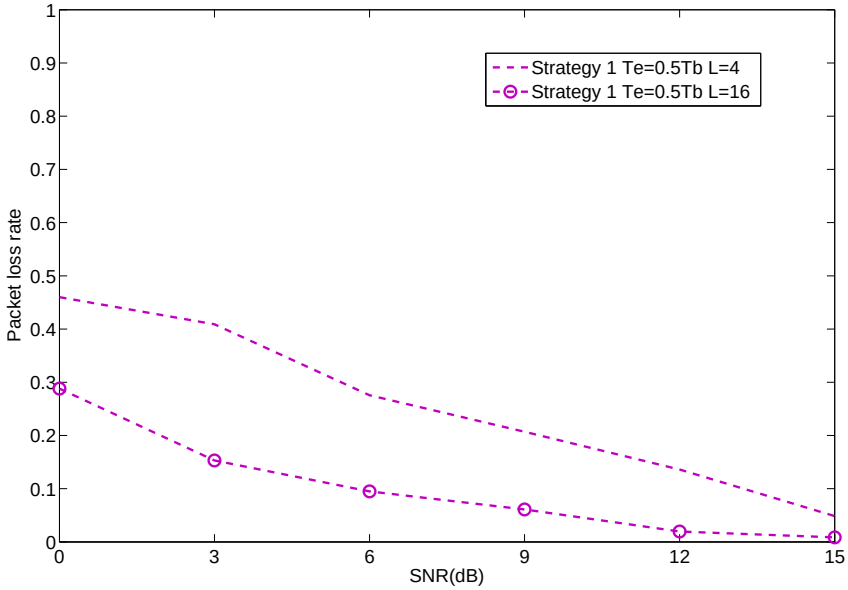

Figure 3.8: Packet loss rate for the first strategy using ML method for synchronization estimation

shown in Figure 3.7, using the first strategy, the BER performance achieves theoretical value with no synchronization error. It doesn't depend on the length of the synchronization sequence. The gain of the BER performance is obtained at the cost of the retransmission of these packets. So it introduces more traffic latency. Figure 3.8 shows the relation between the packet loss rate and the synchronization sequence length. We can see that the longer the synchronization sequence is, the less the packet loss rate will be. This is due to the fact that longer synchronization sequence makes the estimation of the synchronization error more accurate. So the feedback of the synchronization error is more accurate. The synchronization process will be quicker to be stable. Meanwhile, more accurate estimation makes the false alarm of the synchronization error to be less. It reduces the unnecessary drop of the packet.

Considering the second strategy, the threshold of the best BER performance depends on the granularity of the estimation as shown in Figure 3.7. With the initial synchronization error of $0.5T_b$ and using granularity factor of 4, the BER performance, for long synchronization sequence of 16 symbols, approaches to the result of cooperative transmission with constant synchronization error of $0.25T_b$. While for the ML estimation using 4 symbols, the BER performance is worse. So, the applications that need higher BER performance can use the first strategy or the second strategy with larger granularity factor. Therefore, considering the energy consumption of the communication, there is a trade-off between more transmission energy for retransmission and more processing energy for synchronization estimation.

3.5 Two Other Candidate Solutions

In the previous sections, we discussed two problems that will be met on the practical implementation of Alamouti coded cooperative communication. One is how precise the two distributed nodes should be synchronized, the other is how we can achieve the required synchronization. Although some asynchronous cooperative schemes have been proposed in [56, 57], the complexity of the decoding process requires a stronger signal processing capability at the sensor nodes. It makes more demands on the circuits, and its energy efficiency should also be considered. In wireless sensor networks, the sensor nodes are typically constrained by hardware resource and processing capability. So the cooperative communication scheme with

	time slot 1	time slot 2
CTN 1	$s_1(0) \quad \cdots \quad s_1(N-1)$	$-s_2^*(0) \quad \cdots \quad -s_2^*(N-1)$
CTN 2	$s_2(0) \quad \cdots \quad s_2(N-1)$	$s_1^*(0) \quad \cdots \quad s_1^*(N-1)$

(a) Traditional Alamouti coding scheme

	time slot 1	time slot 2
CTN 1	$s_1(0) \quad \cdots \quad s_1(N-1)$	$-s_2^*(N-1) \quad \cdots \quad -s_2^*(0)$
CTN 2	$s_2(0) \quad \cdots \quad s_2(N-1)$	$s_1^*(N-1) \quad \cdots \quad s_1^*(0)$

(b) Time-reverse Alamouti coding scheme

Figure 3.9: Cooperative scheme with traditional Alamouti coding and time-reverse Alamouti coding

simple linear decoding process is more desirable. In this section, we will discuss two categories of distributed cooperative communication schemes which can loose or get rid of the requirement on time synchronization but have a relative low complexity on the coding and decoding process.

3.5.1 Time-Reverse Space-Time Coding

Typically, distributed cooperative communication utilizing Alamouti code requires the two cooperative transmit nodes (*CTN1* and *CTN2*) to be synchronized as we have discussed in the previous sections. The work in [58] has proposed a time-reverse Alamouti code which could tolerate the asynchronous transmission from the two cooperative transmit nodes. The traditional Alamouti coding scheme and the time-reverse Alamouti coding scheme are shown in Figure 3.9. In the first time slot, the coded blocks transmitted by the two cooperative nodes are the same in these two schemes. In the second time slot, the time reversed versions of the Alamouti coded blocks are transmitted in the time-reverse Alamouti coding scheme. With the assumption of independent Rayleigh fading channels between

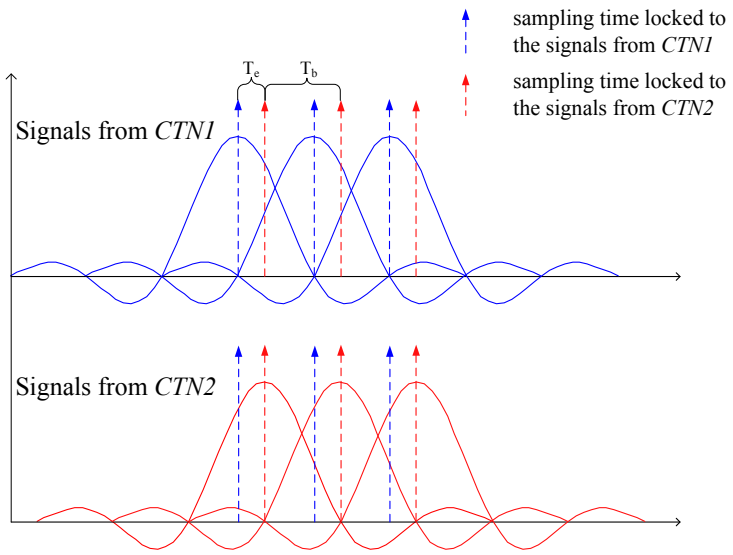

Figure 3.10: Illustration of the sampling time at the receive node CRN1

the transmit and receive node pairs, the received signals in the first time slot is:

$$r_1(t) = \sqrt{E_{n1}} h_1(t) s_1(t) + \sqrt{E_{n2}} h_2(t) s_2(t - T_e) + n_1(t) \tag{3.26}$$

Since we take the clock in *CTN1* as the reference clock, so T_e refers to the synchronization error between *CTN1* and *CTN2*. We note that, the transmitted signals $s_1(t)$ and $s_2(t)$ in equation (3.26) already capture the accumulation of interferences from the the side lobes. The summation of the side lobes' interferences as shown in equation (3.1) is not necessary to be represented. In the second time slot, the received signals is:

$$r_2(t) = -\sqrt{E_{n1}} h_1(t) s_2^*((N-1)T_b - t) + \sqrt{E_{n2}} h_2(t) s_1^*((N-1)T_b - t + T_e) + n_2(t) \tag{3.27}$$

At the receive node *CRN1*, we suppose that the synchronization error T_e could be estimated using our proposed maximum likelihood method in section 3.4. So that the sampling time could be determined according to the synchronization error T_e as shown in Figure 3.10. It is oversampled as twice as typical Alamouti

decoder does. The two sampling sequences are locked to the arrival signals from *CTN1* and *CTN2* respectively. Therefore, for time-reverse Alamouti decoding, the oversampling process to eliminate the effect of synchronization error could be performed as: firstly, sampling the received signals for the decoding of $s_1(t)$ as:

$$r_{s1}(nT_b) = \left[\begin{array}{cc} r_1\left(nT_b\right) & r_2^*\left((N-1)T_b - nT_b + T_e\right) \end{array} \right] \tag{3.28}$$

and secondly sampling the received signals for the decoding of $s_2(t)$ as:

$$r_{s2}(nT_b) = \left[\begin{array}{cc} r_1\left(nT_b + T_e\right) & r_2^*\left((N-1)T_b - nT_b\right) \end{array} \right] \tag{3.29}$$

Then, the transmitted signals can be estimated as:

$$\tilde{s}_1(nT_b) = \frac{1}{E_{n1}+E_{n2}} \left[\begin{array}{cc} \sqrt{E_{n1}}h_1^*(nT_b) & \sqrt{E_{n2}}h_2(nT_b) \end{array} \right] \left[r_{s1}\left(nT_b\right)\right]^T \tag{3.30}$$

$$\tilde{s}_2(nT_b) = \frac{1}{E_{n1}+E_{n2}} \left[\begin{array}{cc} \sqrt{E_{n2}}h_2^*(nT_b) & -\sqrt{E_{n1}}h_1(nT_b) \end{array} \right] \left[r_{s2}\left(nT_b\right)\right]^T \tag{3.31}$$

Taking equations (3.26 - 3.29) into account, the estimated signals shown in equations (3.30) and (3.31) can be deduced as:

$$\begin{aligned} \tilde{s}_1(nT_b) &= \left(|h_1(nT_b)|^2 + |h_2(nT_b)|^2\right) s_1(nT_b) \\ &+ \tfrac{1}{E_{n1}+E_{n2}} \left(\sqrt{E_{n1}}h_1^*(nT_b)n_1(nT_b) + \sqrt{E_{n2}}h_2(nT_b)n_2^*((N-1)T_b - nT_b + T_e)\right) \end{aligned} \tag{3.32}$$

$$\begin{aligned} \tilde{s}_2(nT_b) &= \left(|h_1(nT_b)|^2 + |h_2(nT_b)|^2\right) s_2(nT_b) \\ &+ \tfrac{1}{E_{n1}+E_{n2}} \left(\sqrt{E_{n2}}h_2^*(nT_b)n_1(nT_b + T_e) - \sqrt{E_{n1}}h_1(nT_b)n_2^*((N-1)T_b - nT_b)\right) \end{aligned} \tag{3.33}$$

It is obvious that, by twice oversampling the asynchronous signals, the effect of

the synchronization error can be totally reduced. The diversity performance of time-reverse Alamouti coding scheme is the same as the typical Alamouti coding scheme. In order to further increase the efficiency of cooperative communication, the time-reverse Alamouti coding scheme can be co-designed with the strategy of time synchronization which is discussed in the previous section. So that, at the receiver side, once the synchronization error is within the acceptable range, typical Alamouti decoding process is performed and oversampling is not necessary. Otherwise, when the synchronization error is large, the time-reverse Alamouti decoding with oversampling of the received signals will be chosen. So the time-reverse Alamouti coding scheme could be a good candidate solution for the cooperative communication in the distributed wireless sensor networks.

However, we have to mention that the oversampling process make a few demands on the analog circuit designs. Meanwhile, as the length of the coded block increases, more memory resources are required to cache the sampling symbols. So the coded block could not be too long. Considering a transmitted packet consists of several coded blocks, the guard sequence between the coded blocks should be inserted to eliminate the inter block interference. The length of the guard sequence is necessary to be long enough to go through the time of synchronization error. On the other hand, the length of the coded block should be long to increase the efficiency of transmission. As a result, the length of the coded blocks and the guard sequence should be elaborately designed.

3.5.2 OFDM-Based Cooperative Scheme

OFDM is a popular modulation scheme for wide-band communication. It divides the original data into several parallel data streams. Each data stream is equivalent to a sub-carrier. Due to this parallel transmission, the OFDM symbol rate is reduced. A guard time interval is introduced for each OFDM symbol. It is chosen to be larger than the maximum expected delay spread of the channel, so that the multipath delayed components can not interfere with the next symbol. Furthermore, cyclic prefix of the OFDM symbol is inserted into the guard time interval to reduce the inter-carrier interference [59]. The primary advantage of OFDM over single-carrier scheme is its ability to cope with frequency-selective fading which is due to multipath delay.

In our works, we consider the flat Rayleigh fading channel where the maximum multipath delay of the single link signals is within the symbol time interval.

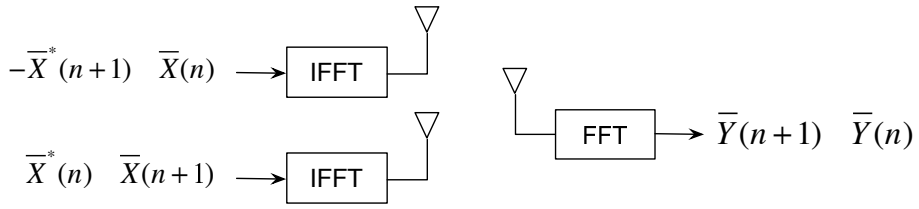

Figure 3.11: Block diagram of space-time OFDM-based cooperative scheme

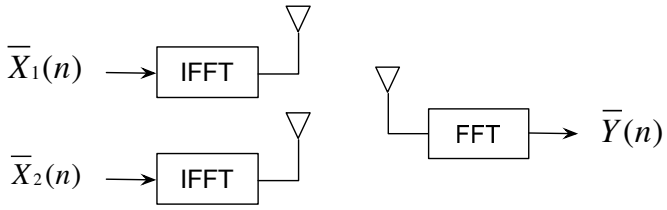

Figure 3.12: Block diagram of space-frequency OFDM-based cooperative scheme

However, when we consider virtual MISO cooperative communication, signals from the distributed nodes normally arrive at the receiver with unequal delays due to different propagation paths or the errors on time synchronization. If this unequal delays are within the symbol time interval, the coherent combination of the cooperative symbols will still have inter-symbol interference as shown in equation (3.5). As the cyclic prefix of the OFDM symbol can be used to loose the requirement on time synchronization, OFDM modulation could facilitate the implementation of cooperative communication in wireless sensor networks. Therefore, a combination of OFDM modulation and *virtual MISO cooperative scheme* could be another candidate to deal with this arrival time synchronization problem.

In [60] and [61], space-time coded OFDM scheme has been proposed for the channels with large delay spread. A variant, space-frequency coded OFDM scheme, has been proposed in [62] to offer the coding gain in frequency dimension. In fact, in those works, the schemes were proposed to explore diversity in selective fading channel. The multipath delays were only caused by the different propagation paths, because the two antenna were assumed to be collocated. In this dissertation, we consider the OFDM scheme as a way to cope with the arrival time synchronization problem for the distributed implementation of *virtual MISO cooperative scheme*. We refer to this as *OFDM-based cooperative scheme*. Figure 3.11 and Figure 3.12 show the diagrams of these cooperative schemes implemented on two distributed transmit nodes.

In space-time OFDM-based cooperative scheme shown in Figure 3.11, source information sequences are divided into vectors in the two transmit nodes. The scale of the vectors is according to the number of available sub-carriers. Each pair of the vectors are encoded by Alamouti code and arranged in series as the same as the Virtual MISO cooperative scheme. Two subsequent encoded vectors at the two transmit nodes can be shown as:

$$\begin{aligned}\overline{X}(n) &= \left[\begin{array}{cccc} X_0(n) & X_1(n) & \cdots & X_{N-2}(n) & X_{N-1}(n) \end{array}\right]^T \\ -\overline{X}^*(n+1) &= \left[\begin{array}{cccc} -X_0^*(n+1) & -X_1^*(n+1) & \cdots & -X_{N-2}^*(n+1) & -X_{N-1}^*(n+1) \end{array}\right]^T \end{aligned} \tag{3.34}$$

and

$$\begin{aligned}\overline{X}(n+1) &= \left[\begin{array}{cccc} X_0(n+1) & X_1(n+1) & \cdots & X_{N-2}(n+1) & X_{N-1}(n+1) \end{array}\right]^T \\ \overline{X}^*(n) &= \left[\begin{array}{cccc} X_0^*(n) & X_1^*(n) & \cdots & X_{N-2}^*(n) & X_{N-1}^*(n) \end{array}\right]^T \end{aligned} \tag{3.35}$$

In space-frequency OFDM-based cooperative scheme shown in Figure 3.12, the source information is divided into vectors and each vector is encoded to $\overline{X}_1$ and $\overline{X}_2$ as [62]:

$$\begin{aligned}\overline{X}_1(n) &= \left[\begin{array}{cccc} X_0(n) & -X_1^*(n) & \cdots & X_{N-2}(n) & -X_{N-1}^*(n) \end{array}\right]^T \\ \overline{X}_2(n) &= \left[\begin{array}{cccc} X_1(n) & X_0^*(n) & \cdots & X_{N-1}(n) & -X_{N-2}^*(n) \end{array}\right]^T \end{aligned} \tag{3.36}$$

In fact, each vector would append the pilot and the guard sequences. As we aim at discussing the effect of multi-nodes synchronization, we consider the vectors that are only loaded with data symbols in both of the OFDM-based cooperative schemes. Supposing N sub-carriers are allocated to the coded information, the modulator performs a N-point inverse fast Fourier transform (IFFT) to the $N \times 1$ symbol vectors after space time coded. The receive node performs N-point fast Fourier transform (FFT) to the combined receiving signals. We use small letters to represent time domain signals (after IFFT and before FFT) , and capital letters

to represent frequency domain signals (before IFFT or after FFT). Supposing the symbol vector $[D_0 \cdots D_{N-1}]$ as a representation of the coded vector in both of the OFDM-based cooperative schemes, the equivalent baseband OFDM samples, which produce pure OFDM signal, can be obtained as:

$$x[n] = \sum_{k=0}^{N-1} D_k e^{j2\pi k \frac{n}{N}} \tag{3.37}$$

After that, a cyclic prefix of L_{cp} samples is appended in front of the OFDM samples to avoid the effect of arrival time synchronization error. To simplify the signal representation, we will not consider the transmit windowing. Correspondingly, each complete OFDM symbol would consist of $L = N + L_{cp}$ samples. The transmit signal for each complete OFDM symbol can be expressed as:

$$x(t) = \sum_{n=0}^{L-1} x[(n - L_{cp}) \bmod N] \times p(t - nt_s) \tag{3.38}$$

where $p(t)$ is the pulse of the shaping filter with duration of t_s. In order to illustrate how the cyclic prefix can eliminate the effect of arrival time synchronization error, we take the space-frequency OFDM-based cooperative scheme as an example. Then, the received baseband signal with both timing errors and frequency offsets can be represented as:

$$r(t) = h_1 e^{j\theta_1(t)} x_1(t - \tau_1) + h_2 e^{j\theta_2(t)} x_2(t - \tau_2) + n(t) \tag{3.39}$$

where $x_1(t)$ and $x_2(t)$ are the complete OFDM symbols obtained from equations (3.37) and (3.38), $\theta_1(t)$ and $\theta_2(t)$ are the phase rotations caused by different frequency offsets, τ_1 and τ_2 are the different delays from the two nodes. We align the receive window at a delay of $\tau_1 + t_{cp}$, where t_{cp} is the interval of the cyclic prefix sequence. Then the signal with an interval of $0 \leq t \leq (N-1)t_s$ will be used for OFDM demodulation and can be expressed as:

$$\begin{aligned} r(t) = {} & h_1 e^{j\theta_1(t+\tau_1+t_{cp})} x_1(t + t_{cp}) + h_2 e^{j\theta_2(t+\tau_1+t_{cp})} x_2(t + \tau_1 - \tau_2 + t_{cp}) \\ & + n(t + \tau_1 + t_{cp}) \end{aligned} \tag{3.40}$$

We note that, in equation (3.40), the first term of $x_1(t + t_{cp})$ can be taken as the pure OFDM signal and the second term of $x_2(t + \tau_1 - \tau_2 + t_{cp})$ can be taken as the pure OFDM signal appended with a cyclic prefix of the interval $\tau_1 - \tau_2$. Therefore, after FFT modulation, the arrival time synchronization error will not alter the orthogonality of the space time code. In a word, from the viewpoint of time domain, the longer OFDM symbol duration along with the use of cyclic prefix provides robust scheme to time synchronization.

However, the phase rotation parts in equation (3.40) will introduce another factor that destroy the orthogonality property. The OFDM symbol from the distributed nodes become more sensitive to frequency offsets. Some works in [63] and [64] have proposed OFDM-based cooperative schemes that are robust to both time error and synchronization offsets, But they require either a pre-compensation for the channel [63] or strong capability on baseband signal processing [64]. Furthermore, the problem on peak-to-average power reduction will constrain the energy efficient implementation of OFDM-based technology to wireless sensor networks. So the OFDM-based cooperative communication for wireless sensor networks is still an open problem.

3.6 Summary

Signal arrival time synchronization is required for the virtual MISO cooperative communication in wireless sensor networks. In this chapter, a physical layer synchronization scheme has been proposed. Considering the effect of the synchronization error, the proposed scheme is adequate but introduces less complexity to the network design. A ML method has been proposed for the synchronization error estimation in cooperative reception. It shows better performance even with shorter synchronization sequence. The decision matrix can be pre-calculated and reused in the process of synchronization error estimation before Alamouti decoding. Considering two strategies after synchronization error estimation, better BER performance can be obtained even in the existence of an initial synchronization error between the two cooperative transmit nodes.

Our proposed time synchronization scheme provides better BER performance in the existence of initial synchronization error. According to the simulated results, it is supposed to be practically implemented in the sensor nodes before the

Alamouti decoding. Upon this assumption, power control schemes, which can further improve the energy efficiency, are proposed in the next chapter for cooperative communication in wireless sensor networks.

Chapter 4

Power Control in Cooperative Communication

4.1 Introduction

Two kinds of cooperative scheme, cooperative relaying scheme and virtual MIMO cooperative scheme, have been proposed for wireless sensor networks in recent works [19, 18, 25, 27, 1, 21]. In the cooperative relaying scheme, one or a set of sensor nodes between the source and destination nodes will be selected as the relays to cooperate on data transmission. Some efficient algorithms on node selection have been proposed in [25] and [65]. Based on the implementation at the relay nodes, cooperative relaying schemes can be classified into decode-and-forward (DF) scheme and amplify-and-forward (AF) scheme [19]. The work in [18] has shown that, for low spectrum efficiency regime, cooperative relaying schemes decrease the transmit power for the same reliability. It is suitable for the applications in wireless sensor networks where energy efficiency is important. By selecting multiple nodes to form a virtual antenna array, virtual MIMO cooperative scheme provides a comparable performance to multi-antenna systems [27]. The works in [1] and [21] have investigated the energy efficiency of cooperative communication utilizing virtual MIMO scheme. For long distance communication in Rayleigh fading channels, it is shown to be more energy efficient than the single-input single-output (SISO) scheme.

Power control among the nodes can further improve the performance of the cooperative communication schemes. For the cooperative relaying scheme, the

works in [66, 67, 68] and [69] considered the power allocation strategy aiming at minimizing outage probability at high signal-noise-ratio (SNR) region. In [66], subject to a total power constraint, the strategy of optimal power allocation between the source and relaying nodes was presented. In addition, the works in [67] also considered the situation of no direct link between source node and destination node. In [68] and [69], power allocation was considered on the cooperative relaying nodes. They resulted in an optimal set of relaying nodes [68] or an optimal region for the relaying nodes [69], and both with an equal power allocation at the relaying nodes. Other than minimizing outage probability, the works in [70] and [71] explored the transmit power allocation among the source and relay nodes to maximize the received SNR at the destination node. For the space-time block code MIMO system, power allocation was investigated in [72] and [73] to improve the receive BER performance. They required that the transmit antennas have partial or complete knowledge of channel state. In [74], an algorithmic solution is proposed for power allocation on the multi-antenna system. Instantaneous attenuations of the channels were supposed to be known at the transmit antennas. It results in a threshold, above which the corresponding antenna can be activated.

In this chapter, we consider a power allocation strategy aiming at minimizing the total transmit power with a constraint on the average BER performance. This criterion is straightforward for obtaining energy efficiency in cooperative communications. Furthermore, in the case of no direct link between the source and destination nodes, we propose two cooperative strategies to employ the AF cooperative relaying scheme and the virtual MISO cooperative scheme. They are more energy efficient and achieve fair allocation of the transmit power among the sensor nodes. On the view of cross layer design as shown in [75] and [76], these cooperative strategies applied in physical layer could be co-designed with medium access control and routing layers to provide reliable and efficient links in the networks. According to different topologies, different sets of cooperative nodes might be available. We propose a heuristic policy to select the optimal cooperative nodes and employ the cooperative strategies.

We note that BPSK modulation is assumed throughout our analysis. The rest of this chapter is organized as follows. In section 4.2, system models of the cooperative relaying scheme and the virtual MISO cooperative scheme will be introduced. In section 4.3, the optimal power allocation strategy will be investigated. In section 4.4, two proposed cooperative strategies will be analysed. In section 4.5, the

optimized performance will be discussed.

4.2 System Models

In this chapter, we consider two kinds of cooperative scheme: cooperative relaying scheme and virtual MISO cooperative scheme. We assume that the channels between the sensor nodes are independent Rayleigh fading channels and static during the transmission of each packet. In addition, communication channels among these nodes could suffer from propagation attenuation coming from the path loss effect.

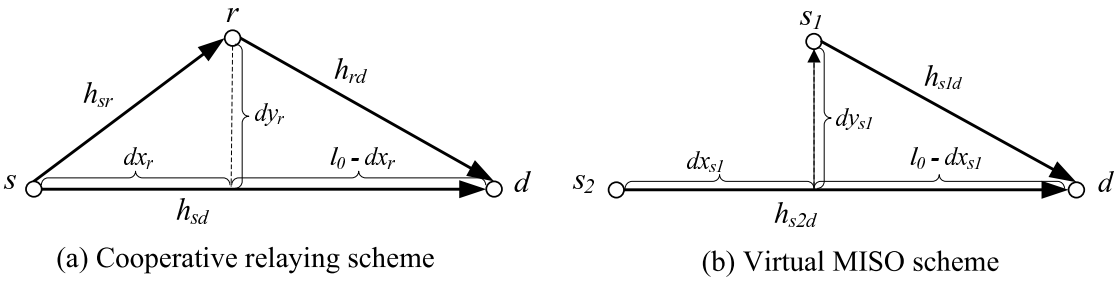

(a) Cooperative relaying scheme

(b) Virtual MISO scheme

Figure 4.1: Cooperative communication in wireless sensor networks

For the cooperative relaying scheme, we consider that the relay node applies the AF method. A cooperative relaying scheme consists of three nodes as shown in Figure 4.1(a). The relay node is selected among the nodes that are located between the source and destination nodes. The cooperative relaying scheme comprises two time slots. In the first time slot, the source node s transmits the information to the relay node r and the destination node d. In the second time slot, the relay node r amplify-and-forwards the received signal to the destination node d. Then the received signals at the relay node and the destination node in the first time slot are:

$$\begin{aligned} r_{sr} &= h_{sr}\sqrt{P_s}s_0 + n_1 \\ r_{sd} &= h_{sd}\sqrt{P_s}s_0 + n_2 \end{aligned} \tag{4.1}$$

where s_0 is the modulated symbol of the transmit sequences. h_{ij} captures the effect of Rayleigh fading and propagation attenuation from node i to node j, where $i \in \{s, r\}$ and $j \in \{r, d\}$. n_1 and n_2 are the additive white Gaussian noises (AWGN) with power spectral density of N_0 determined by $N_0 = k_B T_0$ for the

typical temperature value $T_0 = 27^oC \approx 300K$ and the Boltzmann's constant $k_B = 1.38 \times 10^{-23} W \cdot s/K$. The transmit power at the source node s is assumed to be P_s. So in the first time slot, the received SNR at the relay node and the destination node are:

$$\begin{aligned} \gamma_{sr} &= \frac{|h_{sr}|^2 P_s}{N_0 B} \\ \gamma_{sd} &= \frac{|h_{sd}|^2 P_s}{N_0 B} \end{aligned} \tag{4.2}$$

where B is the bandwidth of the baseband signal. We constrain the transmit power at the relay node to be P_r. Then the amplification factor imposed on the relay node is:

$$\alpha_r = \sqrt{\frac{P_r}{|h_{sr}|^2 P_s + N_0 B}} \tag{4.3}$$

It is determined by the power allocation strategy and also the instantaneous channel gain $|h_{sr}|^2$. In the second time slot, the destination node receives signal from the relay path as:

$$r_{rd} = \alpha_r h_{rd} r_{sr} + n_3 \tag{4.4}$$

where n_3 is the AWGN with power spectral density of N_0. We consider the maximum ratio combination (MRC) of the received signals r_{sd} and r_{rd} at the destination node. Then the received SNR after combination is:

$$\gamma_{AF} = \gamma_{sd} + \frac{\gamma_{sr}\gamma_{rd}}{1+\gamma_{sr}+\gamma_{rd}} \quad with \quad \gamma_{rd} = \frac{|h_{rd}|^2 P_r}{N_0 B} \tag{4.5}$$

We note that the selection of the relay node could be based on the distance range of the radio, the operational states (active or idle) and energy status of the node, etc. While differing from selective relaying where the relay selection is performed for each packet's transmission [25, 65], we assume that the selected relay node will function for a relative long time. It is a reasonable assumption in the clustered sensor network [76]. Since in most case, common nodes will be switched to idle state during the cluster-heads' communication. The selection of the relay node for each transmission will be inefficient. The configuration of cooperative

relaying scheme is better to be fixed for a relative long term in this case.

Another cooperative communication scheme, which we consider in this chapter, is the virtual MISO cooperative scheme. It can be achieved by selecting m cooperative nodes from a set of potential relaying nodes to constitute a virtual multi-antenna system. Data are encoded by a $m \times n$ space time coding matrix [26] and split into m streams with n symbols at each stream. They are simultaneously transmitted by the m cooperative nodes. Alamouti code [28] is well known as one kind of space time code. It can be used in distributed cooperative transmissions. Figure 4.1(b) shows the virtual MISO cooperative scheme utilizing Alamouti code. This cooperative scheme can be implemented by two cooperative transmit nodes as the source and one receiver node as the destination to form a virtual MISO system. In our works, we limit our analysis to the cooperative scheme utilizing Alamouti code for two reasons. Firstly, the energy consumption of the analog circuit is a prominent part of energy depletion. Hence, the participation of more nodes in the cooperative transmission may not be more energy efficient [77]. Secondly, this configuration reduces the complexity of coordination between the distributed nodes.

Considering Alamouti coding, each symbol will be encoded and then transmitted in two sub-timeslots from the two cooperative transmit nodes. The received signal r'_1 and r'_2 can be expressed as:

$$\begin{aligned} r'_1 &= h_{s_1 d}\sqrt{P_{T1}}s_1 + h_{s_2 d}\sqrt{P_{T2}}s_2 + n'_1 \\ r'_2 &= -h_{s_1 d}\sqrt{P_{T1}}s_2^* + h_{s_2 d}\sqrt{P_{T2}}s_1^* + n'_2 \end{aligned} \tag{4.6}$$

where s_1 and s_2 represent the modulated symbols of the transmit sequence, $h_{s_1 d}$ and $h_{s_2 d}$ capture the effect of Rayleigh fading and propagation attenuation between the transmit and receive nodes, * refers to the complex conjugate, n'_1 and n'_2 are the AWGN with power spectral density of N_0. Supposing the transmit power at the two cooperative transmit nodes to be P_{T1} and P_{T2}, the received SNR from the two paths are:

$$\begin{aligned} \gamma'_1 &= \frac{\left|h_{s_1 d}\right|^2 P_{T1}}{N_0 B} \\ \gamma'_2 &= \frac{\left|h_{s_2 d}\right|^2 P_{T2}}{N_0 B} \end{aligned} \tag{4.7}$$

At the Alamouti decoder, the input signals are the combined signals passed through the two paths. After Alamouti decoding, the SNR at the detector is $\gamma_1' + \gamma_2'$ [28]. Practically, we note that these signals may experience propagation delays from the two cooperative transmit nodes. Moreover, the clocks of the two nodes may not be perfectly synchronized. Misalignment of the signals from the two paths will introduce inter-symbol interference. In this chapter, we assume that the synchronization problem could be solved properly. On the other hand, the Alamouti decoding process requires accurate estimation of the channel state information. In our works, the channel state is assumed to be static during each packet transmission, whereas it will change to another state for the next packet. A pilot sequence can be inserted into the front part of the transmit packet to realize the channel estimation. We suppose that, for both cooperative relaying scheme and virtual MISO cooperative scheme, the receiver knows the channel state information by using a pilot sequence and an adequate estimation method.

4.3 Power Allocation Strategy

In this work, we assume that the power allocation strategy is defined for a relative long term communication. So we only consider the mean attenuation of the channels. For some instant, channels between the source and destination may suffer from severe fading effect. We ignore the effect of this instantaneous degradation for the reason that its compensation requires high-speed feedback information, which is beyond the scope of this chapter. While for the case where the channels are all in long time severe fading, the network layer could change another route for the data transmission.

In wireless sensor networks, energy efficiency is an important consideration during the deployment of the network. When considering the power allocation among the nodes, it is more straightforward to minimize the total transmit power for each data transmission. On the other hand, one method of evaluating the communication performance among the nodes is the reception BER. It is a more appropriate and explicit criterion for wireless sensor networks where most nodes are working on moderate SNR region. In our power allocation scheme, we consider the minimization of total transmit power while data transmission can be provided by an average reception BER performance. Furthermore, the maximum transmit power at each node is constrained due to the limited energy supply and efficiency of

the analog circuit, especially the power amplifier. So the power allocation strategy should also consider a transmit power limitation on the nodes.

4.3.1 Cooperative Relaying Scheme

The works in [78] show that the BER probability for the AF communication with one relay node can be adequately lower bounded by:

$$P_e \geq \frac{3}{16}(1+\overline{\gamma}_{sd})^{-1}(1+\frac{\overline{\gamma}_{sr}\overline{\gamma}_{rd}}{\overline{\gamma}_{sr}+\overline{\gamma}_{rd}})^{-1} \tag{4.8}$$

where $\overline{\gamma}_{ij}$ is the mean value of γ_{ij}, so $\overline{\gamma}_{ij} = \frac{\sigma_{ij}^2 P_i}{N_0 B}$, and σ_{ij}^2 is the mean strength of the channel between node i and node j. In our works, we suppose that the relay node is located between the source and destination nodes. The links from source to relay and from relay to destination respectively have a stronger mean strength than the direct link from source to destination. In order to obtain a relative low BER, the average SNR $\overline{\gamma}_{sr}$ and $\overline{\gamma}_{rd}$ satisfy the conditions $\overline{\gamma}_{sr} \gg 1$ and $\overline{\gamma}_{rd} \gg 1$. So equation (4.8) could be appropriately simplified as:

$$P_e \approx \frac{3}{16}(1+\overline{\gamma}_{sd})^{-1}(\frac{\overline{\gamma}_{sr}\overline{\gamma}_{rd}}{\overline{\gamma}_{sr}+\overline{\gamma}_{rd}})^{-1} \tag{4.9}$$

We note that, although the approximated expression will be utilized to determine the predefined BER requirement, it shows to be a tight lower bound on the exact BER. The numerical and simulated results that will be presented later in section 4.5 indicate that our approximated results are with little deviation. Thus, we propose the power allocation strategy that minimizes the total transmit power at the source and relay nodes, while with a predefined BER requirement P_{eThr} to be met. The optimization problem can be formulated as:

$$\min \quad f = P_s + P_r \tag{4.10}$$

$$\begin{aligned} & & P_e &= P_{eThr} \\ & subject \quad to & P_s &\leq P_{\max} \\ & & P_r &\leq P_{\max} \end{aligned}$$

where $P_{\max}$ is a constraint on maximum transmit power. To obtain the optimal

solutions, we firstly release the constraints on the maximum transmit power. Then, considering the Lagrange multiplier λ_1 with one constraint, the problem can be solved as following.

We obtain the objective function L_1 as:

$$L_1 = P_s + P_r + \lambda_1(\frac{3}{16}(1+\overline{\gamma}_{sd})^{-1}(\frac{\overline{\gamma}_{sr}\overline{\gamma}_{rd}}{\overline{\gamma}_{sr}+\overline{\gamma}_{rd}})^{-1} - P_{eThr}) \tag{4.11}$$

Setting $\nabla_{P_s} L_1 = 0$ and $\nabla_{P_r} L_1 = 0$ gives:

$$\begin{aligned} \nabla_{P_s} L_1 &= 1 - \tfrac{3\lambda_1}{16} \cdot \tfrac{(N_0B)^2}{(\sigma_{sd}^2 P_s + N_0 B)} \cdot (\tfrac{\sigma_{sd}^2}{\sigma_{sr}^2 P_s \sigma_{rd}^2 P_r} \cdot \tfrac{\sigma_{sr}^2 P_s + \sigma_{rd}^2 P_r}{\sigma_{sd}^2 P_s + N_0 B} + \tfrac{1}{\sigma_{sr}^2 P_s^2}) = 0 \\ \nabla_{P_r} L_1 &= 1 - \tfrac{3\lambda_1}{16} \cdot \tfrac{(N_0B)^2}{(\sigma_{sd}^2 P_s + N_0 B)} \cdot \tfrac{1}{\sigma_{rd}^2 P_r^2} = 0 \end{aligned} \tag{4.12}$$

By eliminating the Lagrange multiplier λ_1, equation array (4.12) yields:

$$\frac{\sigma_{sr}^2 P_s + \sigma_{rd}^2 P_r}{\sigma_{sd}^2 P_s + N_0 B} = \frac{\sigma_{sr}^2 P_s^2 - \sigma_{rd}^2 P_r^2}{\sigma_{sd}^2 P_s P_r} \tag{4.13}$$

Considering the predefined BER threshold on equation (4.9) and substituting it into equation (4.13), we get:

$$\frac{3}{16} \cdot \frac{(N_0B)^2}{P_r^2 \sigma_{sd}^2 \sigma_{rd}^2} - \frac{3}{16} \cdot \frac{(N_0B)^2}{P_s^2 \sigma_{sd}^2 \sigma_{sr}^2} = P_{eThr} \tag{4.14}$$

The optimal allocated power P_s and P_r represent the intersection point of the two curves determined by (4.9) and (4.14). However, simple analytical solutions seem not easy to be obtained from these two equations. Considering the BER performance for the MRC of two paths signals [7], the expression $\frac{3}{16} \cdot \frac{(N_0B)^2}{P_s^2 \sigma_{sd}^2 \sigma_{sr}^2}$, which represents the MRC of the source-to-relay and source-to-destination signals, could be approximated as much smaller than P_{eThr}. Thus, the approximated solutions can be obtained by neglecting the effect of $\frac{3}{16} \cdot \frac{(N_0B)^2}{P_s^2 \sigma_{sd}^2 \sigma_{sr}^2}$. Then the asymptote result can be given as:

$$P_r = N_0 B \sqrt{\frac{3}{16 P_{eThr} \sigma_{sd}^2 \sigma_{rd}^2}} \tag{4.15}$$

Hence, the optimal allocated power P_r can be approximated therein. By combining equations (4.9) and (4.15), the optimal allocated power P_s is:

$$P_s = N_0 B \frac{\sqrt{\frac{3}{16 P_{eThr} \sigma_{sd}^2 \sigma_{rd}^2}} - \frac{1}{\sigma_{sd}^2} + \sqrt{(\sqrt{\frac{3}{16 P_{eThr} \sigma_{sd}^2 \sigma_{rd}^2}} - \frac{1}{\sigma_{sd}^2})^2 + \frac{3}{4 P_{eThr} \sigma_{sd}^2 \sigma_{sr}^2}}}{2} \quad (4.16)$$

As shown in equations (4.15) and (4.16), optimal transmit power P_s is reasonable to be larger than P_r. Considering the constraints on the maximum transmit power, the Kuhn-Tucker conditions are utilized to justify the optimization results. The whole process is considered in Appendix A. But a simplified process can be summarized as: if the approximated transmit power P_s and P_r are under the constraints, the solutions are feasible. Otherwise, if P_s exceeds the maximum constraint, the allocated transmit power to the source node should be truncated to $P_{\max}$. Then, the transmit power of the relay node is determined by considering equation (4.9). If P_r also exceeds the maximum constraint, the required BER for the cooperative relaying system cannot be attained.

4.3.2 Virtual MISO Cooperative Scheme

For the cooperative transmission using Alamouti code, the average BER after Alamouti decoding is [7]:

$$P_e' = \frac{3}{4}(1 - \sqrt{\frac{\bar{\gamma}_1'}{1 + \bar{\gamma}_1'}})(1 - \sqrt{\frac{\bar{\gamma}_2'}{1 + \bar{\gamma}_2'}}) \quad (4.17)$$

where $\overline{\gamma}_1'$ and $\overline{\gamma}_2'$ are the mean value of γ_1' and γ_2', with $\overline{\gamma}_1' = \frac{\sigma_1^2 P_{T1}}{N_0 B}$ and $\overline{\gamma}_2' = \frac{\sigma_2^2 P_{T2}}{N_0 B}$. σ_1^2 and σ_2^2 are respectively the mean strength of the channels from node s_1 to d and from node s_2 to d. The power allocation scheme, which minimizes the total transmit power of the two cooperative nodes and with a given average BER requirement P_{eThr}, can be defined as:

$$\min \quad f' = P_{T1} + P_{T2} \quad (4.18)$$

$$\begin{aligned} & P_e' = P_{eThr} \\ subject \quad to \quad & P_{T1} \le P_{\max} \\ & P_{T2} \le P_{\max} \end{aligned}$$

To find the solutions, we firstly loose the constraints on the maximum transmit power. Then, the optimization problem of minimizing the total transmit power can be solved by considering the Lagrange multiplier λ_3 with one constraint. The objective function L_2 can be obtained as:

$$L_2 = P_{T1} + P_{T2} + \lambda_3(\frac{3}{4}(1 - \sqrt{\frac{\bar{\gamma}_1'}{1+\bar{\gamma}_1'}})(1 - \sqrt{\frac{\bar{\gamma}_2'}{1+\bar{\gamma}_2'}}) - P_{eThr}) \tag{4.19}$$

Setting $\nabla_{P_{T1}} L_2 = 0$ and $\nabla_{P_{T2}} L_2 = 0$ gives:

$$\nabla_{P_{T1}} L_2 = 1 - \frac{3}{8}\lambda_3(1 - \sqrt{\frac{\sigma_2^2 P_{T2}}{N_0 B + \sigma_2^2 P_{T2}}})(\frac{\sigma_1 N_0 B}{P_{T1}^{1/2}(N_0 B + \sigma_1^2 P_{T1})^{3/2}}) = 0 \tag{4.20}$$

$$\nabla_{P_{T2}} L_2 = 1 - \frac{3}{8}\lambda_3(1 - \sqrt{\frac{\sigma_1^2 P_{T1}}{N_0 B + \sigma_1^2 P_{T1}}})(\frac{\sigma_2 N_0 B}{P_{T2}^{1/2}(N_0 B + \sigma_2^2 P_{T2})^{3/2}}) = 0 \tag{4.21}$$

By eliminating the Lagrange multiplier λ_3, equations (4.20) and (4.21) yield:

$$\begin{aligned} & (1 - \sqrt{\tfrac{\sigma_2^2 P_{T2}}{N_0 B + \sigma_2^2 P_{T2}}})(\tfrac{\sigma_1}{P_{T1}^{1/2}(N_0 B + \sigma_1^2 P_{T1})^{3/2}}) \\ & = (1 - \sqrt{\tfrac{\sigma_1^2 P_{T1}}{N_0 B + \sigma_1^2 P_{T1}}})(\tfrac{\sigma_2}{P_{T2}^{1/2}(N_0 B + \sigma_2^2 P_{T2})^{3/2}}) \end{aligned} \tag{4.22}$$

Without any loss of generality, we suppose that the mean strengths of the channels satisfy $\sigma_1^2 \ge \sigma_2^2$. In order to obtain a relative low BER probability, the average SNR $\overline{\gamma}_1'$ for the better channel normally satisfies the condition $\overline{\gamma}_1' \gg 1$. So we can make the following approximation:

$$1 - \sqrt{\frac{\overline{\gamma}_1'}{1+\overline{\gamma}_1'}} \approx \frac{1}{2\overline{\gamma}_1'} \tag{4.23}$$

thus

$$(1 - \sqrt{\frac{\sigma_1^2 P_{T1}}{N_0 B + \sigma_1^2 P_{T1}}}) \approx \frac{N_0 B}{2\sigma_1^2 P_{T1}} \tag{4.24}$$

After substituting equation (4.24) into (4.22) and considering equation (4.17) gives:

$$\frac{3}{16} \cdot \frac{\sigma_2 (N_0 B)^2}{\sigma_1^2 P_{T2}^{1/2} (N_0 B + \sigma_2^2 P_{T2})^{3/2} P_{eThr}} = (\frac{\sigma_1^2 P_{T1}}{N_0 B + \sigma_1^2 P_{T1}})^{3/2} \tag{4.25}$$

Define

$$A_1 = \frac{3}{16} \cdot \frac{\sigma_2 (N_0 B)^2}{\sigma_1^2 P_{T2}^{1/2} (N_0 B + \sigma_2^2 P_{T2})^{3/2} P_{eThr}}$$

The relation between transmit power P_{T1} and P_{T2} is:

$$P_{T1} = \frac{N_0 B}{\sigma_1^2 (A_1^{-2/3} - 1)} \tag{4.26}$$

The optimal allocated power P_{T1} and P_{T2} are determined by the intersection point of the two curves according to equations (4.17) and (4.26). But it is hard to get the analytical solutions. While considering equation (4.26), it has the similar form as the rectangular hyperbola. So the optimal allocated power P_{T1} and P_{T2} can be approximated by equation (4.17) and one asymptote of the rectangular hyperbola determined by equation (4.26). Therefore, the approximated optimal power P_{T2} can be determined by setting $A_1 = 1$. It makes:

$$\frac{3\sigma_2^2 (N_0 B)^2}{16\sigma_1^2 P_{eThr}} = (\sigma_2^2 P_{T2})^{1/2} (N_0 B + \sigma_2^2 P_{T2})^{3/2} \tag{4.27}$$

Define

$$A_2 = \frac{3\sigma_2^2 (N_0 B)^2}{16\sigma_1^2 P_{eThr}}$$

Considering

$$A_2 = (\sigma_2^2 P_{T2})^{1/2}(N_0 B + \sigma_2^2 P_{T2})^{3/2} \leq (N_0 B/2 + \sigma_2^2 P_{T2})(N_0 B + \sigma_2^2 P_{T2})$$

We get:

$$P_{T2} \geq \frac{\sqrt{(N_0 B)^2 + 16A_2} - 3N_0 B}{4\sigma_2^2} \tag{4.28}$$

So P_{T2} can be approximated by this lower bound and P_{T1} can therefore be determined by considering equation (4.17), such as:

$$P_{T1} = \frac{N_0 B}{\sigma_1^2}((1 - (\frac{4P_{eThr}}{3(1 - \sqrt{\sigma_2^2 P_{T2}/(N_0 B + \sigma_2^2 P_{T2})})})^{-2} - 1)^{-1} \tag{4.29}$$

While considering the constraints on the maximum transmit power, the Kuhn-Tucker conditions can also be utilized. It is similar to the discussion of the cooperative relaying scheme. For briefly presenting, we will not illustrate the verification. The simplified process can be summarized as: If the approximated transmit power P_{T1} and P_{T2} are under the constraints, the solutions are feasible. Supposing one of these optimal allocated powers is larger than the maximum constraint on transmit power, the optimal transmit power should be truncated. In this case, the transmit node on better channel condition should be allocated with the maximum available transmit power. The transmit power of the other node is determined by equation (4.17). If it still cannot satisfy the constraint on maximum transmit power, the BER performance for the Virtual MISO system cannot be attained.

4.4 Cooperative Strategies

Considering a network topology of four sensor nodes, one or two relay nodes might help the communication between the source and destination nodes. We suppose that every node knows the mean channel strength of each link in this topology. Two cooperative strategies, as shown in Figure 4.2, will be investigated in this section. They consist of relaying cooperation or virtual MISO cooperation at different stages. In these two strategies, direct link between the source and destination nodes is assumed to be unavailable. It is reasonable when the distance between

them is large, and the transmit power is constrained by a maximum threshold. Otherwise, direct implementation of cooperative relaying scheme might be applied by choosing a relaying node among the source and destination nodes.

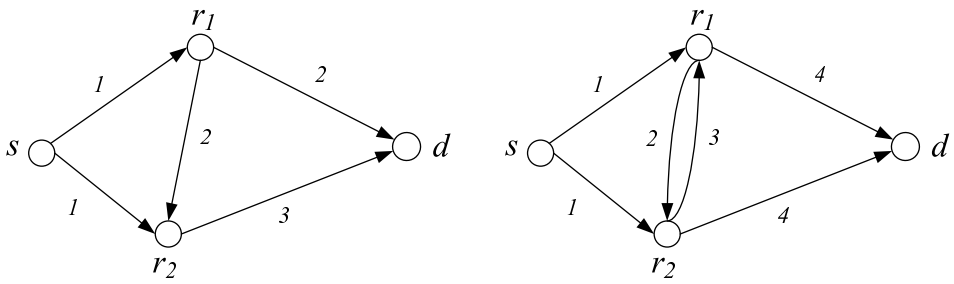

(a) Cooperative strategy 1 (b) Cooperative strategy 2

Figure 4.2: Proposed cooperative strategies by applying cooperative communication

In the previous section, we obtained the approximated optimal power allocation for the cooperative relaying scheme and the virtual MISO cooperative scheme. The results will be utilized to allocate the transmit power in our proposed cooperative strategies. In order to determine the transmit power at each node, not only the mean channel strengths for the corresponding links should be known, but also the required BER probability for each stage should be decided. Hence, in the following analysis for each cooperative strategy, we will explain the process of cooperation and deduce the approximated required BER probability for different cooperation stages.

4.4.1 Cooperative Strategy 1

In strategy 1, a modified cooperative relaying scheme is implemented among the four nodes. As shown in Figure 4.3, at the first time slot, the information is broadcasted by the source node s. For the implementation, we suppose that one of the relay nodes, for example r_1, performs as an amplifier. It amplify-and-forwards the received signal towards the other relay node r_2 and the destination node d at the second time slot. After receiving the signals from the source node s and the relay node r_1, MRC combination and information decoding are performed at the relay node r_2. Then, at the third time slot, the decoded information is retransmitted to the destination node. At the destination, decoding decision is performed based on

a MRC combination of the signals from the relay node r_1 in the second time slot and from the relay node r_2 in the third time slot. So in the strategy 1, the roles of the two relaying nodes are different. One performs the amplify-and-forward; the other performs the decode-and-forward.

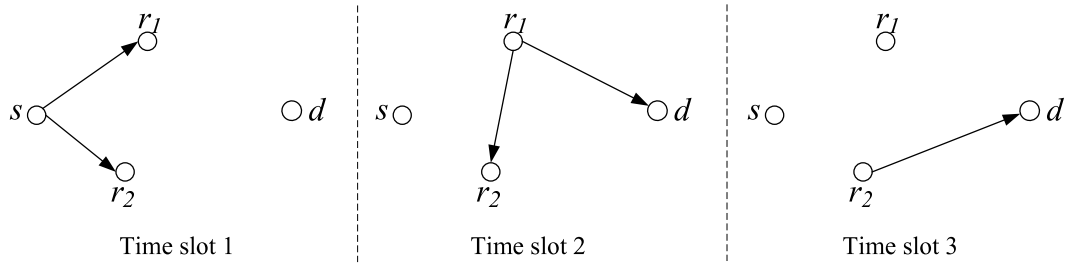

Figure 4.3: Time division channel allocation for cooperative strategy 1 in three time slots

We notice that the strategy 1 could be basically decomposed into two cooperative relaying stages. The first cooperative relaying stage is performed at the first and second time slots and employs three nodes $\{s, r_1, r_2\}$. The second cooperative relaying stage is performed at the second and third time slots and employs the nodes $\{r_2, r_1, d\}$. Moreover, as the destination node d could receive the amplify-and-forwarded signal from node r_1 at the second time slot, the relay node r_1 has no need to relay the signal retransmitted by node r_2 in the second cooperative relaying stage.

Considering power allocation among the nodes in the strategy 1, the results of optimal power allocation for the cooperative relaying scheme, which are obtained in section 4.3.1, will be used. As the source node also acts as a source in the first cooperative relaying stage, its transmit power can be determined according to equation (4.16), where the channel parameters should be altered to those among the three nodes $\{s, r_1, r_2\}$ and the required BER performance is restricted to P_{e1} in the first cooperative relaying stage. Note that the node r_1 performs as the relay node in both cooperative relaying stages. According to equation (4.15), the optimal transmit power at the relay node, in cooperative relaying scheme shown in Figure 4.1(a), is determined by the required BER performance and the mean channel strengths of source-to-destination link (s to d) and relay-to-destination link (r to d). Therefore, considering the two cooperative relaying stages, the transmit power at the node r_1 is determined either by the required BER P_{e1} of the first cooperative relaying stage and the mean channel strengths of $\sigma^2_{sr_2}$ and $\sigma^2_{r_1r_2}$, or

by the required BER P_{e2} of the second cooperative relaying stage and the mean channel strengths of $\sigma^2_{r_2d}$ and $\sigma^2_{r_1d}$. In order to guarantee the receive performance for both of the cooperative relaying stages, we suppose that the transmit power of the node r_1 employs the maximum one. That is:

$$P_{r_1} = \max\left\{ N_0 B \sqrt{\frac{3}{16 P_{e1} \sigma^2_{sr_2} \sigma^2_{r_1 r_2}}}, N_0 B \sqrt{\frac{3}{16 P_{e2} \sigma^2_{r_2 d} \sigma^2_{r_1 d}}} \right\} \tag{4.30}$$

Recalling that, at the second cooperative relaying stage, the destination node d obtains the relaying signal which is actually the amplify-and-forwarded version from the node s. We exclude the so-called source-to-relay link (r_2 to r_1) at the second cooperative relaying stage. It is in nature substituted by the source-to-relay link (s to r_1) at the first cooperative relaying stage. So that, considering the transmit power using equation (4.16) at the node r_2, which performs as a source node at the second cooperative relaying stage, the mean channel strength of $\sigma^2_{sr_1}$ will take the place of $\sigma^2_{r_1 r_2}$. That is:

$$P_{r_2} = N_0 B \frac{\sqrt{\frac{3}{16 P_{e2} \sigma^2_{r_2 d} \sigma^2_{r_1 d}}} - \frac{1}{\sigma^2_{r_2 d}} + \sqrt{(\sqrt{\frac{3}{16 P_{e2} \sigma^2_{r_2 d} \sigma^2_{r_1 d}}} - \frac{1}{\sigma^2_{r_2 d}})^2 + \frac{3}{4 P_{e2} \sigma^2_{r_2 d} \sigma^2_{sr_1}}}}{2} \tag{4.31}$$

As we have mentioned, we suppose that the nodes know the mean channel strengths among them. So in order to determine the transmit power, the required BER P_{e1} and P_{e2} for the two cooperative relaying stages are to be decided. Meanwhile, we note that, the global required BER performance $P_e^{(1)}$ for the cooperative strategy 1 is the receive performance at the destination node d. It would be different from the receive BER performance (P_{e1} and P_{e2}) for the two cooperative relaying stages, since false detection at the relay node would be propagated to the destination node. In order to sustain a reliable communication, it is reasonable to suppose $P_{e1} << 1$ and $P_{e2} << 1$. In addition, as the channel conditions for these two stages are supposed to be independent, we assume that P_{e1} and P_{e2} are uncorrelated and their error symbols happen in different positions. Therefore, on considering $P_e^{(1)}$, we analyse the effect of P_{e1} and P_{e2} separately as follows.

Firstly, considering the decoding result at the relay node r_2, it decoded a symbol without error at the probability of $1 - P_{e1}$. As the relay node r_1 chooses the larger required transmit power shown in equation (4.30), the required BER performance

at the second cooperative relaying stage could be sustained. Therefore, in the condition that a symbol is correctly decoded at the relay node r_2, the destination node could receive it with a BER probability no more than $(1-P_{e1})P_{e2}$. Secondly, we only consider the error signals (with the probability of P_{e1}) decoded in the relay node r_2. They will be propagated to the destination node d through the path of $r_2 \rightarrow d$ link. On the other hand, the relay node r_1 does not make a decoding but amplify-and-forwards the receive signals from the source node s. These signals are propagated through a path comprising the $s \rightarrow r_1$ link and $r_1 \rightarrow d$ link to the destination. In the condition of relative worse fading in the $r_2 \rightarrow d$ link, the signal from the $s \rightarrow r_1 \rightarrow d$ path might rectify the false signal from the node r_2. So its error probability could be supposed to be no more than P_{e1} in this case. At last, considering the both cases, $P_e^{(1)}$ could be upper bounded by the sum of $(1-P_{e1})P_{e2}$ and P_{e1}. So that:

$$\begin{aligned} P_e^{(1)} &\leq (1-P_{e1})P_{e2} + P_{e1} \\ &\leq P_{e1} + P_{e2} \end{aligned} \tag{4.32}$$

Given a pre-required BER performance $P_e^{(1)}$ in the strategy 1, the choices of P_{e1} and P_{e2} must satisfy equation (4.32). So that, the transmit power at different cooperative nodes can be determined.

4.4.2 Cooperative Strategy 2

Figure 4.4 shows the time division channel allocation for the cooperative strategy 2. It is a combination of cooperative relaying scheme and virtual MISO cooperative scheme. Firstly, the two relay nodes receive the source information by cooperative relaying scheme. As it is shown in Figure 4.4, information is broadcasted by the source node s in the first time slot. In the second and third time slots, the relay nodes r_1 and r_2 amplify-and-forward their received signals to each other respectively. After that, MRC combination and information decoding are performed at the relay nodes r_1 and r_2. The virtual MISO cooperative scheme is applied among two relay nodes and one destination node in the fourth time slot.

Considering the strategy 2, the transmit power at the source node is determined by two cooperative relaying schemes. Since the two relay nodes will make

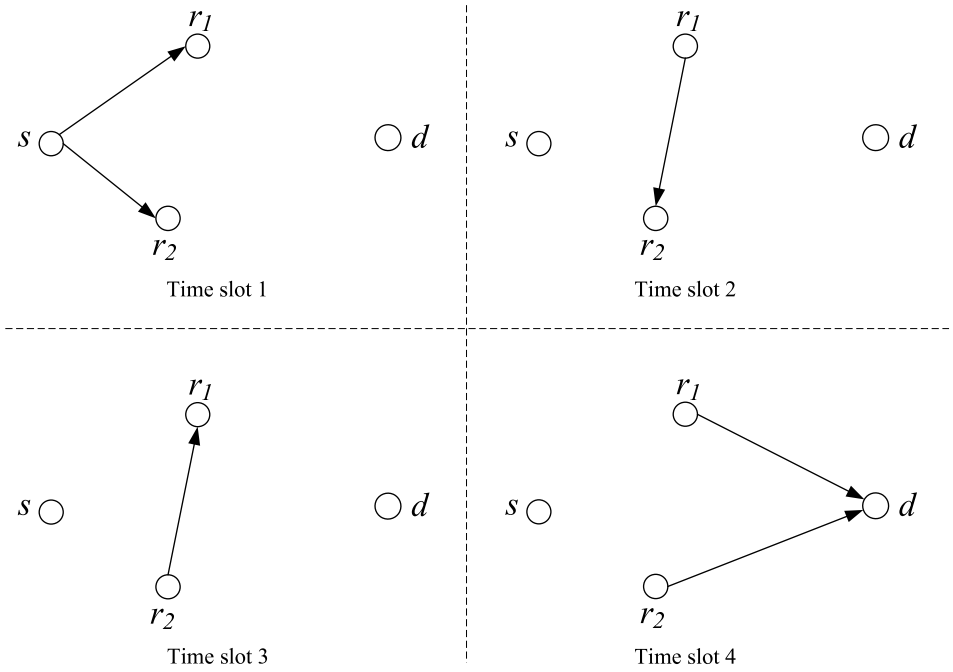

Figure 4.4: Time division channel allocation for cooperative strategy 2 in four time slots

decisions of the source information utilizing the two cooperative relaying schemes respectively, their decision BER performances are supposed to be P'_{e1} and P'_{e2}. We consider P_{s1} and P_{s2} as the required transmit power at the source node for the two cooperative relaying schemes. They can be determined by considering equation (4.16) with the corresponding channel and BER parameters (P'_{e1} and P'_{e2}). We assume that the source node employs the larger one. That is:

$$P_s = \max\{P_{s1}, P_{s2}\} \tag{4.33}$$

In the second and third time slots, according to their cooperative relaying schemes respectively, the transmit power at the two relay nodes is determined by equation (4.15). After the information detection at the two relay nodes, they transmit the decoded information to the destination utilizing a virtual MISO cooperative scheme. At this stage, the optimal transmit power by the two relay nodes is determined by equations (4.28) and (4.29).

Similar to the discussion for the strategy 1, we assume that the required BER P'_{e1} and P'_{e2} at the cooperative relaying stage and P'_{e3} at the virtual MISO coop-

eration stage could be low enough. Thus they satisfy that $P'_{e1} << 1$, $P'_{e2} << 1$ and $P'_{e3} << 1$. The symbol corruptions happening at the two cooperative relaying stages could be supposed to be independent and in different positions. Furthermore, we assume that burst error can be avoided by interleaving at the two relay nodes if it is necessary. Considering the property of Alamouti code, the number of source information symbols would be even in our cooperative strategy. In order to analyse the error propagation in different cooperative stages and without any loss of generality, we consider that a block of two information symbols are transmitted at the source node. Denoting a *node* with a block of two information symbols $(i\ j)$ as $node(i\ j)$, where $node \in \{s, r_1, r_2, d\}$ and $i, j \in \{0, 1\}$, we suppose that two symbols $s(0\ 0)$ are transmitted at the source node. Taking into account the assumption that no burst errors and low BER at the relay nodes, we could only consider the two relay nodes decode the block $s(0\ 0)$ in three cases, such as $r_1(0\ 0)$ $r_2(0\ 0)$ without error, $r_1(1\ 0)$ $r_2(0\ 0)$ or $r_1(0\ 1)$ $r_2(0\ 0)$ with one error at the relay node r_1, and $r_1(0\ 0)$ $r_2(1\ 0)$ or $r_1(0\ 0)$ $r_2(0\ 1)$ with one error at the relay node r_2. They happen with the probabilities of $(1 - P'_{e1})(1 - P'_{e2})$, $P'_{e1}(1 - P'_{e1}) \approx P'_{e1}$ and $P'_{e2}(1 - P'_{e2}) \approx P'_{e2}$ respectively.

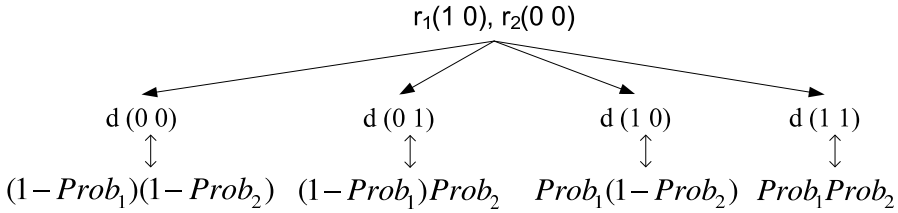

Figure 4.5: The examples of decoding probability for the virtual MISO cooperative scheme

After the source information detection, the two relay nodes employ the virtual MISO cooperative scheme to relay the decoded information to the destination node. Recalling the orthogonal property of Alamouti code, neighbor symbols in the same block will affect the signal detection after decoding combination. We take $Prob_1$ and $Prob_2$ referring to the conditional symbol error probabilities at the destination node d. Specifically, $Prob_1$ is in the condition that two relay nodes had different detections on the decoded symbol but the neighbor symbol in the same block was correctly detected. For example, supposing a block of two symbols $s(0\ 0)$ are transmitted, the two relay nodes detect them as $r_1(1\ 0)$ $r_2(0\ 0)$ separately. So they have different detection on the first symbol while they have correct detection on the

second symbol. After the virtual MISO cooperative transmission, the destination node d decodes the two symbols employing Alamouti code. $Prob_1$ refers to the symbol error probability of decoding the first symbol. Accordingly, since $Prob_2$ is in the condition that two relays have correct detection on the decoded symbol but the neighbor symbol in the same block has been falsely detected at one relay node, it refers to the symbol error probability of decoding the second symbol. Figure 4.5 shows the examples of decoding probability at the destination node. So that, utilizing the strategy 2, the reception BER $P_e^{(2)}$ for the transmitted source block $s(0\ 0)$ can be approximated as:

$$\begin{aligned} P_e^{(2)} &= \tfrac{1}{2}\,(E\,[\text{number of errors} \mid \text{no error at the relay nodes}] \\ &\quad + E\,[\text{number of errors} \mid \text{one error at relay node } \mathrm{r}_1] \\ &\quad + E\,[\text{number of errors} \mid \text{one error at relay node } \mathrm{r}_2]) \\ &\approx \tfrac{1}{2}\,\{(1-P'_{e1})(1-P'_{e2})\,[(1-P'_{e3})P'_{e3} + P'_{e3}(1-P'_{e3}) + 2P'_{e3}P'_{e3}] \\ &\quad + 2P'_{e1}\,[(1-Prob_1)Prob_2 + Prob_1(1-Prob_2) + 2Prob_1Prob_2] \\ &\quad + 2P'_{e2}\,[(1-Prob_1)Prob_2 + Prob_1(1-Prob_2) + 2Prob_1Prob_2]\} \\ &= (1-P'_{e1})(1-P'_{e2})P'_{e3} + (P'_{e1}+P'_{e2})(Prob_1+Prob_2) \end{aligned} \tag{4.34}$$

Generally, equation (4.34) could upper bound the approximated BER for the strategy 2. Furthermore, considering equation (4.6), the detection symbol producing $Prob_1$ will be:

$$\widetilde{s_i} = \left(|h_{r1d}|^2 P_{r1} - |h_{r2d}|^2 P_{r2}\right)s_i + h^*_{r1d}\sqrt{P_{r1}}n'_1 + h_{r2d}\sqrt{P_{r2}}n'^*_2 \tag{4.35}$$

For the special condition of two equal propagation paths at the virtual MISO transmission, that is $E\left[|h_{r1d}|^2 P_{r1}\right] = E\left[|h_{r2d}|^2 P_{r2}\right]$, the conditional error probability $Prob_1$ would be 0.5. Meanwhile, the detection symbol producing $Prob_2$ will be:

$$\widetilde{s_i} = \left(|h_{r1d}|^2 P_{r1} + |h_{r2d}|^2 P_{r2}\right)s_i \pm 2h^*_{r1d}h_{r2d}\sqrt{P_{r1}P_{r2}}s_j + h^*_{r1d}\sqrt{P_{r1}}n'_1 + h_{r2d}\sqrt{P_{r2}}n'^*_2 \tag{4.36}$$

It shows that the interference from the neighbour symbol (in the same block, such as s_j) will degrade the decoding performance. However, since the interfer-

ence is phase rotated by the fading channel parameters, $Prob_2$ is reasonable to be much lower than $Prob_1$. Therefore, by the approximation of taking $P'_{e1}P'_{e3}$, $P'_{e2}P'_{e3}$, $P'_{e1}P'_{e2}P'_{e3}$and $(P'_{e1} + P'_{e2})Prob_2$ approach to zero, the reception BER $P_e^{(2)}$ for the strategy 2 can be simplified as:

$$P_e^{(2)} \leq P'_{e3} + (P'_{e1} + P'_{e2})Prob_1 \tag{4.37}$$

Considering equation (4.37), the required BER (P'_{e1}, $P'_{e2}$and P'_{e3}) for different stages in the strategy 2 can be approximated according to the required source to destination BER $P_e^{(2)}$. Hence, the transmit power for the cooperative nodes can also be determined as stated previously.

4.5 Performance Analysis and Discussion

In this section, we investigate the performance of power allocation strategy. Then we discuss the energy efficiency of the proposed cooperative strategies in two topologies. Data is supposed to be initiated from a source node to a destination node, which are separated by a distance of $l_0 = 100m$. Candidate cooperative nodes, for the relaying cooperation or the virtual MISO cooperation, are located between the source and destination nodes. As shown in Figure 4.8, the relative location of the cooperative node i can be determined by the distance information (l_0, dx_i, dy_i), for example of the node r_1 by (l_0, dx_{r1}, dy_{r1}) and the node r_2 by (l_0, dx_{r2}, dy_{r2}). Recalling the channel model of Rayleigh fading effect superimposed on propagation path loss, the channel mean strength has the form of $\sigma_{ij}^2 = 1/PL(d_{ij})$ where $PL(d_{ij})_{(dB)} = 20\log_{10}(4\pi d_0/\lambda) + 10n\log_{10}(d_{ij}/d_0)$ is the path loss equation with d_0 as the reference distance, d_{ij} as the distance between the transmitter i and the receiver j, λ as the wave length, n as the mean path loss exponent. We take $n = 3.5$ and consider the BPSK modulation with a transmit symbol rate $250k$ symbols per second in our analysis.

4.5.1 Performance of Power Allocation Strategies

On the consideration of the power allocation performances, we suppose that the cooperative node is located on the straight line of source to destination link (that is $dy_r = 0$ and $dy_{s1} = 0$ in Figure 4.1). Thus its distance to the source node is represented by a distance ratio, which is obtained as dx_r/l_0 or dx_{s1}/l_0. Supposing

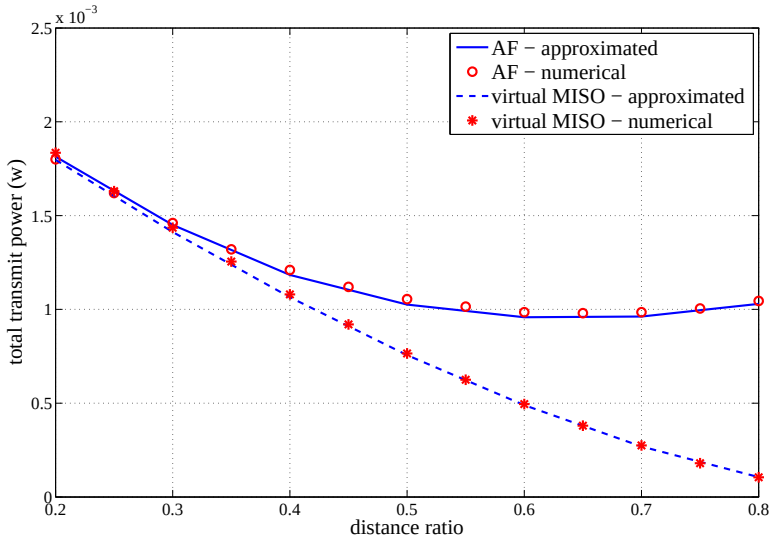

(a)

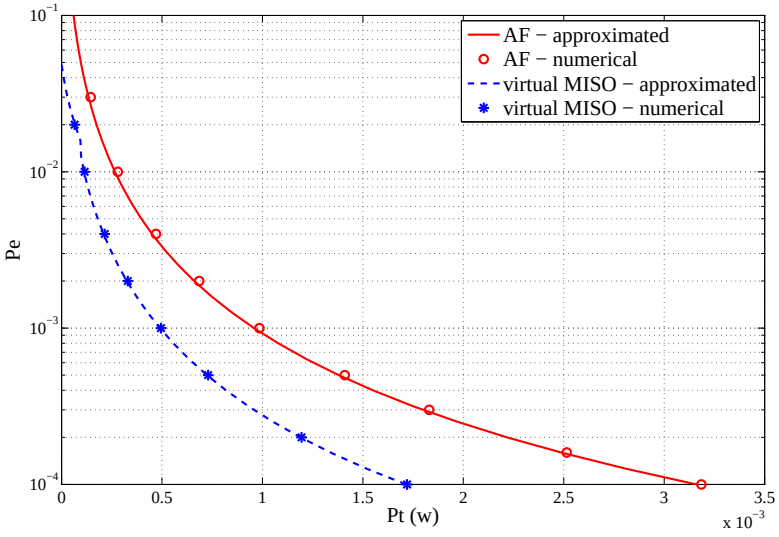

(b)

Figure 4.6: The approximated and numerical results of optimal power allocation for the AF cooperative relaying scheme and the virtual MISO cooperative scheme: (a) we constrain the required BER to be 10^{-3}, the cooperative node (r or s_1 in Figure 4.1) is located at different distance ratios and $dy_i = 0, i \in \{r, s_1\}$; (b) the position of the cooperative node is supposed to be located at a distance ratio of 0.6 and $dy_i = 0, i \in \{r, s_1\}$.

the required BER to be 10^{-3}, Figure 4.6 shows the fidelity of our approximation on the optimal power allocation strategy. The numerical results are obtained by considering the optimization problem (4.10) or (4.18) with the corresponding exact BER. For both of the AF cooperative relaying scheme and the virtual MISO cooperative scheme, the optimal total transmit power obtained by the results in section 4.3 matches well with the numerical results. The optimal total transmit power for the virtual MISO cooperative scheme is decreasing as the cooperative node approaches to the destination node. However, it is due to the implied condition that two nodes s_1 and s_2 in Figure 4.1(b) already know the source information. While for the AF cooperative relaying scheme, only the node s, as shown in Figure 4.1(a), knows the source information. We notice that, when the cooperative relaying node is located at a region near to the destination node, the AF cooperative relaying scheme requires less optimal total transmit power. The minimum point arrives at a place where the distance ratio approaches to 0.6. At this location, the AF cooperative relaying scheme obtains the best energy efficiency. Then, considering that the cooperative node is located at the point with distance ratio of 0.6, the fidelity performances of the optimal power allocation strategies, with different BER requirements, are shown in Figure 4.6(b). It shows that the approximated results of our optimal power allocation strategies are accurate enough for a wide range of BER requirements.

With a constraint on the required BER performance, we refer to the optimal power allocation gain as P_{t_eql}/P_{t_opl}, where P_{t_eql} and P_{t_opl} are the total transmit power for the optimal power allocation strategy and the equal power allocation strategy respectively. Supposing the required BER is 10^{-3}, the optimal power allocation gains are shown in Figure 4.7. For the AF cooperative relaying scheme, more gain is achieved by applying the optimal power allocation strategy when the relay node is approaching to the destination node. When the relaying node is located at a place where the distance ratio is less than 0.4, optimal power allocation achieves no gain as compared to the equal power allocation strategy. Figure 4.7 shows that the virtual MISO cooperative scheme achieves little gain with the optimal power allocation. As we have stated it in [79], the benefit of minimizing the total transmit power by employing the optimal power allocation scheme is very limited. But in the unbalanced channel condition, the precise value could only be obtained by a numerical method. Our proposed approximated optimal power allocation strategy gives this minimal total transmit power in the

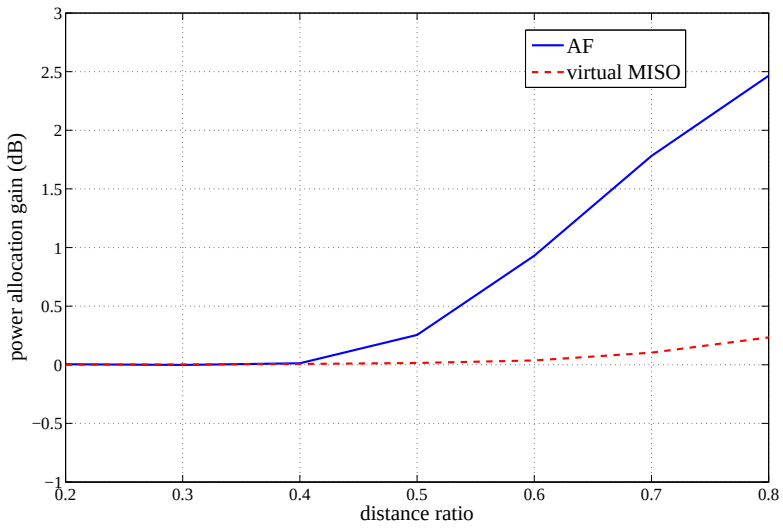

Figure 4.7: The gain of optimal power allocation with the constraint of received BER to be 10^{-3}

analytical way, and with a little deviation.

4.5.2 Discussion on Cooperative Strategies

In the discussion of the cooperative strategies, we consider two kinds of topologies as shown in Figure 4.8. We refer to them as *horizontal symmetric topology* and *diagonal symmetric topology*. In the *horizontal symmetric topology*, two cooperative nodes are assumed to be symmetrically located at the two sides of the straight line of source-to-destination direct link with $dy_{r1} = dy_{r2}$. They are also at the same distance to the source node, so that $dx_{r1} = dx_{r2}$. In the *diagonal symmetric topology*, two cooperative nodes are located at different sides of the source-to-destination direct link and at the same distance to it ($dy_{r1} = dy_{r2}$). The distance of the source node s to r_1 equals the distance of the destination node d to r_2, such as $dx_{r1} = l_0 - dx_{r2}$. For both of the topologies, we define the distance ratio as dx_{r1}/l_0 in the following analysis. We notice that, in the *diagonal symmetric topology*, one relay node is located at (dx_{r1}, dy_{r2}) while the other relay node locates at $(l_0 - dx_{r1}, dy_{r2})$ for a distance ratio of dx_{r1}/l_0.

Our proposed cooperative strategies require that the BER performance at different stages should be predetermined. As we have discussed in section 4.4, the

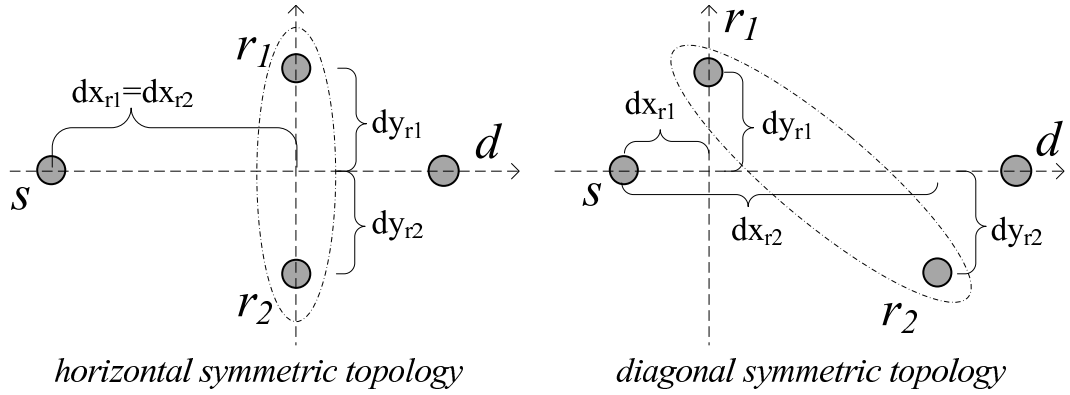

Figure 4.8: Two kinds of topologies, the length of source-to-destination direct link is taken as l_0

relation between the overall BER performance $P_e^{(i)}$ and the BER performance P_{ei} at different stages can be approximated as equation (4.32) for the cooperative strategy 1 and equation (4.37) for cooperative strategy 2. We note that, the decoded source information at the relay nodes might be useful for other nodes besides the desired destination node, and it has a meaning to keep the network with a balanced link quality. So in our discussion, we assume that the predetermined BER performances at different stages of the cooperative strategy are identical. That is $P_{e1} = P_{e2}$ in the cooperative strategy 1 and $P'_{e1} = P'_{e2} = P'_{e3}$ in the cooperative strategy 2. Considering equations (4.32) and (4.37), we take $P_{e1} = P_{e2} = 0.5P_e^{(1)}$ for the cooperative strategy 1 and $P'_{e1} = P'_{e2} = P'_{e3} = 0.5P_e^{(2)}$ for the cooperative strategy 2. In the following discussion, we suppose that the required overall BER between the source node and the destination node is 10^{-3} for all kinds of cooperative communications.

For the *horizontal symmetric topology*, two cooperative nodes could be located in vicinity or separated by a relative long distance. Figure 4.9 shows the allocated transmit power among the sensor nodes in the case where two cooperative nodes are in vicinity with $dy_{r1} + dy_{r2} = 1m$. In the AF cooperative relaying scheme, only one of the two cooperative nodes is utilized. Figure 4.9 shows that it requires more total transmit power than the two cooperative strategies. Our proposed cooperative strategies are more energy efficient no matter what the distance ratio is. Figure 4.10 shows the case where the distance between the two cooperative nodes increases to be $dy_{r1}+dy_{r2} = 40m$. In this case, the AF cooperative relaying scheme will be more energy efficient when the cooperative nodes close to the destination

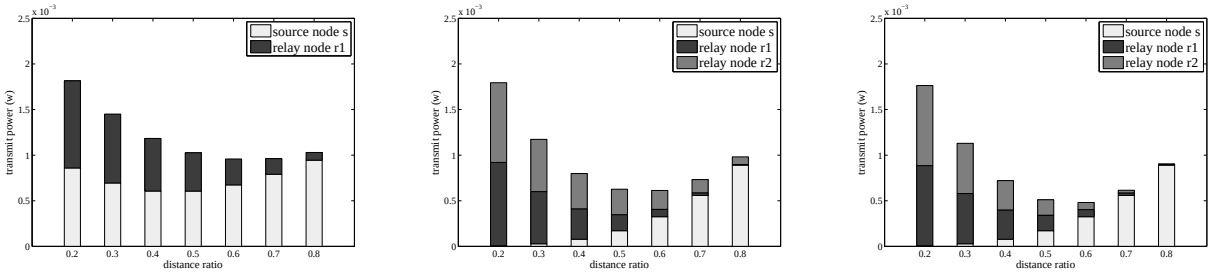

(a) (b) (c)

Figure 4.9: The transmit power consumption among the sensor nodes for (a) AF cooperative relaying scheme, (b) cooperative strategy 1 and (c) cooperative strategy 2. The nodes are supposed to be located in the *horizontal symmetric topology* with $dy_{r1} + dy_{r2} = 1m$.

node as shown in Figure 4.10. At the distance ratio of 0.8, the AF cooperative relaying scheme saves more than 30% of the total transmit power as compared to the two cooperative strategies. However, when the cooperative nodes are located in the middle region, with distance ratio around 0.5, the two cooperative strategies will also be more energy efficient than the AF cooperative relaying scheme.

As we compare the two cooperative strategies in Figure 4.9b and Figure 4.9c with that in Figure 4.10b and Figure 4.10c, the cooperative strategy 1 is more energy efficient when the distance between the two cooperative nodes increases. In the cooperative strategy 2, more power will be consumed for the information exchange between the two cooperative nodes as the distance between them increases. When this growth draws off the energy saving brought by the implementation of the virtual MISO scheme, the cooperative strategy 2 will be less energy efficient.

On the other hand, we compare the power allocation among the source node and cooperative nodes. As shown in Figure 4.9(b,c) and Figure 4.10(b,c), our proposed cooperative strategies achieve fair allocation of the transmit power among the nodes at distance ratio of 0.5. It helps to balance the energy consumption in wireless sensor networks. We note that, the fair allocation is different from the equal allocation strategy which is mentioned in the power allocation strategy. Since each node already employed the optimal power allocation strategy at different stages, and then results in a fair distribution of the total transmit power. Figure 4.9a and Figure 4.10a show that, the source node requires more transmit power than the relay node when applying the optimal power allocation strategy to

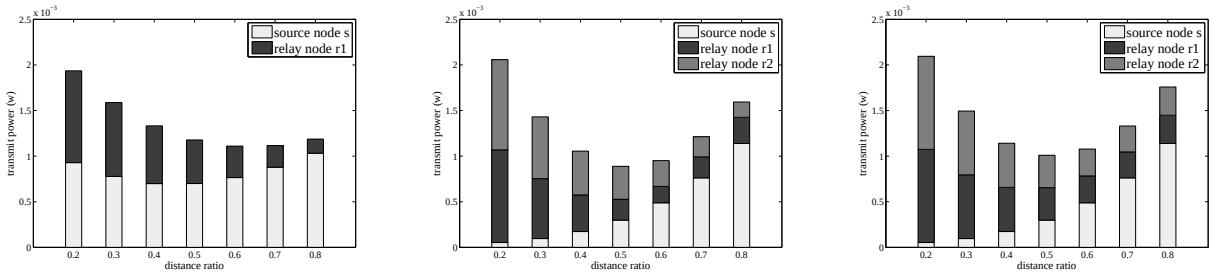

(a) (b) (c)

Figure 4.10: The transmit power consumption among the sensor nodes for (a) AF cooperative relaying scheme, (b) cooperative strategy 1 and (c) cooperative strategy 2. The nodes are supposed to be located in the *horizontal symmetric topology* with $dy_{r1} + dy_{r2} = 40m$.

the AF cooperative relaying scheme in most cases. Although the AF cooperative relaying scheme can obtain fair power allocation at the distance ratio of 0.2, the source and relay nodes require more transmit power which is not energy efficient.

When both cooperative nodes are located in a region near to the source node or destination node, the power allocation among the nodes is either not energy efficient or not fair. So in the *horizontal symmetric topology*, cooperative nodes are better to be located in the middle region of the source-to-destination path. In the case where only cooperative nodes could be found near the source and destination nodes, the *diagonal symmetric topology*, as shown in Figure 4.8, could be a good candidate. Figure 4.11a shows that, the cooperative strategy 1 could be more energy efficient when one cooperative relay node is near to the source node and the other is near to the destination node. It achieve also fair allocation of the total transmit power. In the *diagonal symmetric topology*, the cooperative strategy 2 could obtain relative stable performance on the power consumption as shown in Figure 4.11b.

As a result, in the *horizontal symmetric topology*, cooperative nodes should be located in the middle region of the source-to-destination path. Meanwhile, when the two cooperative nodes are near to each other, the cooperative strategy 2 is preferred. Otherwise, the cooperative strategy 1 is more energy efficient. In the *diagonal symmetric topology*, both of the two proposed cooperative strategies provide good performance on power consumption when the two cooperative nodes are separately near to the source node and the destination node. We take these

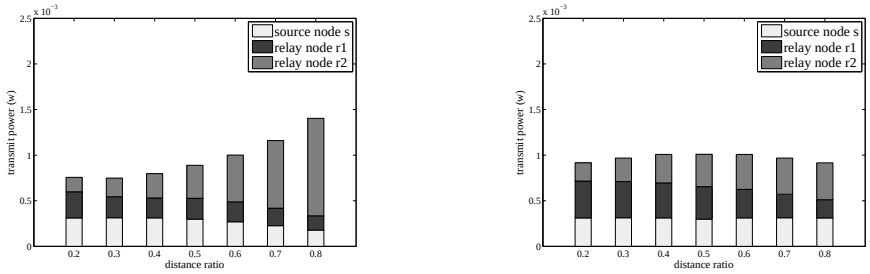

(a) (b)

Figure 4.11: The transmit power consumption among the sensor nodes for (a) cooperative strategy 1 with r1 performs AF and (b) cooperative strategy 2. The nodes are supposed to be located in the *diagonal symmetric topology* with $dy_{r1} = 20m$ and $dy_{r2} = 20m$.

as a heuristic policy to select the cooperative nodes and choose the appropriate cooperative communication for wireless sensor networks.

Considering the cases that comply with the heuristic policy, we show the simulated results of the two cooperative strategies under various BER constraints in Figure 4.12a and Figure 4.12b. The cooperative nodes are supposed to be at the relative optimal regions for two topologies. For example, in Figure 4.12a, we consider that two cooperative nodes are located at a distance ratio of 0.5 in the *horizontal symmetric topology*. Based on our previous discuss, we showed that the strategy 2 is more energy efficient in the case that the two relay nodes locate in vicinity and the strategy 1 is more profitable in the case that the two relay nodes are separated at a larger distance. Therefore, for faire comparison, we suppose that the two relay nodes are separated with $1m$ by using the cooperative strategy 2 and $40m$ by using the cooperative strategy 1. As shown in Figure 4.12a, the simulated BER results match well with the predetermined values obtained by our cooperative strategies. Moreover, we compare our cooperative strategies with equal allocation scheme, where each node is allocated with the equal transmit power. It shows that our cooperative strategies utilize less transmit power than the equal allocation scheme in the corresponding topologies.

On the other hand, in Figure 4.12b, we consider that the cooperative nodes are located at distance ratio of 0.2 and $dy_{r1} = dy_{r2} = 20m$ in the *diagonal symmetric topology*. Consistent simulated results can also be found when the cooperative strategy 2 is used. While using the predetermined transmit power of the coop-

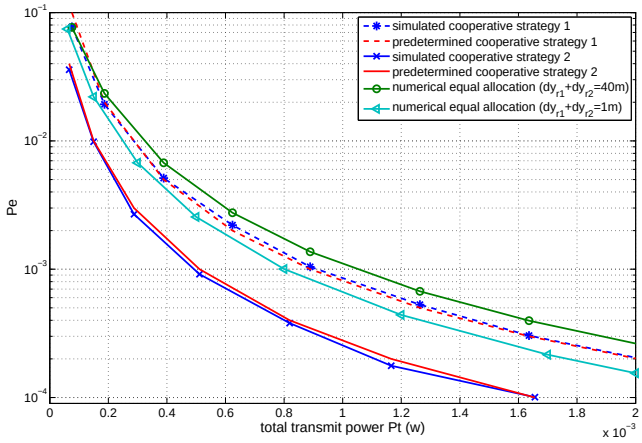

(a)

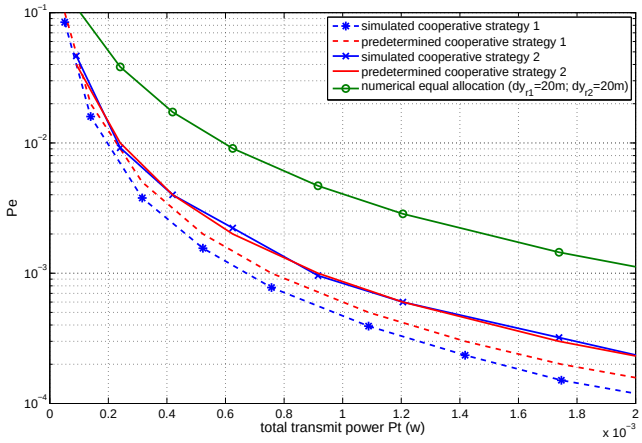

(b)

Figure 4.12: For various requirements on the BER performance and using the predefined power allocation of each cooperative strategy, the simulated results of BER: (a) in the *horizontal symmetric topology* with distance ratio of 0.5, (b) in the *diagonal symmetric topology* with distance ratio of 0.2

erative strategy 1, the simulated BER performance can be better. Since in the cooperative strategy 1, the relay node r_1 amplifies the received signal with a larger factor, as shown in equation (4.30), to preserve the desired BER performance. The conservative method will slightly increase the transmit power at the relay node in this asymmetric topology. But it is still more energy efficient as compared to the equal allocation scheme. It shows that in this asymmetric topology, our proposed cooperative strategy achieve more power gain than in the symmetric topology.

4.6 Summary

In this chapter, we proposed an optimal power allocation strategy for cooperative communications in wireless sensor networks. With a given requirement on the BER performance, it helps to minimize the total transmit power for the AF cooperative relaying scheme and the virtual MISO cooperative scheme in Rayleigh fading channel. The approximated power allocation for each node can be calculated in analytical way. The approximated performance matches well with the precise results obtained in numerical way. Moreover, without direct link between the source and destination nodes, we proposed two energy efficient cooperative strategies where the optimal power allocation strategy is applied at different stages. We compared the performance of the two topologies and derived a heuristic policy to select the cooperative nodes and choose the appropriate cooperative communication for wireless sensor networks. In the *horizontal symmetric topology*, cooperative nodes are better to be located in the middle region of the source-to-destination path. Meanwhile, when the two cooperative nodes are near to each other, the cooperative strategy 2 is preferred. Otherwise, the cooperative strategy 1 is more energy efficient. In the *diagonal symmetric topology*, both of the two proposed cooperative strategies provide good performance on the power consumption when the two cooperative nodes are near to the source node and the destination node respectively.

Until now, we consider cooperative communications without taking the error control schemes into account. In fact, the transmission of the data packets can not be assumed to be successful at each trial. Error control codes and automatic repeat request mechanism are the tradition ways to provide error control for data transmission. In the next chapter, we will consider these error control schemes in wireless sensor networks and analyse their energy efficiency for both SISO and MISO cooperative communication.

Chapter 5

Energy Efficiency in Wireless Sensor Networks

5.1 Introduction

In wireless sensor networks, the information data are usually sensitive to transmission errors. Error control schemes, such as error control codes (ECC) and automatic repeat request (ARQ), could be utilized to provide reliable wireless communications. Since the error control schemes will introduce redundancy to the information data or lower the bandwidth efficiency of the communication, these will cause extra energy consumption. When considering their implementation in wireless sensor networks, the energy efficiency should be investigated.

In this chapter, we consider three kinds of error control protocols: Basic ARQ, Hybrid ARQ-I and Hybrid ARQ-II. They are assumed to be incorporated in the SISO and MISO cooperative systems. In all of these protocols, a cyclic redundancy check sequence is used as error detection code to detect the transmission error on information data. Additionally, error correction codes are employed in Hybrid ARQ-I and Hybrid ARQ-II. The processing of error correction is performed before the error detection in these two schemes. In Hybrid ARQ-II, the coded redundancy of error correction code is transmitted only when it is necessary. Since stronger codes provide more coding gain but at a cost of longer coded redundancy and more complex coding/decoding process, the choice of error correction codes would have influence on the efficiency of the error control protocols. To analyse their energy efficiency, we consider the total energy consumption including the transmit energy

and the energy consumption for the coding and decoding processing and for the involved analog circuitry. In AWGN channel, since a low transmit power can provide reliable link for short distance connection, more consideration should be given to reduce the energy consumption on analog circuitry. On the other hand, in Rayleigh fading channel, the fading attenuation should be compensated by more transmit power in SISO system or exploring cooperative diversity in MISO system. In both cases, more transmit energy consumption is required. It will be comparable to or even larger that analog circuitry consumption, An energy efficient consideration should make a tradeoff between the transmit energy consumption and the rest. By employing error control protocols, these could be reflected by the choices of error correction codes and the ARQ protocols. Therefore, in the analysis of this chapter, according to different channel conditions, we investigate the requirement on the error correction codes and their energy efficient implementation in error control protocols.

The remainder of this chapter is organized as follows. In section 5.2, we make a brief introduction to the error control schemes, including the types of error control codes and ARQ scheme, which will be considered in our works. In section 5.3, the energy consumption models of error control codes and analog circuitry are presented. In section 5.4, the basic ARQ protocol and hybrid ARQ protocols are discussed. In section 5.5, the performance of error control protocols are analysed.

5.2 Error Control Scheme

Error control scheme that employs error control code and automatic repeat request is the typical way, which could be used at the data link layer, to provide reliable wireless communication with lower transmit power. However, the ECC will introduce extra redundancy appended to the information data and the ARQ requires data retransmission, so their improvement on reducing transmit power comes at a cost of bandwidth efficiency. For the ECC, additional decoding complexity might deplete its energy efficiency as well. In order to explore the energy efficient implementation of the ECC and ARQ, a brief introduction to them are presented in the following.

5.2.1 Error Control Code

The error control codes introduce redundancy to the information data. The redundant information allows the decoder to detect or/and correct the transmission errors. We consider the ECC that only has the capability of detecting errors as the error detection code, and the ECC that can detect and correct errors as the error correction code. Considering the error correction code, the ability to correct errors in the received message means that, for the same SNR, a system using the error correction code over a noisy channel provides better BER performance than the uncoded system in most SNR region. It is a classic approach to lower the transmit power while maintaining the link reliability.

Sophisticated codes may provide better coding gain but require more complicated decoding algorithm, and need more power consumption at the decoding process. Therefore, when considering the implementation of error correction codes in wireless sensor networks, low complex codes would be advisable. In the most recent standard of IEEE 802.15.4 [5], only the error detection code is introduced in the data link layer. In our works, we examine one kind of error detection codes and two kinds of error correction codes as briefly introduced in the follows. More details about the fundamentals of these codes are referred in [80].

CRC

Cyclic redundancy check (CRC) is an error detecting scheme based on cyclic codes. Commonly, it is used to detect errors caused by the noise in transmission channels. The CRC codes can be constructed using the finite field GF(2), which has only two elements 0 and 1. It is obtained as the remainder of the polynomial division of the input sequence by the generator polynomial. As the length of the remainder is always less than that of the divisor, so we can change the length of CRC code by choosing the corresponding generator polynomial. A 16-bit CRC code is used in IEEE 802.15.4 standard [5] at the MAC sublayer. It is calculated by the following generator polynomial:

$$G_{16}(x) = x^{16} + x^{12} + x^5 + 1 \tag{5.1}$$

In our works, we also use this generator polynomial to generate the CRC sequence. If the recalculated CRC code does not match the received CRC code, the received

frame will be considered erroneous and additional procedures, which will be discussed later in this chapter, should be taken into account.

Hamming code

Hamming codes are a class of linear block codes devised for error correction. Generally, the encoding and decoding procedures of Hamming codes can be processed by linear operations and with little extra requirement on signal processing. Considering binary Hamming codes, for each integer $m \geq 3$, there is one type of Hamming codes with the codeword length of n and the data bits length of k. These parameters follow the relationship as $(n, k) = (2^m - 1, 2^m - m - 1)$. Hence, the code rate is given by $r = k/n$. The Hamming codes have a minimum distance $d_{min} = 3$, which means that they can detect $(d_{\min} - 1) = 2$ error bits, but correct $t = \left\lfloor \frac{1}{2}(d_{\min} - 1) \right\rfloor = 1$ error bit from a codeword.

Considering the Hamming code (n, k), if the received codeword has i errors, where $i > 1$, the decoder will decode it to an unexpected one which might have a maximum difference of $i + \left\lfloor \frac{1}{2}(d_{min} - 1) \right\rfloor = i + t$ bits to the original codeword. So we can get a maximum bound of the BER for the coded system in AWGN channel as [7]:

$$P_{eb} \leq \frac{1}{n} \sum_{i=t+1}^{n} (i + t) C_n^i P_e^i (1 - P_e)^{n-i} \tag{5.2}$$

where P_e is the uncoded BER of the binary symmetric AWGN channel but taking the code rate into account. Without considering higher order of the P_e, the coded BER in AWGN channel can be further approximated as:

$$P_{eb} \approx \frac{1}{n}(2t + 1) C_n^{t+1} P_e^{t+1} \tag{5.3}$$

Reed-Solomon code

Reed-Solomon codes are non-binary cyclic error-correcting codes. The codewords can also be constructed using the finite field GF(2). They are selected from an alphabet of 2^m symbols, from which m-bits information can be mapped into. Typ-

ically, a series of Reed-Solomon codes on m-bits symbols can be described by the parameters $(n, k) = (2^m - 1, 2^m - 1 - 2t)$, where n is the total number of codeword symbols, k is the number of information symbols and $2t$ is the number of the redundancy symbols. Therefore, this kind of Reed-Solomon code RS(n, k) has the capability of correcting t erroneous symbols.

When the received codeword is affected by a number of errors more than its error correction capability t, a codeword error is made. For the hard-decision decoder of Reed-Solomon codes, the corresponding symbol error probability in AWGN channel can be expressed as [7]:

$$P_{es} = \frac{1}{n} \sum_{i=t+1}^{n} iC_n^i P_m^i (1 - P_m)^{n-i} \tag{5.4}$$

where P_m is m-bits symbol error probability given as $P_m = 1 - (1 - P_e)^m$. If the symbols are converted to binary digits, the corresponding BER of the coded system in AWGN channel can be presented as:

$$P_{eb} = \frac{2^{m-1}}{2^m - 1} P_{es} \tag{5.5}$$

5.2.2 Automatic Repeat reQuest

ARQ is another error control scheme for data transmission. It makes use of acknowledgement and retransmission to achieve reliable data transmission. An acknowledgement is sent by the receiver and indicates to the transmitter that it has correctly received a data frame. Many sophisticated ARQ schemes have been proposed for packet retransmission in computer networks [81]. In this chapter, we consider the data transmission in wireless sensor networks is sporadic and the requirement on accuracy is stringent. So the simplest Wait-and-Go scheme might be more appropriate. It is specified in the standard of IEEE 802.15.4. In this scheme, the transmitter sends a packet and waits for its acknowledgement (ACK) before proceeding with the transmission of the next packet. The CRC is utilized to detect the transmission error. A correctly received packet will be acknowledged by the receiver. A packet is retransmitted if its ACK is not received within a certain time-out interval noted as the Round Trip Time (RTT). The retransmission will stop until the packet is either correctly received or the tries of retransmission is beyond a predetermined threshold. In our works, we consider the combination of

CRC and ARQ as the basic ARQ protocol. Furthermore, error correction codes will be incorporated and a few modification to the basic ARQ protocol will be taken into account in Hybrid ARQ schemes.

5.3 Energy Consumption Model

In order to explore the energy efficient communication in wireless sensor networks, energy consumption models for data transmission in the networks should be determined. In this chapter, we investigate the joint optimization of energy consumption on the physical layer and data link layer. Therefore, for communication link between sensor nodes, we consider the total energy consumption including the energy consumption of the baseband signal processing blocks, the analog circuitry and the radio transmission.

5.3.1 Baseband Codec

Nowadays, since the signal processing techniques applied on sensor nodes are not complicated, the energy consumption on those blocks are neglected in recent works. Whereas, as the development of digital integrated circuits and the extension of applications on wireless sensor networks, more complicated signal processing techniques (such as multiuser detection or adaptive equalization) might be feasible and preferable even on the tiny sensor nodes. In this case, the effect of energy consumption of the signal processing should be investigated. In addition, it is well-known that applying error correction codes reduces the transmit power with a given target BER probability to be met. However, some error correction codes might require complex algorithms on the decoder side. The effect of the extra decoding energy consumption should also be explored in the evaluation of the energy efficiency of error correction codes. Therefore, the effect of energy consumption on the signal processing blocks is interesting to be investigated. We note that, a common behaviour between the sophisticated signal processing techniques and the error correction codes is that more requirement on energy consumption results in better receiver performance. Hence, in our analysis, we consider the examples of error correction codes as a representation for the behaviour of baseband signal processing. We use the term *codec* as referred to the encoder and decoder of the error correction codes.

In the analysis of the energy efficiency of error correction codes, two modelling methods are usually employed. One is to consider the energy consumption on the encoding and decoding processes as proportional to the computational complexity of their algorithms. For example, in the Hamming code (n, k), the encoding and decoding processes can be accounted as linear operations of the related matrices. The energy consumption for the coding can be obtained as:

$$\begin{aligned} E_{enc} &= \tfrac{n(2k-1)}{k} E_{add} \\ E_{dec} &= \tfrac{(n-k)(2n-1)}{k} E_{add} \end{aligned} \tag{5.6}$$

For RS code (n, k), the model presented at [82] shows that the energy consumption can be calculated as:

$$\begin{aligned} E_{enc} &= \tfrac{2t}{m}(E_{mult} + E_{add}) \\ E_{dec} &= \tfrac{(4tn+10t^2)E_{mult}+(4tn+6t^2)E_{add}+3tE_{inv}}{m(n-2t)} \end{aligned} \tag{5.7}$$

where E_{add}, E_{mult} and E_{inv} are the energy consumption per bit of addition, multiplication and inversion. Assuming the digital process units of the encoder and decoder employ the technology of $0.18\mu m$ $2.5V$ CMOS as in [82], the energy consumption per m-bits for different operations can be characterized as in Table 5.1:

Table 5.1: Energy consumption per m-bits for different operations

E_{add}	$3.3 \times 10^{-2} m \quad \mu W/MHz$
E_{mult}	$3.7 \times 10^{-2} m^3 \quad \mu W/MHz$
E_{inv}	$3.3 \times 10^{-2}(2m-3)m^3 \quad \mu W/MHz$

Considering the models described by equations (5.6) and (5.7), Figure 5.1 (a) and (b) show the total energy consumption per bit considering both the encoding and decoding processes. As the encoding and decoding processes in Hamming code are much simpler, they consume much less energy than Reed Solomon codes do. Furthermore, another distinction has to be mentioned. We observe that the total energy consumption for the Hamming codes will increase as the code rate approaches to one, whereas the error correction capability is still one-bit error. We note that it is due to the property of block coding. For example, for Hamming code (31,26), each 26-bits block vector will be encoded and 31-bits block vector is

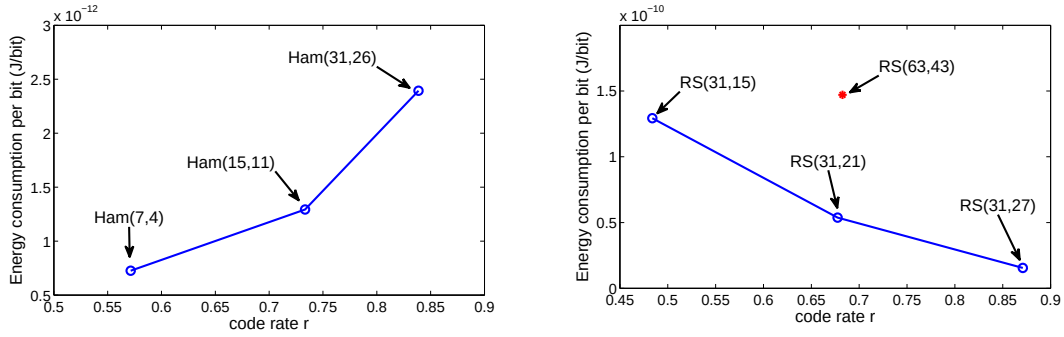

(a) (b)

Figure 5.1: Total energy consumption per bit for the encoding and decoding processes. (a) Hamming codes (b) Reed Solomon codes

to be decoded. The dimension of the encoding and decoding matrices are increased as compared to the Hamming code (7,4) and (15,11). Therefore, the coding complexity represented by equation (5.6) will intrinsically be increased. Although the Reed Solomon codes are not linear block codes as Hamming codes, the same phenomena can also be observed as we compare the total energy consumption of RS (31,21) and (63,43), which have similar code rate. So we may conclude that with longer codeword vector (as in Hamming codes) or larger mapping constellation (as in Reed Solomon codes), the operation of coding procedures will be increased and therefore the energy consumption might also be increased, if no additional optimization is applied. On the other hand, if we constrain the dimension of the mapping constellation in Reed Solomon, we observe that the coding energy consumption will decrease as the code rate increases. It is reasonable that lower the error correction capability can decrease the coding complexity and therefore the energy consumption.

Another modelling method to evaluate the energy consumption on the coding processes is to consider the power consumption at the digital CMOS logic, which is assumed to have dynamic and static power consumption. This method is considered in [83] to discuss the energy efficiency of the error correction codes. Typically, the dynamic power consumption of the CMOS logic can be modelled as $P_d \approx CV_{dd}^2 f$, where C is the total switched capacitance, V_{dd} is the power supply voltage and f is the operating frequency that is proportional to the codec throughput. The static power consumption part can be modelled as $P_s = I_{leak} V_{dd}$, which is due to the leakage current I_{leak}. Therefore, the total power consumption at the

CMOS logic can be evaluated as:

$$P_{codec} = P_d + P_s \approx CV_{dd}^2 f + I_{leak} V_{dd} \tag{5.8}$$

We note that this model does not differentiate the classes of error correction codes. The coding and decoding processes are enclosed in the CMOS logic. It could be a good experimental method to analyse the power consumption at the codec. In contrast, the first modelling method that we introduced before considers more about the algorithm complexity of different error correction codes. But its accuracy might be violated by the practical implementation or some hardware optimization. For example, parallel operation might be applied to long codeword, so the energy efficiency of the Hamming codes with longer codeword as shown in Figure 5.1a might be improved. Therefore, in our works, we don't use a specific model to evaluate the energy efficiency of error correction codes. Instead, we propose a general model that captures the coding energy consumption according to the code rate. The model can be expressed as:

$$Eb_{codec} = \Psi(r) \tag{5.9}$$

It is supposed to be applied to a heuristic evaluation on energy efficiency that helps for further design and implementation of error control codes.

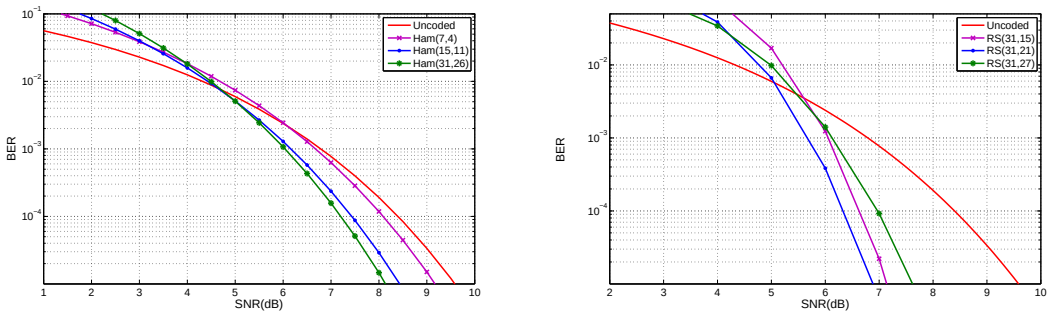

(a) (b)

Figure 5.2: BER performance for the error control codes in AWGN channel: (a)Hamming codes; (b) Reed Solomon codes.

Figure 5.2 (a) and (b) show the BER performance of the Hamming codes and

Reed Solomon codes in AWGN channel. We consider the achievable gain of error correction codes as the coding gain that can be expressed as:

$$G_{(dB)} = SNR_{U(dB)} - SNR_{C(dB)} \tag{5.10}$$

where SNR_U and SNR_C represent the required SNR for a common BER in the uncoded system and the coded system. For the same class of the error correction codes, different code rates will exhibit varied coding gain as shown in Figure 5.2. Therefore, for a class of error correction codes, the coding gain can be modelled as a variable according to the code rate, such as:

$$G = g(r) \tag{5.11}$$

We observe that, the coding gain will also vary at different BER performances as shown in Figure 5.2. In our works, we consider that the BER performance is predetermined during the system design. Thus, for a given BER performance, the coding gain is dominated by the specific error correction code. The effect of the BER on the coding gain will be neglected in the analysis. But we note that the energy efficient conditions obtained in section 5.5.4 should take the corresponding BER performance into account. In addition, considering the Rayleigh fading channel, as we will discuss in section 5.5, outage probability is utilized to analyse the communication performance. Then, for obtaining the coding gain in equation (5.10), the predetermined performance for uncoded and coded systems will be referred to as the outage probability other than the BER probability.

On the other hand, the error correction code with similar code rate can obtain different coding gain due to their coding complexities. More complex code is reasonable to exhibit higher coding gain at the same code rate. Hence, energy consumption model described by equation (5.9) and the available coding gain model in equation (5.11) should be jointly taken into account to capture the behaviours of the error correction codes. We note that the works in this chapter are not to specify the $\Psi(r)$ and $g(r)$ for the error correction codes, but to determine in what kind of condition that $\Psi(r)$ and especially $g(r)$ can make the communication energy efficient.

5.3.2 Transceiver Circuitry

For traditional wireless links where the transmission distance is large, the transmit energy dominates the total energy consumption. In wireless sensor networks, sensor nodes might be located in a short distance range. Then, the circuit energy consumption along the signal path is the major part as compared to the transmit energy consumption. So the energy consumption on the RF circuitry should be taken into account to explore energy efficient communication. In order to evaluate the energy consumption of analog circuits in the transceiver, the model presented in [84] will be used in our analysis. Figure 5.3 and Figure 5.4 present the general diagrams of the analog blocks at the transmitter and the receiver.

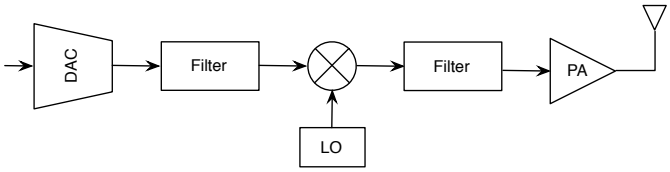

Figure 5.3: Analog circuit blocks for the transmitter

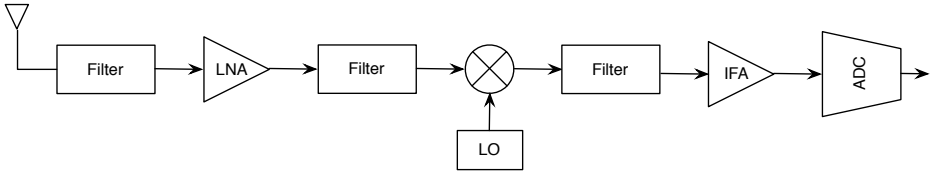

Figure 5.4: Analog circuit blocks for the receiver

According to the model in Figure 5.3, the energy consumption per bit at the analog blocks of the transmitter can be calculated from:

$$\begin{aligned} Eb_{tx} &= \frac{(P_T+P_{amp})}{R} + \frac{P_{ct}}{R} + \frac{P_{tr}T_{tr}}{L} \\ &= Eb_T + Eb_{ct} + Eb_{tr} \end{aligned} \tag{5.12}$$

where R is the transmit bit rate, L is the length of the packet in bits, T_{tr} is the time needed for a sensor to change from *sleep* mode to *awake* mode. Those power consumption values P_T, P_{amp} ,P_{ct} and P_{tr} are defined as follows:

P_T is the transmit power which should take antenna gain, channel condition, transmission distance, carrier frequency, requested BER and the modulation

scheme into account. It can be calculated by the link budget equation for BPSK modulation scheme as described in [7]:

$$P_{T(dBw)} = PL(d)_{(dB)} + E_b/N_{0(dB)} + R_{(dBHz)} - 204_{(dBW/Hz)} + M_{(dB)} \tag{5.13}$$

where $PL(d)$ is the path loss equation as stated in Chapter 4 section 4.5. E_b/N_0 is the received SNR that depends on the requested BER. When considering the error control protocols, it also depends on the applied error correction code. R refers to the transmit bit rate. M is the safety margin accounting for other attenuation and interference. -204 dBW/Hz is the typical value for the white noise spectrum density at the temperature $T_0 = 27^oC \approx 300K$. It is determined by $N_0 = k_B T_0$, with k_B is the Boltzmann's constant (1.38×10^{-23}W-s/K) and T_0 is the noise temperature in Kelvin.

P_{amp} is the power consumption at the power amplifier. It can be approximated by equation (5.11) as described in [84]:

$$P_{amp} = \alpha P_T \tag{5.14}$$

where $\alpha = \xi/\eta - 1$ with η the drain efficiency of the RF power amplifier and ξ the Peak-to-Average Ratio (PAR) which depends on the modulation scheme and the associated constellation size, for BPSK we take it as $\xi = 3\frac{\sqrt{2}-1}{\sqrt{2}+1} = 0.5147$ in [84]. Since the energy consumption at the amplifier is determined by the transmit power, we include the energy consumption of the amplifier into Eb_T to represent the energy consumption due to the transmit power.

P_{ct} is the power consumed by the other circuits at the transmitter, including the Digital-to-Analog Converter (DAC) (P_{DAC}), the transmit active filters (P_{filter_T}), the mixer (P_{mixer}) and the frequency synthesizer (P_{syn}):

$$P_{ct} = P_{DAC} + 2P_{filter\_T} + P_{mixer} + P_{syn} \tag{5.15}$$

P_{tr} is the power needed by the transmitter to switch from *sleep* mode to *awake* mode. As in this transient state, the most energy consumed component is the frequency synthesizer, P_{tr} can be approximated as equal to P_{syn}.

On the other side, according to the receiver model in Figure 5.4, the energy

consumption per bit at the RF of the receiver can be obtained easily as:

$$\begin{aligned} Eb_{rx} &= \frac{(3P_{filter\_R}+P_{LNA}+P_{mixer}+P_{IFA}+P_{ADC}+P_{syn})}{R} + \frac{P_{syn}T_{tr}}{L} \\ &= \frac{P_{cr}}{R} + \frac{P_{syn}T_{tr}}{L} = Eb_{cr} + Eb_{tr} \end{aligned} \tag{5.16}$$

where P_{cr} is the power consumed by the other circuits at the receiver. It comprises P_{filter_R}, P_{LNA}, P_{IFA}, P_{ADC} and P_{syn} which are respectively the power consumption at the receive active filters, the Low Noise Amplifier (LNA), the Intermediate Frequency Amplifier (IFA), the Analog-to-Digital Converter (ADC) and frequency synthesizer.

5.4 Error Control Protocols

5.4.1 Basic ARQ Protocol

The error control protocol that combines CRC and ARQ is specified in IEEE 802.15.4 standard at the MAC sublayer. In this protocol, the transmitter sends the packet with a request on the acknowledgement of successful reception. By checking the calculated checksum of CRC, the receiver sends an acknowledgement frame back to the transmitter if the packet is correctly received. Once this acknowledgement frame is received within the predefined duration, the transmission is considered successful, and no further action regarding retransmission should be taken. On the other hand, if the packet is not correctly received, no acknowledgement frame will be sent back to the transmitter. Therefore, if an acknowledgement for the original transmission is not received within the acknowledgement waiting duration, the transmitter should conclude that the previous transmission attempt has failed. If the maximum retry times for the retransmission is not attained, original packet will be retransmitted again. Otherwise, the transmitter assumes that the transmission has failed.

We assume that the CRC can detect all the transmission errors. If we allow infinite retries for the retransmission, the packet will make it through eventually. Denoting the packet error probability to be P_{epkt}, the packet will be received intact during the first transmission with the probability of $(1 - P_{epkt})$. Otherwise, it will be received correctly after n times retransmissions with the probability of $P_{epkt}^{n}(1 - P_{epkt})$. Therefore, without the limits on retransmission tries, the mean

times τ_0 required for a successful reception is:

$$\begin{aligned}\tau_0 &= (1 - P_{epkt}) + 2P_{epkt}(1 - P_{epkt}) + \cdots + nP_{epkt}^{n-1}(1 - P_{epkt}) + \cdots \\ &= 1 + P_{epkt} + P_{epkt}^2 + P_{epkt}^3 + \cdots + P_{epkt}^n + \cdots \\ &= \tfrac{1}{1-P_{epkt}}\end{aligned} \tag{5.17}$$

5.4.2 Hybrid ARQ Protocols

In addition to the error detection code, error correction codes are also used in Hybrid ARQ (HARQ) schemes. The HARQ schemes can exploit the advantage of ARQ and error correction codes to provide reliable communication. Using the redundancy of the error correction code, a few error bits in the reception sequence can be corrected. After that, error detection is processed to check the accuracy of the information data. In our works, we consider two hybrid ARQ schemes as discussed in the follows.

HARQ-I : The difference between the HARQ-I protocol and the basic ARQ protocol is that packet frames will be encoded with error correction codes in HARQ-I protocol. Therefore, similar to the classic ARQ protocol, the mean times τ_1 required for successful communication is:

$$\tau_1 = \frac{1}{1 - P_{epkt}^{(c)}} \tag{5.18}$$

where $P_{epkt}^{(c)}$ is the packet error rate for the coded packet frames. We note that the corresponding coding gain could lower the transmit power for the same packet error rate as compared to the uncoded system.

HARQ-II : As the redundancy of error correction codes could be appended systematically, such as Hamming codes and Reed-Solomon codes etc., the HARQ-II considers the retransmission only for the redundancy. Supposing one type of error control code (n,k) with the error correction capability of t error bits is used in HARQ-II, we consider the transmission of k-bits information as an example. If the k-bit information is corrupted during the first transmission try, only $(n - k)$ bit redundancy will be transmitted at the retransmission frame. On receiving the redundant frame, error correction decoding will be performed by combining with

the redundancy with the first received k-bits information. We consider this as coded combination. Considering the m-th retransmission redundancy, the combined n-bit codeword can be correctly decoded with the probability of:

$$\begin{aligned}\rho_m &= \sum_{i=1}^{t} P(i\ errors\ in\ the\ first\ k\ bits \\ &\qquad and\ no\ more\ than\ (t-i)\ errors\ in\ the\ redundant\ (n-k)\ bits) \\ &= \sum_{i=1}^{t} C_k^i (P_{e,1})^i (1-P_{e,1})^{k-i} \sum_{j=0}^{t-i} C_{n-k}^j (P_{e,m+1})^j (1-P_{e,m+1})^{n-k-j}\end{aligned} \tag{5.19}$$

where $P_{e,1}$ and $P_{e,m+1}$ are the BER performances for the first transmission and the m-th retransmission respectively. In AWGN channel, since the BER performances $P_{e,m+1}$ are identical for each retransmission redundancy, ρ_m could also be assumed to be identical. Extending this analysis to the whole packet frame, the combination of the first transmitted information sequence and the later retransmitted redundancy could be considered as equivalent to an once coded transmission. Then, the packet error rate $P_{epkt}^{(c)}$ for each coded combination could be assumed to be equal. Therefore, the mean transmission times for the HARQ-II protocol in AWGN channel can be approximated as:

$$\begin{aligned}\tau_2 &= (1-P_{epkt}) + 2P_{epkt}(1-P_{epkt}^{(c)}) + \cdots + nP_{epkt}(P_{epkt}^{(c)})^{n-2}(1-P_{epkt}^{(c)}) + \cdots \\ &= 1 + P_{epkt} + P_{epkt}P_{epkt}^{(c)} + P_{epkt}(P_{epkt}^{(c)})^2 + \cdots + P_{epkt}(P_{epkt}^{(c)})^n + \cdots \\ &= 1 + P_{epkt}\frac{1}{1-P_{epkt}^{(c)}} = \frac{1+P_{epkt}-P_{epkt}^{(c)}}{1-P_{epkt}^{(c)}}\end{aligned} \tag{5.20}$$

5.5 Performance Analysis

In this section, we will investigate the HARQ schemes in AWGN channel and Rayleigh fading channel respectively. We propose a cross layer optimization strategy by implementing SISO non-cooperative and MISO cooperative communication schemes. In order to make a choice between the SISO and MISO schemes, we compare their energy consumption in the following subsection.

5.5.1 Energy Consumption Comparison

The works in [1] have shown that cooperative MIMO communications are more energy efficient than SISO systems at long distance communication in Rayleigh fading channel. In order to analyse the energy efficiency of the HARQ schemes, we extend the works in [1] by investigating the energy consumption components in the sensor nodes. Furthermore, The AWGN channel and Rayleigh fading channel conditions will be considered respectively. In this subsection, since we try to investigate and compare the energy consumption components in SISO scheme and MISO scheme, we assume no ARQ protocol is employed, and the performance metric is the average BER of the total transmit packets.

We consider the MISO Alamouti scheme as a candidate cooperative scheme. It employs two cooperative transmit nodes and one receive node. Each of them is equipped with one antenna. Assuming the transmit power is equally allocated to the two transmit nodes, which are located at the same distance from the receive node, the average BER of the MISO Alamouti scheme in Rayleigh fading channel can be approximated as [7]:

$$P_e = \frac{3}{16}(\frac{\bar{E}_b}{N_0})^{-2} \tag{5.21}$$

where $\bar{E}_b/N_0$ is the average received SNR from one path in Rayleigh fading channel. On the other hand, taking the SISO communication in AWGN channel and in Rayleigh fading channel into account, the average BER of SISO communication in AWGN channel and Rayleigh fading channel can respectively be expressed as:

$$AWGN: \quad P_e = \tfrac{1}{2} erfc(\sqrt{\tfrac{E_b}{N_0}}) \tag{5.22}$$

$$Rayleigh \quad fading: \quad P_e = \tfrac{1}{4}(\tfrac{\bar{E}_b}{N_0})^{-1} \tag{5.23}$$

where E_b/N_0 is the received SNR in AWGN channel. Considering equation (5.13), the corresponding transmit power P_T for a given BER performance can be deduced according to equations (5.21), (5.22) and (5.23) in different scenarios.

Therefore, the total energy consumption per information bit for one transmission can be summarized as:

$$
\begin{aligned}
Eb &= \frac{(1+\alpha)P_T}{R} + \frac{M_T P_{ct} + M_R P_{cr}}{R} + \frac{(M_T + M_R)P_{syn}T_{tr}}{L} \\
&= Eb_T + M_T Eb_{ct} + M_R Eb_{cr} + (M_T + M_R)Eb_{tr}
\end{aligned}
\tag{5.24}
$$

We note that, in MISO Alamouti scheme, P_T is used to represent the total transmit power of the cooperative nodes. In addition, except for the power amplifier, we assume that the power consumption P_{ct} and P_{cr} at the analog circuitry are quasi invariant for a given transmit bit rate. Therefore, employing the system parameters as shown in Table 5.2 and considering the parameters of transmit bit rate as 250 *kbps*, the required BER as 10^{-3} and the packet length L as 100 *bits*, the comparison of total energy consumption for SISO and MISO Alamouti communication is shown in Figure 5.5. Since the advantage of MISO Alamouti scheme is the capability of eliminating fading degradation and it has no extra benefits in AWGN channel, so it is only considered for Rayleigh fading channel in our analysis.

Table 5.2: System parameters[1]

$P_{DAC} = 15mW$	$P_{syn} = 50mW$
$P_{ADC} = 7mW$	$P_{LNA} = 20mW$
$P_{filter\_T} = P_{filter\_R} = 2.5mW$	$P_{IFA} = 3mW$
$P_{mixer} = 30.3mW$	$T_{tr} = 5\mu m$
$\eta = 0.35$	$M = 40dB$

Figure 5.5 shows that MISO Alamouti scheme consumes less total energy than SISO scheme when the distance between the transmitter and receiver is larger than a threshold value in Rayleigh fading channel. This observation coincides with the analysis in [1]. Furthermore, we notice that, for MISO scheme in Rayleigh fading channel, the growth of the total energy consumption increases smoothly as the distance become larger. The same phenomena can also be observed for SISO scheme in AWGN channel. The reason for that can be explained in Figure 5.6 where we consider the ratio of energy consumption Eb_T to the total energy consumption expressed as:

$$
\varepsilon = \frac{Eb_T}{Eb_T + M_T Eb_{ct} + M_R Eb_{cr} + (M_T + M_R)Eb_{tr}} \tag{5.25}
$$

It shows that, for SISO scheme in AWGN channel and MISO scheme in Rayleigh fading channel, the required transmit energy increases slowly and accounts for a

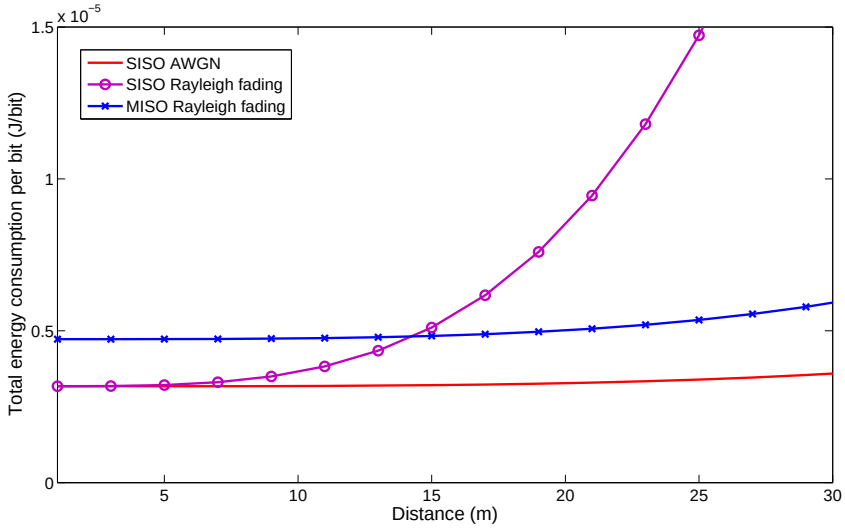

Figure 5.5: Total energy consumption per bit for communication in different distances, with BPSK, $R = 250kbps$, $P_e = 10^{-3}$ and $L = 100bits$

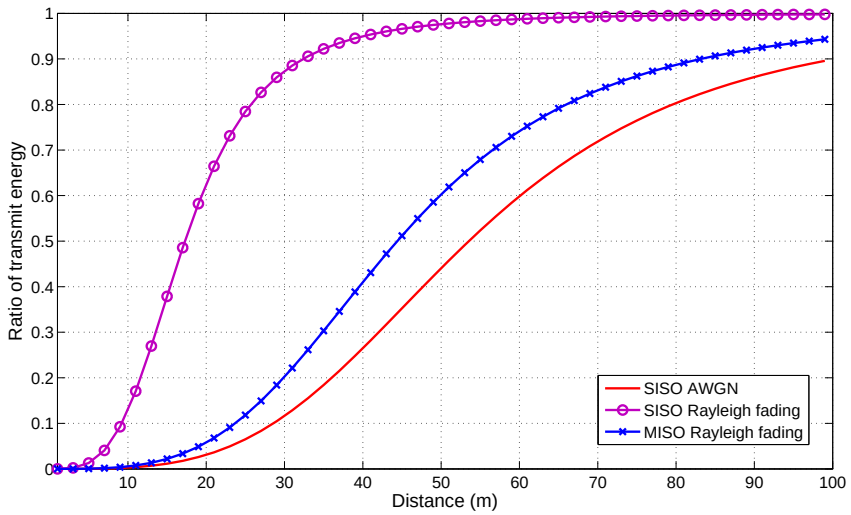

Figure 5.6: Ratio of transmit energy to total energy consumption for communication in different distances, with BPSK, $R = 250kbps$, $P_e = 10^{-3}$ and $L = 100bits$

small ratio (less than 0.1) in the total energy consumption for the distance less than 20 meters. In this region, the energy consumption on the circuitries dominates the total energy consumption. So the increase of total energy consumption is stable in Figure 5.5. On the other hand, when the communication distance increases, the required transmit power becomes larger and the ratio of the transmit energy to total energy increases fastest in the SISO scheme of Rayleigh fading channel. It approaches to one when the distance is larger than 50 meters. Therefore, in Rayleigh fading channel, the SISO scheme consumes much more transmit energy than the MISO Alamouti scheme. The MISO Alamouti scheme is more energy efficient when the saving of the transmit energy exceeds the extra circuit energy consumption.

In Figure 5.5 and Figure 5.6, we fixed the transmit bit rate and the packet length. Whereas, equation (5.24) shows that increasing the transmit bit rate or the packet length can lower the energy consumption per bit on the circuitry or at the transient state, but the transmit energy per bit will not change for a given BER. Consequently, the saving of the transmit energy by MISO Alamouti scheme can easily surpass the extra circuit energy consumption. Hence, the threshold distance where the energy efficiency of the MISO scheme outperforms the SISO scheme in Rayleigh fading channel will decrease. As shown in Figure 5.7, the more the transmit bit rate or the packet length is, the less the threshold distance will be.

In the deployment of wireless sensor networks, the sensor nodes could be located with little obstacle in the near distance region where AWGN channel is usually assumed, or with many scatters in the far distance region where Rayleigh fading channel is more applicable. As we have discussed in the previous analysis, SISO scheme consumes less energy on the analog circuitry and could be energy efficient in AWGN channel, while the MISO scheme is more energy efficient beyond the threshold distance in Rayleigh fading channel. Therefore, in the following analysis, we consider the SISO scheme in short distance communication (for example less than $20m$) with AWGN channel, and MISO scheme in relative long distance (larger than $20m$) communication with Rayleigh fading channel.

5.5.2 SISO System in AWGN Channel

For the communication in the short distance, AWGN channel among the nodes is practical and SISO scheme is more appropriate. In this case, the packet error

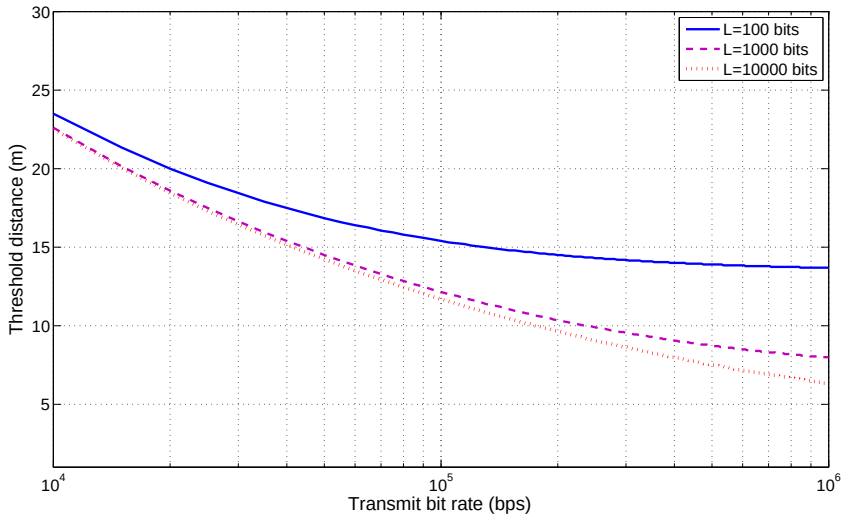

Figure 5.7: Threshold distance of energy efficiency by comparing the SISO scheme with the MISO Alamouti scheme in Rayleigh fading channel

probability for a packet with L bits length can be given as:

$$P_{epkt} = 1 - (1 - P_e)^L \tag{5.26}$$

Considering the basic ARQ protocol, the average times τ_0 required for a successful reception can de determined by equation (5.17). Then, the energy consumption per bit for the transmission in basic ARQ protocol can be expressed as:

$$\begin{aligned} Eb_0 &= \tau_0 \left(\frac{P_T^u + P_{amp}^u + P_{ct} + P_{cr}}{R} \right) + \frac{2P_{tr}T_{tr}}{L} \\ &= \tau_0 \frac{P_T^u}{R\beta_{1,1}} + \frac{2P_{tr}T_{tr}}{L} \qquad with \quad \beta_{i,j} = \frac{P_T^u}{P_T^u + P_{amp}^u + iP_{ct} + jP_{cr}} \end{aligned} \tag{5.27}$$

where $\beta_{i,j}$ is the ratio of the transmit power to the total power consumption for each frame transmission in a system of i transmitters and j receivers. For example, employing the system parameters as shown in Table 5.2, Figure 5.8 (a) and (b) show the total energy consumption per bit and average transmission times by the basic ARQ protocol. We change the separation distance of d=[5m, 10m, 20m]. The minimum energy consumption points appear at the transmit power around -5dBm, 5dBm, and 15dBm. Figure 5.8b shows that at those transmit power, the average

transmission times all approach to one. So it shows that less retransmissions might be preferable to obtain the minimum energy consumption. The reason is that power consumption on the analog circuitry dominates the total power consumption in those cases as shown in Figure 5.9. For a separation distance less than $20m$, the ratio of the optimal transmit power to the total power consumption is almost less than 0.1 by considering the basic ARQ protocol is applied. Therefore, when considering the error control protocols in the SISO AWGN scenario, we should give more consideration to reduce the energy consumption on the analog circuitry and hence reduce the number of average transmission times.

5.5.3 Cooperative System in Rayleigh Fading Channel

Considering the Rayleigh fading channel, the packet error probability expressed by equation (5.26) is valid only if perfect interleaving is applied to the transmission sequences and each information bit fades independently. Since in our works, we assume independent fading on each packet, the perfect interleaving is not feasible considering the low data traffic of wireless sensor networks. Therefore, as stated in [85], we interpret the outage probability at certain bandwidth efficiency Φ as the representation of the packet error rate. Then for the basic ARQ protocol, the mean transmission times in Rayleigh fading channel could be given as:

$$\tau_0 = \frac{1}{1 - P_{epkt}} = \frac{1}{1 - P_{out}(\Phi)} \tag{5.28}$$

where the outage probability $P_{out}(\Phi)$ for the MISO Alamouti scheme is expressed as:

$$P_{out}(\Phi) = Prob\left\{\log_2\left(1 + \frac{\bar{E}_b}{2N_0}(|a_1|^2 + |a_2|^2)\right) < \Phi\right\} \tag{5.29}$$

For Rayleigh fading channel, the channel strengths of two cooperative paths are independent exponentially distributed with $E[|a_1|^2] = E[|a_2|^2]$, the outage probability can be given according to equation (1.22) in Chapter 1 as:

$$P_{out}(\Phi) = 1 - (1 + \gamma)e^{-\gamma} \quad with \quad \gamma = 2\frac{2^{\Phi}-1}{\bar{E}_b/N_0} \tag{5.30}$$

Figure 5.10 shows the case of transmitting $L = 100bits$ or $L = 1000bits$ packet frame in Rayleigh fading channel by MISO Alamouti scheme. It shows that, for

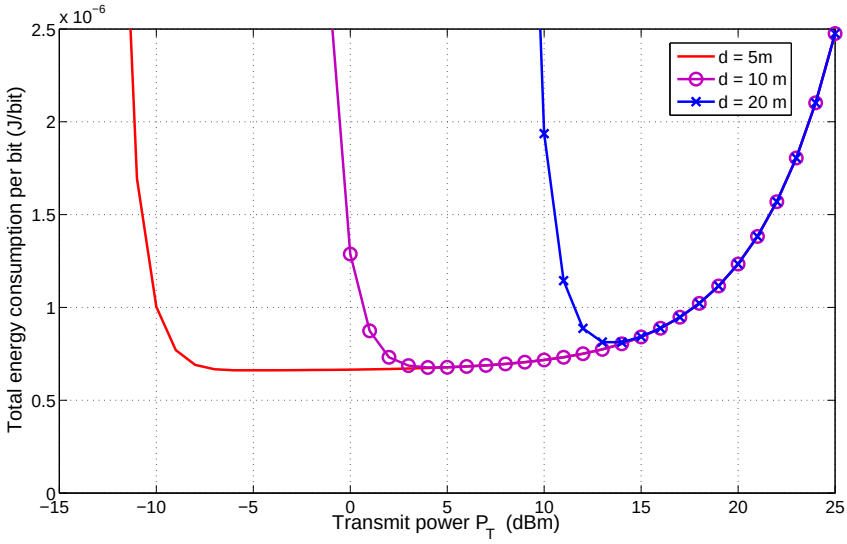

(a)

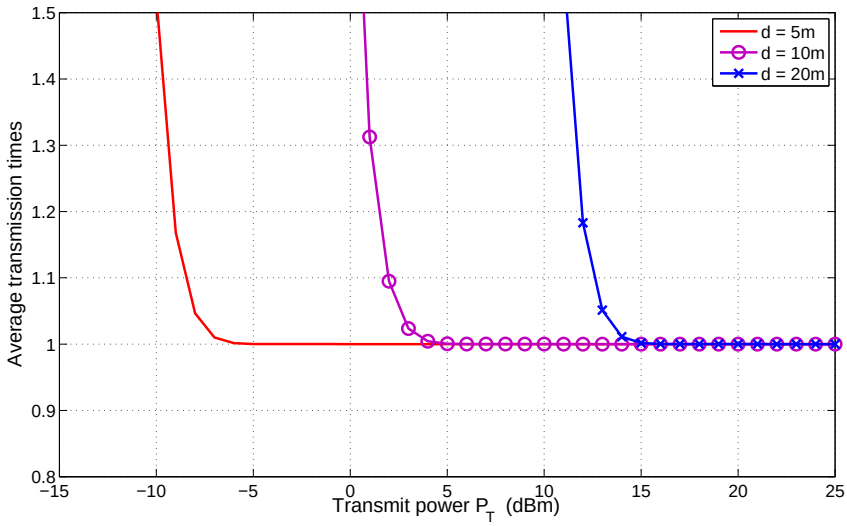

(b)

Figure 5.8: Performance of basic ARQ protocol in AWGN channel by SISO: (a) total energy consumption per bit (b)average transmission time required for a successful reception; with BPSK, $R = 250kbps$ and $L = 100bits$

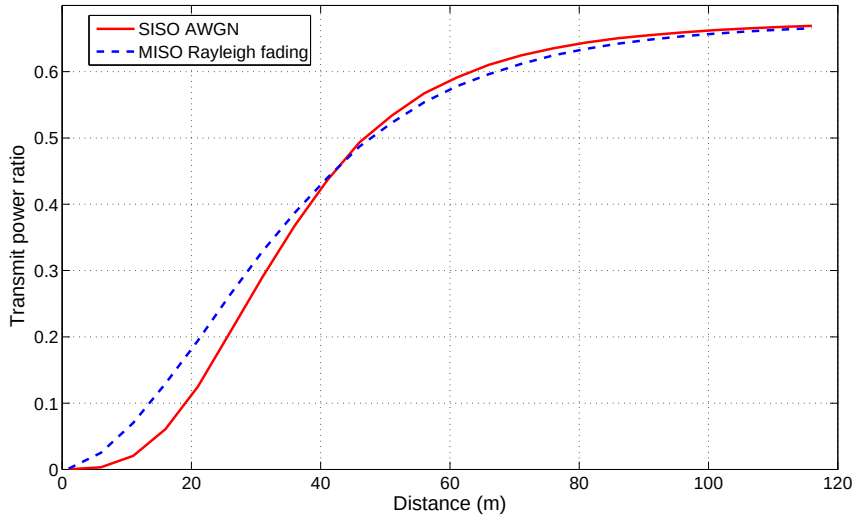

Figure 5.9: Ratio of optimal transmit power to total power consumption for basic ARQ protocol in SISO AWGN channel and MISO Rayleigh fading channel, with BPSK, $R = 250kbps$, and $L = 100bits$

both of the frame length, wide gaps exist between the theoretical results assuming perfect interleaving and the simulated packet error rate without interleaving. On the other hand, by choosing appropriate parameter Φ, the outage probability can represent the packet error rate with good precision. We note that the parameter Φ could be decided in advance according to the length of the packet frame. For example, taking Φ equals to 2, the outage probability matches well with the simulated packet error rate with $L = 100bits$. While for the frame length with 1000 *bits*, Φ equals to 2.6 would be appropriate.

Considering the basic ARQ protocols, the total energy consumption per bit for the transmission in Rayleigh fading channel by MISO Alamouti scheme can be given as:

$$\begin{aligned} Eb_0 &= \tau_0 \left(\frac{P_T^u + P_{amp}^u + M_T P_{ct} + M_R P_{cr}}{R} \right) + \frac{(M_T + M_R) P_{tr} T_{tr}}{L} \\ &= \tau_0 \frac{P_T^u}{R \beta_{M_T, M_R}} + \frac{(M_T + M_R) P_{tr} T_{tr}}{L} \qquad with \quad \beta_{M_T, M_R} = \frac{P_T^u}{P_T^u + P_{amp}^u + M_T P_{ct} + M_R P_{cr}} \end{aligned} \tag{5.31}$$

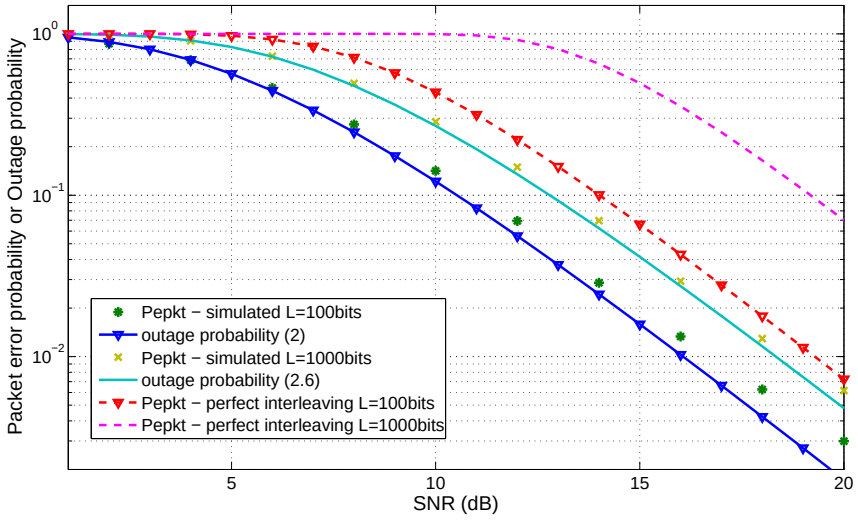

Figure 5.10: The relation between the packet error probability and the outage probability, in outage probability(2): $\Phi = 2$; in outage probability(2.6): $\Phi = 2.6$.

where τ_0 is determined according to equation (5.30). Figure 5.11a shows the energy consumption at a transmission distance of 60 meters. We notice that by increasing the packet length to 1000 bits, the minimum total energy consumption will also increase. Because in this MISO Rayleigh fading scenario, more transmit power should be allocated to provide a comparable packet error rate as shown in Figure 5.10. Furthermore, Figure 5.11 (a) and (b) show that the optimal mean transmission times obtaining the minimum energy consumption approach to 2 at the SNR around 6dB and 8dB for the two packet lengths.

As shown in Figure 5.9, in the MISO Rayleigh fading scenario, the transmit power consumption will dominate the total power consumption for the long distance transmission. By applying the basic ARQ protocol, the transmit power consumption will surpass the other circuitry power consumption at a separation distance larger than $50m$ where the optimal transmit power ratio is larger than 0.5. To the extreme case of $\beta_{M_T,M_R} \approx 1/(1+\alpha)$ where the power consumptions at the analog circuitry and the transient state are trivial, the total energy consumption per bit can be approximated as:

$$Eb_0 \approx \tau_0 \left(\frac{P_T^u + P_{amp}^u}{R} \right) \approx \frac{(1+\alpha)}{(1-P_{out}(\Phi))R} P_T^u \quad with \quad P_T^u >> M_T P_{ct} + M_R P_{cr} \qquad (5.32)$$

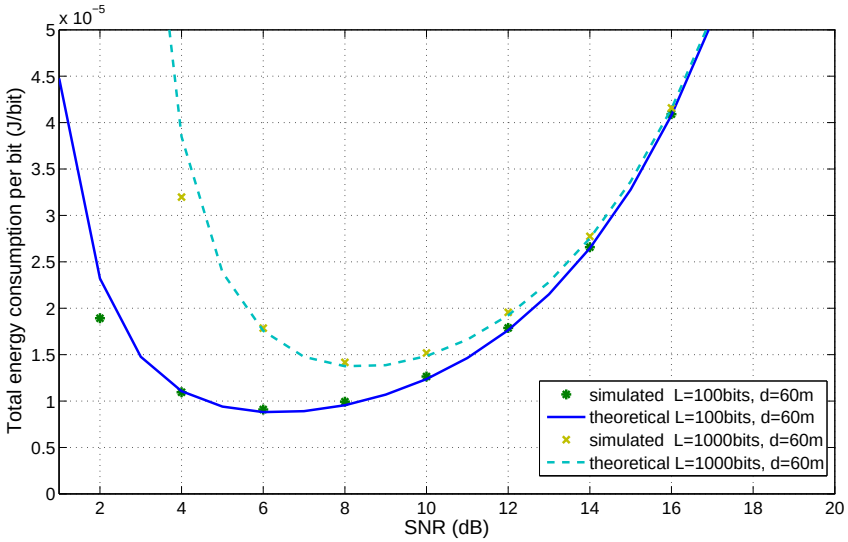

(a)

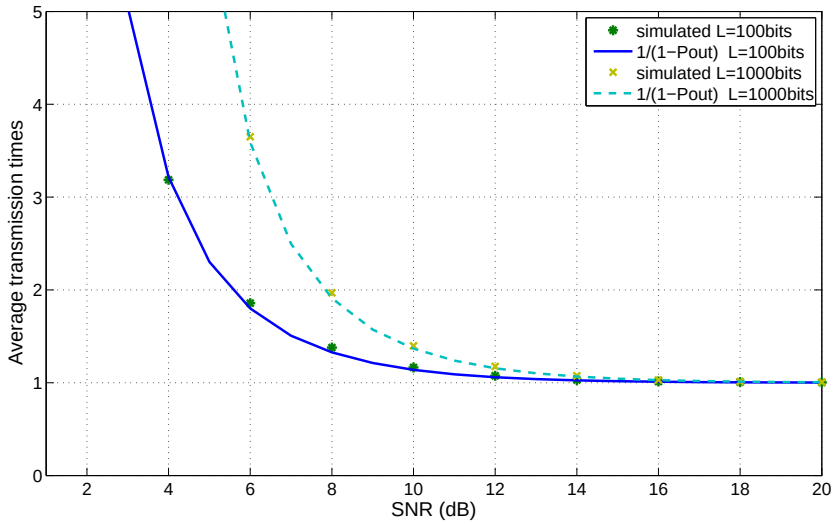

(b)

Figure 5.11: Performance of basic ARQ protocol in Rayleigh fading channel by MISO Alamouti scheme: (a) total energy consumption per bit; (b) average transmission time required for a successful reception; with BPSK, $R = 250kbps$

The function of total energy consumption Eb_0 is easily shown to be convex on the transmit power P_T^u. Therefore, the optimal transmit power can be determined by considering the partial differential equation of:

$$\begin{aligned}\frac{\partial Eb_0}{\partial P_T^u} &= \frac{\partial}{\partial P_T^u}\left(\frac{(1+\alpha)}{(1+\gamma)e^{-\gamma}R}P_T^u\right) \\ &= \frac{\partial}{\partial P_T^u}\left(\frac{(1+\alpha)}{\left(1+2(2^{\Phi}-1)N_0R\cdot PL(d)/P_T^u\right)e^{-2(2^{\Phi}-1)N_0R\cdot PL(d)/P_T^u R}}P_T^u\right) = 0\end{aligned} \tag{5.33}$$

Then, the optimal transmit power or optimal expected SNR for long distance communication can be given as:

$$(P_T^u)_{opt} = (\sqrt{5}-1)(2^{\Phi}-1)N_0R\cdot PL(d) \;\Rightarrow\; \left(\frac{\bar{E}_b}{N_0}\right)_{opt} = (\sqrt{5}-1)(2^{\Phi}-1) \tag{5.34}$$

Considering equations (5.28) and (5.30), the optimal mean transmission times can also be determined as:

$$\tau_{opt} = \frac{1}{(1+2\frac{2^{\Phi}-1}{(\bar{E}_b/N_0)_{opt}})e^{-2\frac{2^{\Phi}-1}{(\bar{E}_b/N_0)_{opt}}}} = \frac{1}{(1+\frac{2}{\sqrt{5}-1})e^{-2\frac{2}{\sqrt{5}-1}}} \approx 1.93 \tag{5.35}$$

It shows that packet retransmission is expected in this extreme case. According to equation (5.28), the expectation of packet retransmission means that larger outage probability is presented as compared to less expectation on packet retransmission. Hence, lower transmit power is utilized at the price of more packet retransmission. Since transmit energy consumption dominates the total energy consumption in this scenario, decreasing the transmit power is reasonable to be energy efficient.

5.5.4 Energy Efficiency of Hybrid ARQ Protocols

In the hybrid ARQ protocols, error correction codes will be applied. They bring the coding gain but at a cost of decreasing the bandwidth efficiency. Hence, more

energy consumption on the analog circuitry is required at the same transmit bit rate. The energy efficiency of employing hybrid ARQ protocols should be investigated. We note that optimizing the transmit bit rate could help to eliminate the effect of energy consumption on analog circuitry. Whereas, changing the bit rate will also alter the ratio of the transmit power $\beta_{i,j}$. Since in our works, we try to analyse the energy efficiency by considering the effect of power consumption on analog circuitry, so the ratio of the transmit power to the total power consumption will be primarily taken into account and we will not consider the optimization of the transmit bit rate. But we mention that our works can be extended to optimize the transmit bit rate if we consider that the ratio $\beta_{i,j}$ changes with the transmit bit rate. Therefore, in the following analysis, we only consider that the bit rate is constant and equals to 250 *kbps* which is the largest bit rate in current IEEE standard [5] for wireless sensor networks.

SISO AWGN scenario

As shown in Figure 5.8a, the average transmission times for optimal energy consumption approaches to one in the SISO AWGN scenario. The BER should be already low enough for the optimal transmission. So the main purpose of applying error correction codes is not to decrease the communication BER, but to reduce the possibility of retransmission requirement. On the other hand, the energy consumption of analog circuitry dominates the total energy consumption in this scenario, so the energy efficient implementation of error control codes should satisfy that the reduced transmit energy can compensate the extra energy consumption of the redundant sequence and the codec. As a result, when we consider the schemes of the different HARQ protocols in AWGN channel, we assume that the retransmission, if it is required, at least could maintain the same BER performance as the first try.

Specifically, in HARQ-I, since the coded sequence will be transmitted at the first try and also during the required retransmissions. The BER performance can be obtained as equal to the basic ARQ protocol by choosing an appropriate transmit power. The coding gain expressed in equation (5.10) can be represented as:

$$G = \frac{E_b^u}{E_b^c} = \frac{P_T^u}{P_T^c}\frac{R_c}{R_u} = \frac{P_T^u}{rP_T^c} \tag{5.36}$$

where E_b^u and E_b^c are the required signal energy per bit to maintain the same BER performance. P_T^u and P_T^c represent the according transmit powers by assuming the uncoded and coded systems have the same bandwidth efficiency, that is the transmit bit rates for the uncoded and coded systems have the relation of $R_u = rR_c$.

In HARQ-II, the incremental redundancy will be transmitted only on the request for retransmission. The BER performances of the first transmission sequence and the combined coded sequence are not easy to keep the same. Considering the previous analysis of basic ARQ protocol, packet retransmission is seldom required in SISO AWGN scenario on the view of energy efficiency. Hence, it is reasonable that the retransmission of incremental redundancy happens with little occasion. Therefore, we assume that the transmit bit rates of the first transmission and the retransmission are the same. It is obvious that the BER performance of the coded combining sequence is better than the first transmission sequence. The transmit power for retransmission of incremental redundancy can be determined by the coding gain corresponding to equation (5.10) as:

$$G = \frac{E_b^u}{E_b^c} = \frac{P_T^u}{P_T^c}\frac{R_c}{R_u} = \frac{P_T^u}{P_T^c} \tag{5.37}$$

Therefore, according to the previous discussion, the HARQ-I protocol is supposed to obtain the same BER performance as the basic ARQ protocol, while the HARQ-II protocol is supposed to obtain better BER performance. Since the transmission errors happen independently in AWGN channel, the packet error rate is determined by equation (5.26). Considering equations (5.17), (5.18) and (5.20), the average transmission times for different protocols satisfies:

$$\tau_0 = \tau_1 > \tau_2 \tag{5.38}$$

As the relation between the transmit power for the uncoded transmission and the coded transmission are determined by equations (5.36) and (5.37) in HARQ-I and HARQ-II, hence, in the SISO AWGN scenario, the energy consumption per bit by employing these protocols can be expressed as:

HARQ-I :

$$\begin{aligned} Eb_1 &= \tau_1 \left(r \frac{P_T^c + P_{amp}^c + P_{ct} + P_{cr}}{R} + Eb_{codec} \right) + \frac{2P_{tr}T_{tr}}{L} \\ &= \tau_0 \left(\left(\frac{1+\alpha}{Rg(r)} + r \frac{1-(1+\alpha)\beta_{1,1}}{R\beta_{1,1}} \right) P_T^u + \Psi(r) \right) + \frac{2P_{tr}T_{tr}}{L} \end{aligned} \tag{5.39}$$

HARQ-II :

$$\begin{aligned} Eb_2 &= \frac{P_T^u + P_{amp}^u + P_{ct} + P_{cr}}{R} + (\tau_2 - 1) \left(\frac{(1-r)}{r} \frac{P_T^c + P_{amp}^c + P_{ct} + P_{cr}}{R} + Eb_{codec} \right) + \frac{2P_{tr}T_{tr}}{L} \\ &< \frac{P_T^u}{R\beta_{1,1}} + (\tau_0 - 1) \left(\frac{(1-r)}{r} \left(\frac{1+\alpha}{Rg(r)} + \frac{1-(1+\alpha)\beta_{1,1}}{R\beta_{1,1}} \right) P_T^u + \Psi(r) \right) + \frac{2P_{tr}T_{tr}}{L} \end{aligned} \tag{5.40}$$

MISO Rayleigh fading scenario

In the MISO Rayleigh fading scenario, the energy efficient application of error control codes should also satisfy the condition that, the reduced transmit energy for obtaining the same optimal outage probability can compensate the extra energy consumption on the redundant sequence and the codec. In addition, as we have mentioned that, since the transmit power dominates the total transmit power in this scenario, the opportunistic of one successful transmission by employing a lower transmit power could be profitable. So the HARQ-I protocol, which can reduce the required transmit power as shown in equation (5.36), would be more preferable. Therefore, we only consider HARQ-I in the MISO Rayleigh fading scenario.

Considering the energy consumption per bit by employing the HARQ I protocol, the expression can be obtained as:

HARQ-I :

$$\begin{aligned} Eb_1 &= \tau_1 \left(r \frac{P_T^c + P_{amp}^c + M_T P_{ct} + M_R P_{cr}}{R} + Eb_{codec} \right) + \frac{(M_T + M_R)P_{tr}T_{tr}}{L} \\ &= \tau_0 \left(\left(\frac{1+\alpha}{Rg(r)} + r \frac{1-(1+\alpha)\beta_{M_T,M_R}}{R\beta_{M_T,M_R}} \right) P_T^u + \Psi(r) \right) + \frac{(M_T + M_R)P_{tr}T_{tr}}{L} \end{aligned} \tag{5.41}$$

It has similar expression to equations (5.39) but with differences on the ratio $\beta_{i,j}$ and the energy consumption on the transient state. At the same time, we note that the average transmission times τ_i in the MISO Rayleigh fading scenario is

determined by the outage probability, and the $g(r)$ is referred to as the coding gain of maintaining the same outage probability.

Furthermore, we have to mention that, in the case where the transmit energy consumption is comparable to the energy consumption on the analog circuitry, the optimal implementation of error controls might also try to reduce the transmit power at the same time of decreasing the average transmission times. Our consideration of maintaining the outage probability provides an upper bound of the condition that the HARQ protocols can be more energy efficient.

Therefore, these HARQ protocols can be more energy efficient than the basic ARQ protocol if the following condition is satisfied:

$$\Delta Eb_i = Eb_0 - Eb_i > 0 \tag{5.42}$$

Specifically, for each HARQ protocols, the conditions are given as:

HARQ-I :

$$\Delta Eb_1 = \tau_0 \left[(1+\alpha) \left(rg(r) - 1 \right) \beta_{i,j} + (1-r)g(r) - g(r)\beta_{i,j}\Psi(r)R/P_T^u \right] > 0 \tag{5.43}$$

HARQ-II :

$$\Delta Eb_2 = (\tau_0 - 1) \left[(1+\alpha) \left(1-r \right) \left(g(r) - 1 \right) r\beta_{i,j} + r^2 g(r) - rg(r)\beta_{i,j}\Psi(r)R/P_T^u \right] > 0 \tag{5.44}$$

We notice that, the parameters τ_0 or $\tau_0 - 1$ will only affect the amount of energy savings by the two protocols. Therefore, eliminating the effect of the parameters τ_0 or $\tau_0 - 1$, the general conditions for the protocols to be more energy efficient than basic ARQ are:

HARQ-I :

$$\begin{gathered} g(r) > \frac{(1+\alpha)\beta_{i,j}}{(1+\alpha)r\beta_{i,j} + (1-r) - \beta_{i,j}\Psi(r)R/P_T^u} \approx \frac{(1+\alpha)\beta_{i,j}}{(1+\alpha)r\beta_{i,j} + (1-r)} \\ with \quad (1+\alpha)r\beta_{i,j} + (1-r) - \beta_{i,j}\Psi(r)R/P_T^u > 0 \end{gathered} \tag{5.45}$$

HARQ-II :

$$g(r) > \frac{r(1-r)(1+\alpha)\beta_{i,j}}{r(1-r)(1+\alpha)\beta_{i,j}+r^2-r\beta_{i,j}\Psi(r)R/P_T^u} \approx \frac{(1+\alpha)\beta_{i,j}}{(1+\alpha)\beta_{i,j}+r/(1-r)}$$
$$with \quad r(1-r)(1+\alpha)\beta_{i,j} + r^2 - r\beta_{i,j}\Psi(r)R/P_T^u > 0 \tag{5.46}$$

The two equations provide the requirements on the coding gain to make the employed error control code be energy efficient. Considering the power consumption at the codec ($R\Psi(r)$) is usually much less than P_T^u, the component $\beta_{i,j}\Psi(r)R/P_T^u$ in equations (5.45) and (5.46) is reasonable to be omitted. As we have stated, for the short distance communication less the $20m$, power consumption on the analog circuitry dominates the total power consumption in AWGN channel. So $\beta_{i,j} < 0.1$ is assumed to be satisfied in this case as shown in Figure 5.9. Then, the condition expressed in equation (5.45) requires more coding gain than in equation (5.46). Therefore, the HARQ-II protocol is more easier to be energy efficient in the SISO AWGN scenario.

5.6 Summary

In this chapter, we consider the energy efficiency of three error control protocols in wireless sensor networks. Two scenarios: SISO AWGN for short distance communication and MISO Rayleigh fading for long distance communication are considered in our analysis. In the SISO AWGN scenario, since energy consumption on analog circuitry dominates the total energy consumption, less retransmission is expected. As the HARQ-II protocol transmits the redundancy only when it is necessary, so it shows to be easier to be energy efficient than the others. On the other hand, in the MISO Rayleigh fading scenario, due to the channel fading and relative long separation distance, more transmit power is required. A tradeoff between less transmit power and more retransmission expectation by employing HARQ-I protocol could be made. In this case, we propose the thresholds of the coding gain for various code rates to make the HARQ-I protocol more energy efficient.

Chapter 6

Conclusions

Due to the benefits from virtual multiple antennas, cooperative communication schemes provide good performance on energy efficiency in hostile fading channel condition. The aim of this dissertation was to explore the energy efficient and low complex implementation of cooperative schemes in wireless sensor networks.

In order to reveal the advantage of virtual multiple antennas system, we evaluated the capacity of ergodic Rayleigh fading channel and outage probability in block Rayleigh fading channel for MIMO system in Chapter 1. Although multiple receive antennas could further improve the system, it increases the transceiver complexity, which is not practical for the sensor nodes that are normally equipped with one antenna. Considering the requirement on simple and flexible deployment, we focused on the virtual multiple transmit antennas system in this dissertation. In Chapter 2, various cooperative schemes are discussed. They are implemented either in physical layer or in network layer. Physical layer cooperative communication schemes were the most consideration in our works. We considered the distributed time synchronization problem, power allocation scheme and error control protocol in the application of these cooperative schemes. In the most parts of our works, we focused on the energy efficient implementation of cooperative communications.

The contribution of this dissertation can be summarized as:

- We analysed the synchronization requirement on the virtual MISO cooperative communication, which is based on the Alamouti code. Although signal arrival time synchronization is required for this cooperative scheme, a slight

synchronization error has little effect on the reception performance. Knowing the effect of the synchronization error, we proposed a physical layer synchronization scheme for the virtual MISO cooperative communication in wireless sensor networks. The proposed scheme is adequate while introduces less complexity to the network design. A maximum likelihood method has been proposed for the synchronization error estimation in the reception of cooperative data. It shows better performance even with shorter synchronization sequence. The decision matrix can be pre-calculated and reused in the process of synchronization error estimation before Alamouti decoding. We also considered two strategies after synchronization error estimation. Better BER performance is obtained even in the existence of an initial synchronization error between the two cooperative transmit nodes. Our proposed time synchronization scheme provides better BER performance in the existence of initial synchronization error.

- We proposed the optimal power allocation strategies for AF cooperative relaying scheme and virtual MISO cooperative scheme in wireless sensor networks. With a given requirement on BER performance, they help to minimize the total transmit power in Rayleigh fading channel. The approximated power allocation for each node can be calculated in analytical way and agrees the precise result obtained in numerical way. Moreover, without direct link between the source and destination nodes, we proposed two energy efficient solutions to incorporate the AF cooperative relaying scheme and virtual MISO cooperative scheme. The optimal power allocation strategies are applied at different stages of the cooperation. We compared their performances on the horizontal symmetric topology and diagonal symmetric topology. A heuristic policy to select the cooperative nodes and choose the appropriate cooperative solution is derived.

- We analysed the energy efficiency of three error control protocols in wireless sensor networks. Two scenarios: SISO AWGN for near distance communication and MISO Rayleigh fading for long distance communication are considered. In the SISO AWGN scenario, since energy consumption on analog circuitry dominates the total energy consumption, less retransmission is expected. As the HARQ-II protocol only transmits the redundancy when it is necessary, it shows to be easier to be energy efficient than the others. On the

other hand, in the MISO Rayleigh fading scenario, due to the channel fading and relative long separation distance, more transmit power is required. A tradeoff between less transmit power and more retransmission expectation by employing HARQ-I protocol could be made. In this case, we proposed the thresholds of the coding gain for various code rates to make the HARQ-I protocol to be more energy efficient.

Future Works

In the works of this dissertation, we proposed some solutions to the practical and energy efficient implementation of cooperative communication in wireless sensor networks. There are still a variety of open areas for further research.

Combination with the network coding: In this dissertation, we focused on the cooperative communication in the physical layer and explored their energy efficiency. While we have shown that network coding cooperative scheme can be implemented in the network layer to improve the network throughput. The dynamic switching between the cooperative schemes in network layer and physical layer or a combination of both would be interesting for the networks either with different requirement on data transmission or in different channel conditions.

OFDM based cooperative communication: We have shown that OFDM modulation scheme can be incorporated in the cooperative communication to reduce the requirement on time synchronization. However, it brings another problem of frequency synchronization which might increase the complexity to the signal processing. Although some research have been done on this problem, the energy efficient implementation of that is still an open area. Furthermore, the problem of high peak-to-average-power ratio on OFDM modulation, which might introduce poor energy efficiency to the cooperative communication, is interesting to be investigated.

MAC layer consideration: The cooperative communication schemes require the coordination among the involved sensor nodes. A strict TDMA scheme might affect the energy efficiency or throughput performance on the view of the entire network. On the other hand, the probabilistic MAC protocols, like the CSMA protocol, cannot guarantee the involvement of all the necessary cooperative nodes. Therefore, an efficient MAC layer protocol is interesting to be explored for the

cooperative communication schemes.

Hardware implementation: A number of research works have theoretically proven the advantages of cooperative communication. But little prototype has been implemented with practical supports for amply-and-forward cooperation or virtual multiple antennas system. Most sensor nodes on the shelf are supposed to support the IEEE-15.4 standard that has not proposition for cooperative communication. Our works have proposed a reasonable time synchronization scheme for cooperative communication, but a test-bed implementation would be helpful for revealing other potential issues.

Appendix A

Considering the optimal solutions of the relaxed problem shown in the equations (4.15) and (4.16), if they are under the constraints of the maximum transmit power, the solutions are feasible. Otherwise, we rewrite the objective function L_1 in the equation (4.11) as:

$$L_1 = P_s + P_r + \lambda_1(\frac{3}{16}(1+\bar{\gamma}_{sd})^{-1}(\frac{\bar{\gamma}_{sr}\bar{\gamma}_{rd}}{\bar{\gamma}_{sr}+\bar{\gamma}_{rd}})^{-1} - P_{eThr}) + \lambda_2(P_s - P_{\max}) \quad (7.1)$$

Setting $\nabla_{P_s} L_1 = 0$ and $\nabla_{P_r} L_1 = 0$ gives:

$$\begin{aligned} \nabla_{P_s} L_1 &= 1 - \tfrac{3\lambda_1}{16} \cdot \tfrac{(N_0B)^2}{(\sigma_{sd}^2 P_s + N_0 B)} \cdot (\tfrac{\sigma_{sd}^2}{\sigma_{sr}^2 P_s \sigma_{rd}^2 P_r} \cdot \tfrac{\sigma_{sr}^2 P_s + \sigma_{rd}^2 P_r}{\sigma_{sd}^2 P_s + N_0 B} + \tfrac{1}{\sigma_{sr}^2 P_s^2}) + \lambda_2 = 0 \\ \nabla_{P_r} L_1 &= 1 - \tfrac{3\lambda_1}{16} \cdot \tfrac{(N_0B)^2}{(\sigma_{sd}^2 P_s + N_0 B)} \cdot \tfrac{1}{\sigma_{rd}^2 P_r^2} = 0 \end{aligned} \quad (7.2)$$

Considering the constraint functions of the equation (4.9) and $P_s = P_{\max}$, the optimal allocated power of P_r can be:

$$P_r = (\frac{16P_e}{3}\frac{\sigma_{sd}^2 P_s + N_0 B}{(N_0 B)^2}\sigma_{rd}^2 - \frac{\sigma_{rd}^2}{\sigma_{sr}^2 P_s})^{-1} \quad (7.3)$$

If the obtained P_r is under the maximum power constraint, λ_2 should be used to verify that the solutions are feasible. Thus, by eliminating the Lagrange multiplier λ_1 and considering the equation (4.9), the equation array (7.2) yield:

$$\lambda_2 = \frac{16P_e}{3}\frac{P_r^2 \sigma_{sd}^2 \sigma_{rd}^2}{(N_0 B)^2} - \frac{\sigma_{rd}^2 P_r^2}{\sigma_{sr}^2 P_s^2} - 1 \quad (7.4)$$

Therefore, considering the equations (7.3) and (7.4), if the condition $\lambda_2 \geq 0$ can be verified, the optimal solutions P_s and P_r represented by $P_s = P_{\max}$ and the equation (7.4) are feasible. Otherwise, the required BER for the cooperative relaying system cannot be attained.

Appendix B : Résumé Étendu

Introduction générale

Dans l'histoire de l'évolution de l'informatique, les lois empiriques de Moore prédisent une évolution à long terme de la puissance des ordinateurs et de la complexité du matériel informatique. Une réévaluation de ces lois, formulée en 1975, prédit que le nombre de transistors des microprocesseurs double approximativement tous les deux ans à coût constant. Cette assertion s'avère exacte depuis 1971. Cette tendance à la miniaturisation et à l'augmentation des capacités de calcul permet aux chercheurs de concevoir à faible coût, des dispositifs de communications de faible puissance. Les réseaux de capteurs sans fil, interconnectés à l'aide de ces petits dispositifs (généralement appelés nœuds ou capteurs), sont destinés aux applications militaires, environnementales, médicales, commerciales ou de sécurité. Ils peuvent être déployés à grande ou à petite échelle selon l'application visée.

Les réseaux de capteurs sans fil sont généralement utilisés dans des environnements complexes où les canaux de communications souffrent d'évanouissements et d'effets de masque. Les systèmes multi-antennes peuvent améliorer grandement les performances en exploitant la diversité des canaux. Cependant, pour des raisons de taille, la mise en œuvre d'antennes multiples sur ces nœuds n'est pas envisageable.

Compte tenu de la nature diffuse du signal radio, le message émis par un nœud peut être écouté par les autres nœuds. Ils peuvent ainsi retransmettre la même version du message source en tant que « relais » (répéteurs) ou en utilisant un codage spatio-temporel coopératif. Nous nommerons ces deux méthodes, système coopératif par relais et système coopératif MISO (Multi-Input Single-Output) virtuel. L'utilisation de tels systèmes de communications coopératifs peut aboutir à l'obtention de performances similaires à celles obtenues avec des systèmes multi-antennes. De plus, ces systèmes sont souvent plus efficaces en énergie qu'une simple communication SISO (Single-Input Single-Output) longue distance.

Les nœuds sont généralement soumis à des limitations, comme l'alimentation électrique, la capacité de traitement et la largeur de bande. Les contraintes sur la puissance et l'architecture simple des nœuds doivent être prises en compte lors de la mise en œuvre des schémas coopératifs de communications dans les réseaux de capteurs sans fil. C'est la principale motivation de notre travail. Considérant les communications coopératives MISO virtuel, nous nous concentrons sur le système de codage spatio-temporel de type Alamouti. La mise en œuvre de cette méthode nécessite que les nœuds soient bien synchronisés à la réception du signal. Nous proposons donc un schéma de synchronisation satisfaisant l'exigence de précision tout en introduisant une faible complexité pour la conception du système. En appliquant ce schéma, nous supposons que le problème de synchronisation temporelle peut être résolu de manière appropriée. Puis, différents schémas de contrôle de puissance sont étudiés pour les communications coopératives par relais et les transmissions MISO virtuel afin d'améliorer encore l'efficacité énergétique. Enfin, des protocoles de contrôle d'erreurs pour les communications coopératives sont proposés, afin de déterminer le bon compromis entre la fiabilité des liens et l'efficacité énergétique.

B.1 Concepts associés

Un réseau de capteurs sans fil se compose de capteurs autonomes, spatialement répartis, communiquant entre eux via une connexion sans fil et permettant la perception du monde qui nous entoure et l'Internet des Objets. Les réseaux de capteurs sans fil peuvent être déployés à petite ou à grande échelle : à l'échelle du corps humain pour les réseaux de capteurs « corporels » ou à l'échelle d'une ville, voire plus, pour les réseaux de capteurs de surveillance. Tous les nœuds sont autonomes et combinés pour former un réseau sans fil nécessitant peu ou pas de planification. Les informations collectées par les réseaux de capteurs sans fil peuvent être de natures différentes en fonction de l'intérêt des utilisateurs. Ces réseaux peuvent être consultés par l'intermédiaire d'un nœud spécial, appelé puits, qui fait office de passerelle.

La caractéristique essentielle des réseaux de capteurs sans fil est leur capacité à percevoir le monde, de façon autonome et omniprésente. Ces deux caractéristiques imposent un certain nombre d'exigences :

- Fonctionnement de longue durée avec une alimentation limitée ou des batte-

ries rechargeables (récupération d'énergie),

- Capacité à travailler de manière flexible et inattendue vis-à-vis des nœuds en échec,
- Capacité à résister aux conditions environnementales et de communication difficiles,
- Intégration possible de nœuds hétérogènes,
- Déploiement à grande échelle et dynamique de la topologie du réseau.

Les applications des réseaux de capteurs sans fil sont variées et ont été développées notamment pour la surveillance environnementale, la poursuite de cibles ou encore le contrôle industriel. D'autre part, avec le développement des systèmes MEMS (Micro-Electro-Mechanical Systems) et NEMS (Nano-Electro-Mechanical Systems), les capteurs devraient progresser vers la miniaturisation, à faible coût et à faible consommation. Ainsi, les réseaux de capteurs sans fil auront, à court terme, un grand impact sur la vie moderne.

Les réseaux de capteurs sans fil sont généralement déployés dans des environnements complexes où les canaux de communications souffrent d'évanouissements et d'effets de masque. A ce titre, le canal de propagation radio mobile a un impact important sur le fonctionnement des réseaux. Les conditions rigoureuses du canal exigent l'application d'algorithmes spécifiques, à plusieurs niveaux du protocole.

Le canal BBAG (Bruit Blanc Additif Gaussien) ou AWGN en anglais, est classiquement considéré comme une source élémentaire de dégradation des performances des systèmes de communications. Le principal contributeur au BBAG est le bruit thermique généré dans le récepteur.

Le signal qui se propage dans le canal radio mobile peut être soumis à deux types de phénomènes provoquant des variations de la puissance du signal reçu : les évanouissements à grande et à petite échelle. L'impact de ces évanouissements sur les performances du récepteur est généralement plus important que celui du canal BBAG. Les systèmes coopératifs de codage spatio-temporel et par relais sont des solutions prometteuses pour lutter contre ces phénomènes. La mise en œuvre de ces systèmes coopératifs implique qu'un canal SIMO, MISO ou MIMO devra être établi entre les nœuds.

A titre d'illustration, dans la figure 7.1, nous comparons la capacité d'un canal à évanouissement de Rayleigh pour ces systèmes coopératifs utilisant des canaux de

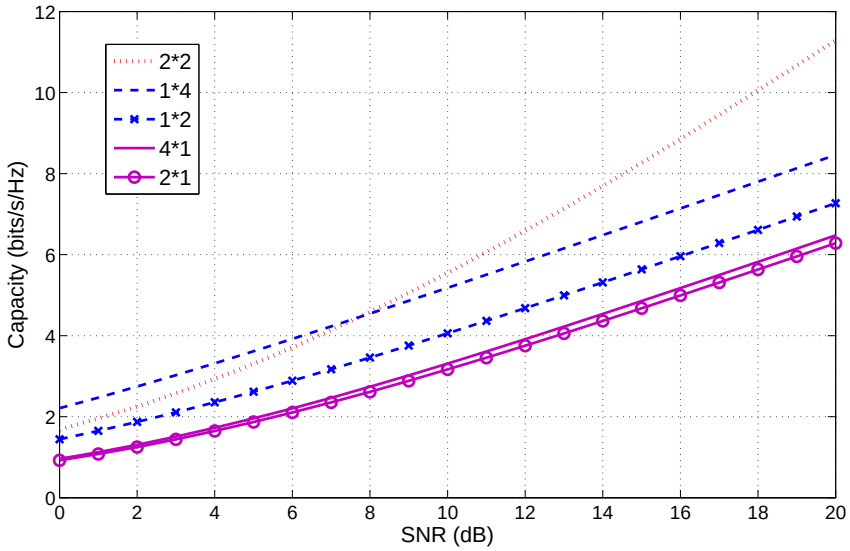

FIGURE 7.1 – Capacité d'un canal à évanouissement de Rayleigh en fonction du RSB pour les systèmes SIMO, MISO et MIMO

propagation 2x2, 1x4 et 4x1 (nombre d'émetteurs x nombre de récepteurs). Dans ces trois cas, quatre liens de Rayleigh indépendants existent. Le cas 2x2 montre une plus grande capacité pour un RSB (Rapport Signal à Bruit) de plus de 8 dB, alors que le cas 1x4 offre un meilleur gain de capacité pour les faibles RSB. En outre, l'augmentation du nombre d'antennes de réception dans les systèmes SIMO permet d'obtenir un meilleur gain de capacité que l'augmentation du nombre d'antennes d'émission dans les systèmes MISO. Cela peut être clairement observé sur la figure 7.2. La capacité sature plus rapidement dans le cas des systèmes MISO. Il semblerait qu'aller au delà de deux antennes d'émission ne soit pas nécessaire dans la perspective d'obtenir un gain de capacité dans le cas d'un canal à évanouissements de Rayleigh. Si la puissance totale transmise disponible pour le système MISO est contrainte, l'emploi d'un nombre plus important d'antennes d'émission, dans la perspective d'obtenir une plus grande capacité de canal, semble être un gaspillage de ressources. Par conséquent, un système de communications avec plusieurs antennes de réception fournit un meilleur gain de capacité qu'un système composé de plusieurs antennes d'émission.

Bien que les systèmes à plusieurs antennes de réception, tels que les systèmes 1x4 et 2x2, permettent d'améliorer les performances des communications, ils aug-

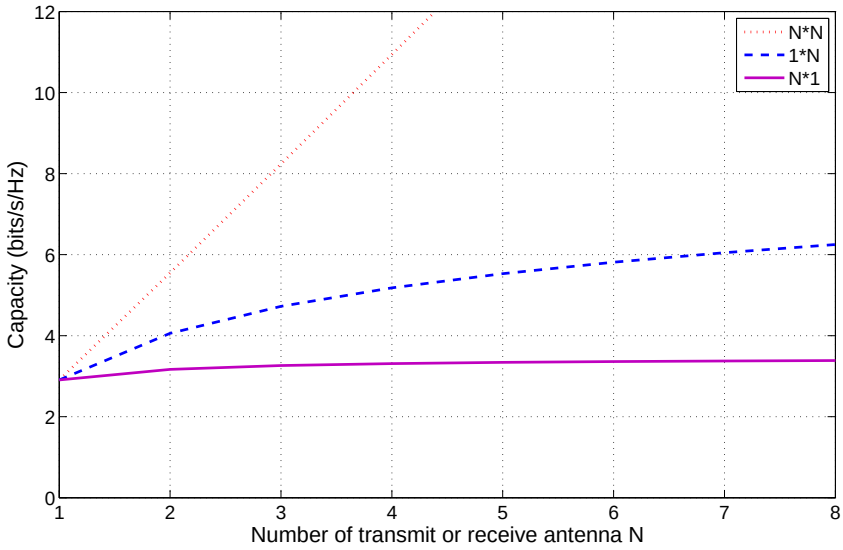

FIGURE 7.2 – Capacité d'un canal à évanouissement de Rayleigh en fonction du nombre d'antennes pour les systèmes SIMO, MISO et MIMO ; $RSB = 10dB$

mentent la complexité des émetteurs-récepteurs. Dans cette thèse, nous nous focalisons sur la problématique des réseaux de capteurs sans fil, où chaque nœud est normalement équipé d'une seule antenne et alimenté à l'aide d'une batterie à puissance limitée. Dans ce cas, l'efficacité énergétique et la simplicité de mise en œuvre sont prépondérantes par rapport à l'augmentation de la capacité. C'est pourquoi nous considérerons essentiellement des systèmes MISO dans cette thèse.

B.2 Communication coopérative dans les réseaux de capteurs sans fil

B.2.1 Introduction

Les systèmes de communications coopératifs peuvent être mis en œuvre à différents niveaux du protocole, telles que la couche réseau ou la couche physique. Dans le premier cas, le codage de réseau est un domaine de recherche très actif ces dernières années. Il peut être également implanté au niveau de la couche physique moyennant une augmentation de la complexité du traitement en bande de base.

Au niveau de la couche physique, deux autres types de systèmes coopératifs sont

principalement proposés. Le premier, que nous appelons système coopératif par relais, utilise l'assistance radio des nœuds relais pour compenser les effets engendrés par les évanouissements. En utilisant le principe de « décodage et retransmission » (decode-and-forward) ou le principe d'« amplification et retransmission » (amplify-and-forward), le nœud relais peut retransmettre le signal reçu du nœud source vers le nœud destinataire. Celui-ci combine les signaux reçus du nœud source et du nœud relais en se basant sur le critère du maximum de vraisemblance ou du maximum du rapport signal à bruit.

Le second système, appelé système coopératif MISO virtuel, exploite des codes spatio-temporels orthogonaux. Le message émis est d'abord codé par un code spatio-temporel au niveau de chaque nœud coopératif. Des copies redondantes du flux de données, sont transmises par ces nœuds au récepteur, afin de bénéficier de la diversité de canal. Le système coopératif MISO virtuel peut être combiné avec une modulation OFDM (Orthogonal Frequency Division Multiplexing) pour surmonter le problème de synchronisation temporelle entre les nœuds distribués.

B.2.2 Codage de réseau

En codage de réseau, les nœuds réalisent une combinaison des paquets à émettre avant transmission. Cette combinaison peut être faite sur les flux de bits ou sur les symboles analogiques modulés. Nous différencierons ces deux méthodes en parlant respectivement de codage de réseau numérique et de codage de réseau analogique.

Pour illustrer le principe de base du codage de réseau, considérons deux nœuds sans fil (A et B) échangeant de manière classique des messages via un nœud routeur (R). En tenant compte du fait qu'un seul canal est utilisé par le système, l'échange de messages entre les deux nœuds A et B nécessite quatre intervalles de temps : les deux premiers sont alloués au recueil des messages et les deux derniers à la diffusion des messages.

En utilisant le codage de réseau numérique, deux intervalles de temps sont encore nécessaires pour le recueil des messages mais un seul est nécessaire pour la diffusion des messages. En effet, le relais diffuse la combinaison de a *xor* b et les nœuds A et B qui connaissent déjà les messages a et b respectivement, peuvent obtenir le message b à partir de [a *xor* (a *xor* b)] et le message a à partir de [b *xor* (a *xor* b)].

B.2.3 Système coopératif par relais

La transmission multi-saut est un principe de communication longue distance couramment utilisé dans les réseaux de capteurs sans fil. En se référant à ce principe et en exploitant la nature diffuse du support de transmission, plusieurs systèmes coopératifs par relais peuvent être considérés. En général, ils peuvent être classifiés en plusieurs catégories : les systèmes par relais fixes exploitant le principe de « décodage et retransmission » (decode-and-forward) ou le principe de l'« amplification et retransmission » (amplify-and-forward), et les systèmes par relais optionnels utilisant des relais sélectifs ou des relais supplémentaires.

Le processus de décodage et de transmission est également utilisé dans la transmission traditionnelle multi-saut. La différence est que, dans le cas du système coopératif par relais, le nœud source S souhaite transmettre un message aux nœuds de destination D avec la collaboration du nœud relais R, alors que classiquement, le nœud R n'est utilisé que pour effectuer un saut de communication. La transmission peut être divisée en deux étapes. Dans un premier temps, le message est diffusé par le nœud source. Le nœud de destination et le nœud relais reçoivent ce message par le biais de la diffusion sans fil. En raison des conditions différentes du canal de propagation, les nœuds relais et de destination détectent le message différemment. Il est raisonnable de penser que, dans la plupart des cas, le nœud relais reçoit ce message avec une probabilité d'erreur moindre que le nœud de destination. Puis, dans un deuxième temps, le nœud relais retransmet le message décodé. En se basant sur les deux signaux reçus, le nœud de destination, par l'intermédiaire de la méthode MRC (maximum Ratio Combining), récupère le signal source avec une probabilité d'erreur plus faible. Le processus d'amplification et de retransmission se compose également de trois nœuds mais, dans ce cas, le nœud relais se contente d'amplifier le signal reçu sans le décoder.

Les systèmes par relais fixes, comme décrits précédemment, correspondent aux cas où le nœud relais est défini à l'avance. Cependant rien ne garanti que ce nœud reste le meilleur candidat pour ce rôle. Ainsi, dans le cas d'un système par sélection de relais, le nœud relais peut être choisi au fil de l'eau en fonction des conditions de transmission et suivant différentes stratégies.

Dans ce qui précède nous avons proposé que le nœud relais choisi participe en permanence à la communication coopérative. Dans certains cas, cette stratégie peut être inefficace. En effet, si le canal entre le nœud source et le nœud de destination est suffisamment bon, il n'est pas nécessaire d'utiliser le relais. On peut alors

envisager que la transmission par relais soit déclenchée par la destination en cas de défaillance de la transmission directe.

Enfin la transmission par relais peut inclure l'utilisation de codes correcteurs d'erreurs afin de protéger l'information transmise, la redondance pouvant être transmise ou non par l'intermédiaire du relais.

B.2.4 Système coopératif MISO virtuel

Le système coopératif MISO virtuel est capable de fournir des performances proches de celles obtenues lors de l'utilisation de systèmes multi-antennaires. Le principe et de sélectionner un ou plusieurs nœuds de coopération parmi un ensemble de nœuds relais potentiels afin de constituer un système virtuel multi-antennes. Les données à transmettre sont codées au moyen d'un code espace-temps puis divisées en autant de flux de données que de nœuds de coopération choisis. Ces flux sont transmis simultanément par l'ensemble des nœuds coopératifs. Dans la suite, nous détaillons les codes en blocs espace-temps distribués, en nous limitant au code d'Alamouti.

Un tel système est constitué de deux nœuds émetteurs et d'un nœud récepteur. Nous supposons que chacun des deux nœuds émetteurs connaît l'information à transmettre. La modulation choisie possède une constellation à 2^b symboles. Dans un premier temps, $2b$ bits sont traités et fournissent deux signaux modulés s_1 et s_2. Ces deux signaux sont alors transmis en parallèle par les deux nœuds émetteurs. Dans un second temps, les signaux $-s_2^*$ et s_1^* sont émis simultanément par ces deux mêmes nœuds émetteurs. L'opérateur * fait référence à la conjugaison complexe. Si le canal est considéré comme statique durant les deux intervalles de temps où les deux émissions simultanées sont effectués, les signaux r_1 et r_2 reçus par le nœud récepteur s'écrivent :

$$\begin{aligned} r_1 &= h_1\sqrt{P_{T1}}s_1 + h_2\sqrt{P_{T2}}s_2 + n_1 \\ r_2 &= -h_1\sqrt{P_{T1}}s_2^* + h_2\sqrt{P_{T2}}s_1^* + n_2 \end{aligned} \tag{7.5}$$

où P_{T1} et P_{T2} sont les puissances d'émission des deux nœuds émetteurs, h_1 et h_2 sont les coefficients complexes des canaux de propagation respectivement définis par $a_1 e^{j\theta_1}$ et $a_2 e^{j\theta_2}$, n_1 et n_2 représentent les bruits blancs additifs gaussien. La méthode du maximum de vraisemblance est utilisée pour effectuer la décision en

réception :

$$\left[\left|r_1 - h_1\sqrt{P_{T1}}s_1 - h_2\sqrt{P_{T2}}s_2\right|^2 + \left|r_2 + h_1\sqrt{P_{T1}}s_2^* - h_2\sqrt{P_{T2}}s_1^*\right|^2\right] \tag{7.6}$$

Ainsi, les signaux combinés reçus au détecteur sont donnés par :

$$\begin{aligned}\tilde{s}_1 &= r_1 h_1^*\sqrt{P_{T1}} + r_2^* h_2\sqrt{P_{T2}} = (a_1^2 P_{T1} + a_2^2 P_{T2})s_1 + h_1^*\sqrt{P_{T1}}n_1 + h_2\sqrt{P_{T2}}n_2^* \\ \tilde{s}_2 &= r_1 h_2^*\sqrt{P_{T2}} - r_2^* h_1\sqrt{P_{T1}} = (a_1^2 P_{T1} + a_2^2 P_{T2})s_2 - h_1\sqrt{P_{T1}}n_2^* + h_2^*\sqrt{P_{T2}}n_1\end{aligned} \tag{7.7}$$

Ce type de système coopératif, utilisant le codage d'Alamouti, fournit deux branches de diversité, et permet donc d'améliorer les performances de la liaison en présence d'évanouissements rapides.

Notons toutefois que l'application d'un système coopératif MISO virtuel à des réseaux de capteurs sans fil, nécessite de résoudre un certain nombre de questions pratiques. Dans l'analyse précédente, nous avons supposé une parfaite synchronisation fréquentielle et temporelle, alors qu'en réalité, en raison de l'incohérence des oscillateurs et du déploiement distribué des nœuds, le problème de synchronisation ne doit pas être ignoré. Pour la synchronisation de la porteuse, on peut supposer qu'une porteuse de référence est transmise sur laquelle tous les nœuds peuvent se synchroniser en utilisant une boucle à verrouillage de phase. On peut également proposer une estimation de la porteuse basée sur la présence de symboles pilotes placées au début de chaque paquet.

Outre le problème de synchronisation de la porteuse, la synchronisation du temps d'arrivée des signaux reçus est plus importante pour un système coopératif MISO virtuel. En effet, les signaux reçus au nœud récepteur provenant de plusieurs émetteurs doivent être recombinés de manière cohérente, ce qui nécessite que le nœud soit correctement synchronisé. Les effets liés au problème de synchronisation seront discutés dans le chapitre 3.

B.2.5 Conclusion

Dans ce chapitre, différents systèmes de communications coopératifs, mis en œuvre soit au niveau de la couche physique soit au niveau de la couche réseau, ont été présentés. Ils peuvent être utilisés pour exploiter la diversité dans l'espace fréquentielle ou dans l'espace temporelle. Dans cette thèse, nous nous concentrons sur les systèmes de communications coopératifs au niveau de la couche physique. Cependant, nous pouvons noter que des systèmes coopératifs au niveau de la couche réseau, tels que le codage de réseau, peuvent être implémentés en parallèle de systèmes coopératifs au niveau de la couche physique.

B.3 Synchronisation pour les communications coopératives

B.3.1 Introduction

La synchronisation temporelle est cruciale pour la mise en œuvre des communications coopératives dans les réseaux de capteurs sans fil. Nous étudions ici les effets de l'erreur de synchronisation sur la communication coopérative utilisant le codage d'Alamouti distribué. Les résultats d'analyse et de simulation montrent qu'une petite erreur de synchronisation a un effet négligeable sur le taux d'erreur binaire (BER). Dans l'optique de synchroniser les nœuds répartis avec une erreur acceptable, nous proposons un schéma de synchronisation au niveau de la couche physique. Ce schéma consiste en une synchronisation initiale des émetteurs coopératifs, une estimation de l'erreur de synchronisation au niveau du récepteur de coopération et enfin une phase de rétroaction. La méthode du maximum de vraisemblance est proposée pour estimer l'erreur de synchronisation. Elle donne des meilleures performances que la méthode du filtre adapté au prix d'une augmentation modérée de la complexité des calculs et de l'occupation mémoire. Deux stratégies, après estimation de l'erreur de synchronisation, ont été analysées. Elles offrent de bonnes performances en termes de taux d'erreur en présence d'une erreur initiale de synchronisation et sont faciles à implémenter au niveau des nœuds avant le décodage d'Alamouti.

B.3.2 Modèle du système

Nous considérons le déploiement de réseaux de capteurs sans fil où les nœuds exploitent un système coopératif utilisant le codage d'Alamouti. Ce système coopératif peut être mis en œuvre par deux nœuds émetteurs coopératifs (CTN1 et CTN2) et un nœud récepteur (CRN1) afin de former un système MISO virtuel. Après codage d'Alamouti, les données sont ensuite séparées en deux flux, transmis simultanément par les deux nœuds émetteurs. Toutefois, en raison de l'utilisation de nœuds séparés, la synchronisation temporelle au niveau symbole ne peut pas être supposée parfaite.

Dans le but de synchroniser les nœuds émetteurs coopératifs, nous assignons un nœud de déclenchement (Trigger) dans chaque Cluster (groupe de nœud) pour initier une première phase de synchronisation. Ce nœud de déclenchement peut également jouer le rôle de « tête » (header) de cluster dans certains scénarios de réseaux de capteurs sans fil organisés en cluster. Il recueille les informations de surveillance au sein du cluster et celles provenant d'autres clusters dans le réseau. Toutes ces informations se trouvant dans un paquet dédié seront envoyés à CTN1 et CTN2. Une séquence d'apprentissage et de synchronisation est insérée au début de chacun de ces paquets. En utilisant cette séquence, le temps d'arrivée du paquet peut être estimé par un filtre adapté et la synchronisation des horloges de CTN1 et CTN2 peut s'effectuer de façon relativement précise.

Dans la suite, nous supposerons que cette phase de synchronisation initiale fournit une précision de l'ordre de la durée du temps symbole.

Après cette première phase, la séquence d'information est transmise de manière collaborative sous le contrôle des horloges synchronisées. Nous montrons dans la suite qu'une petite erreur de synchronisation amène peu de dégradations sur les performances du récepteur en termes de taux d'erreur.

B.3.3 Effet de l'erreur de synchronisation sur le système MISO virtuel

En raison de l'erreur de synchronisation résiduelle entre les deux nœuds émetteurs coopératifs, la combinaison des signaux, fournit des expressions différentes du cas idéal étudié plus haut. Dans notre analyse, nous prenons pour référence l'horloge de CTN1. L'erreur de synchronisation de CTN2 par rapport à CTN1 est notée T_e. Ainsi, les signaux reçus en CRN1 sur deux intervalles de temps successifs

s'expriment par :

$$r_1(t) = \sum_{k=-L_t}^{L+L_t-1} \left\{ \sqrt{E_{n1}} s_1(k) h_1(t) p(t - kT_b) + \sqrt{E_{n2}} s_2(k) h_2(t) p(t - kT_b - T_e) \right\} + n_1(t) \tag{7.8}$$

$$r_2(t) = \sum_{k=-L_t}^{L+L_t-1} \left\{ -\sqrt{E_{n1}} s_2^*(k) h_1(t) p(t - kT_b) + \sqrt{E_{n2}} s_1^*(k) h_2(t) p(t - kT_b - T_e) \right\} + n_2(t) \tag{7.9}$$

où $s_1(k)$ et $s_2(k)$ sont les kième symboles d'information, E_{n1} et E_{n2} représentent l'énergie par symbole reçue par l'intermédiaire du canal entre CTN1 et CRN1 et entre CTN2 et CRN1 respectivement. $p(t)$ est le filtre de mise en forme en racine de cosinus surélevé avec $2L_t + 1$ comme durée effective du symbole ; L est la longueur de la séquence d'information. T_b est la durée symbole. $h_1(t)$ et $h_2(t)$ sont modélisés par des variables aléatoires gaussiennes complexes indépendantes de variance 0.5 par dimension. Le temps de cohérence du canal de propagation est supposé être plus important que le temps de propagation d'un paquet. Ainsi, les canaux sont supposés constants durant la transmission d'un paquet. $n_i(t)$ représente un bruit blanc additif gaussien de moyenne nulle et de variance σ_{ni}^2.

Habituellement, les lobes de la forme de l'impulsion $p(t)$ s'affaiblissent en $1/t^3$ pour un facteur de roll-off supérieur à 0. Par conséquent, une partie de l'interférence entre symboles provenant des lobes secondaires converge vers une valeur négligeable. Afin de simplifier l'analyse, mais en conservant une précision acceptable, nous limitons la forme d'impulsion en cosinus surélevé aux deux lobes latéraux (d'où, $L_t = 2$) et approximons l'impulsion linéairement par morceaux.

Sans perte de généralité, nous considérons le cas où les paquets de CTN1 arrivent les premiers. Les résultats d'analyse et de simulation montrent que, lorsque l'erreur de synchronisation est faible, par exemple $T_e = 0.25T_b$, la dégradation des performances en termes de taux d'erreur du système coopératif est négligeable. Toutefois, lorsque l'erreur de synchronisation augmente jusqu'à $0.5T_b$, la perte est de plus de 3dB pour un taux d'erreur binaire égal à 10^{-2} en comparaison avec le système d'Alamouti parfait (sans erreur de synchronisation). En outre, les performances se dégradent considérablement pour une erreur de synchronisation de l'ordre de $0.6T_b$. Dans cette situation, le système MISO affiche des performances plus mauvaises que celles du système SISO.

En nous basant sur les résultats de cette étude, nous supposerons pour la suite de nos travaux, que $T_e = 0.25T_b$ est une erreur de synchronisation acceptable.

B.3.4 Stratégie de la synchronisation temporelle

Nous considérons que la stratégie de synchronisation est implémentée au niveau de la couche physique dans le cas d'une communication coopérative. Etant donné qu'une petite erreur de synchronisation (typiquement $T_e = 0.25T_b$) fournit une dégradation négligeable des performances en taux d'erreur, le principe du schéma de synchronisation est de confiner l'erreur de synchronisation dans un intervalle de cet ordre. A cause des différents retards de propagation et des incohérences du matériel, le temps d'arrivée des paquets sur les deux nœuds est différent. Nous supposons que, lors d'une communication à l'intérieur d'un même cluster, les signaux reçus sont uniquement perturbés par un bruit blanc additif gaussien. Les signaux reçus sont sur-échantillonnés avant traitement dans les deux nœuds d'un facteur Q. Ils s'expriment alors de la manière suivante :

$$\begin{aligned} x_i\left[l_iQ+m_i\right] = \sqrt{E_{tr}} \sum_{k=-L_t}^{L_0+L_t-1} & s_{tr}(k)p((l_iQ+m_i)T_b/Q - kT_b - \sigma_i T_b) \\ & + n_{tr}\left[(l_iQ+m_i)T_b/Q\right] \qquad , m_i = 0,1,...Q-1 \end{aligned} \tag{7.10}$$

où $s_{tr}(k)$ représente le kième symbole du paquet ; L_0 est l'intervalle d'observation ; σ_i est le retard inconnu normalisé par rapport à la durée symbole T_b ; $n_{tr}(t)$ modélise le bruit blanc additif gaussien ; l_i et m_i sont les indice du symbole et de l'échantillon discrets pour le ième noeud. Nous supposons que l'instant d'échantillonnage m_{i_opt}, le plus proche de l'instant optimal, est choisi après le temps d'acquisition. Ensuite, le calcul de l'intercorrélation entre les signaux reçus et la séquence connue de Barker fournit un maximum chaque fois qu'il y a alignement exact entre ces deux séquences. Par conséquent, le temps d'arrivée du paquet peut être déterminé. L'horloge du nœud est ainsi synchronisée sur le temps d'arrivée du paquet. Cette phase de synchronisation initiale est faite au niveau de la couche physique. Sa précision peut être supposée de l'ordre d'un temps symbole. Les résultats des simulations montrent en effet que la phase de synchronisation initiale peut permettre d'avoir une erreur de synchronisation inférieure à un temps symbole.

Après cette phase de synchronisation initiale, la séquence d'information est

transmise coopérativement sous le contrôle de l'horloge réglée. Comme la phase de synchronisation initiale peut ne pas être parfaite, nous devons estimer l'erreur de synchronisation au niveau du récepteur CRN1 avant le décodage d'Alamouti. Les paquets reçus avec une erreur de synchronisation inférieure à $T_e = 0.25T_b$ ayant un effet négligeable sur les performances, seront acceptés tandis que les paquets reçus avec une plus grande erreur synchronisation seront rejetés.

Nous avons développé une méthode basée sur le principe du maximum de vraisemblance pour estimer cette erreur. La fonction de vraisemblance de l'erreur de synchronisation est donnée par :

$$\begin{aligned} &ML(y(kT_b/M), n_1/M, n_2/M, \sqrt{E_{n1}}h_1, \sqrt{E_{n2}}h_2) \\ &= (\pi\sigma_w^2)^{-L_0} e^{-\frac{\left\| y(kT_b/M) - \sqrt{E_{n1}}h_1 A_{n_1/M} s_1 - \sqrt{E_{n2}}h_2 A_{n_2/M} s_2 \right\|^2}{\sigma_w^2}} \end{aligned} \tag{7.11}$$

où σ_w^2 est la variance du bruit blanc additif gaussien $n(t)$. Alors, la matrice de décision s'écrit :

$$\Lambda(n_1/M, n_2/M) = \mathrm{I} - \left[\begin{array}{cc} A_{n_1/M} s_1 & A_{n_2/M} s_2 \end{array} \right] \cdot R^{-1} \cdot \left[\begin{array}{c} s_1^H A_{n_1/M}^H \\ s_2^H A_{n_2/M}^H \end{array} \right] \tag{7.12}$$

où M est un facteur prédéfini qui représente la granularité de l'estimation de la synchronisation ; n_1 et n_2 sont des entiers. Par exemple, pour estimer l'erreur de synchronisation avec une précision de $0.25T_b$, M est fixé à 4.

Finalement, l'erreur de synchronisation est estimée à partir de l'équation suivante :

$$\hat{n} = \arg\min_{n_1, n_2} \left\| \Lambda(n_1/M, n_2/M) y(kT_b/M) \right\|^2 \tag{7.13}$$

Comme nous l'avons précisé, l'acquisition du temps d'arrivée des signaux peut être faite à partir d'une courte séquence d'apprentissage. Nous avons besoin de déterminer l'erreur de synchronisation relative entre les deux nœuds émetteurs coopératifs. Donc, en supposant que le nœud CTN1 est la référence ($n_1 = 0$), seul le paramètre n_2 doit être estimé. Pour cette raison, les nœuds ont besoin de stocker uniquement la matrice de décision $\Lambda(0, n_2/M)$. Ensuite, l'erreur de synchronisation

estimée est $(n_2/M)T_b$. Cette estimation n'est qu'une approximation de l'erreur de synchronisation. Toutefois, comme nous cherchons seulement à déterminer si l'erreur de synchronisation est acceptable ou non, cette approximation est suffisante.

B.3.5 Conclusion

Dans ce chapitre, un système de synchronisation a été proposé au niveau de la couche physique. Nous avons tout d'abord déterminé la tolérance du système de transmission coopératif aux erreurs de synchronisation. Une méthode basée sur le principe du maximum de vraisemblance a ensuite été proposée pour l'estimation de l'erreur de synchronisation à la réception. Elle montre de meilleures performances que le filtre adapté, surtout avec une courte séquence de synchronisation. La matrice de décision peut être pré-calculée et réutilisée dans le processus d'estimation des erreurs de synchronisation avant le décodage d'Alamouti. Considérant deux stratégies après estimation de l'erreur de synchronisation, de bonnes performances peuvent être obtenues même en présence d'une erreur de synchronisation initiale entre les deux nœuds émetteurs coopératifs.

B.4 Contrôle de puissance dans les communications coopératives

B.4.1 Introduction

Dans ce chapitre, nous considérons le contrôle de puissance pour deux types de systèmes coopératifs : le système coopératif par relais et le système coopératif MISO virtuel. Dans nos travaux, nous proposons une stratégie d'allocation de puissance visant à minimiser la puissance de transmission totale avec une contrainte sur les performances moyennes en termes de taux d'erreur. Cette stratégie cherche à maximiser l'efficacité énergétique des communications coopératives. En outre, dans le cas où aucun lien direct n'existe entre le nœud source et le nœud de destination, nous proposons deux stratégies coopératives : le système coopératif par relais (basé sur le principe « amplification et retransmission ») et le système coopératif MISO virtuel. Ces systèmes sont plus économes en énergie et parviennent à effectuer une répartition équitable de la puissance de transmission entre les nœuds. Du point de vue de la conception multi-couches, ces stratégies coopératives appliquées au niveau

de la couche physique pourraient être conçues conjointement avec les couches de contrôle d'accès au support et de routage afin de fournir des liens fiables et efficaces dans les réseaux. A partir de l'étude de différentes topologies, nous proposons une démarche heuristique permettant de sélectionner les nœuds coopératifs optimaux intervenant dans une transmission coopérative.

B.4.2 Stratégie d'allocation de puissance

La probabilité d'erreur pour la communication coopérative de type « amplification et retransmission » avec un seul nœud relais peut être approximée par l'équation suivante :

$$P_e \geq \frac{3}{16}(1+\overline{\gamma}_{sd})^{-1}(1+\frac{\overline{\gamma}_{sr}\overline{\gamma}_{rd}}{\overline{\gamma}_{sr}+\overline{\gamma}_{rd}})^{-1} \tag{7.14}$$

où $\bar{\gamma}_{ij}$ est la valeur moyenne de γ_{ij}, ainsi $\bar{\gamma}_{ij} = \frac{\sigma_{ij}^2 P_i}{N_0 B}$, et σ_{ij}^2 représente l'atténuation moyenne du canal entre le nœud i et le nœud j. Nous supposons que le nœud relais est situé entre le nœud source et le nœud de destination. Les canaux entre le nœud source et le nœud relais et entre le nœud relais et le nœud de destination, respectivement, subissent en moyenne moins d'atténuation que le canal direct reliant le nœud source au nœud de destination. Afin d'obtenir un taux d'erreur relativement faible, les rapports signal à bruit moyens $\bar{\gamma}_{sr}$ et $\bar{\gamma}_{rd}$ satisfont les conditions $\bar{\gamma}_{sr} >> 1$ et $\bar{\gamma}_{rd} >> 1$. Donc, la formule donnant la probabilité d'erreur peut être simplifiée comme suit :

$$P_e \approx \frac{3}{16}(1+\overline{\gamma}_{sd})^{-1}(\frac{\overline{\gamma}_{sr}\overline{\gamma}_{rd}}{\overline{\gamma}_{sr}+\overline{\gamma}_{rd}})^{-1} \tag{7.15}$$

Dans le cas de la communication coopérative MISO virtuel utilisant le codage d'Alamouti, le taux d'erreur moyen après le décodage d'Alamouti est donné par :

$$P_e = \frac{3}{4}(1-\sqrt{\frac{\bar{\gamma}_1'}{1+\bar{\gamma}_1'}})(1-\sqrt{\frac{\bar{\gamma}_2'}{1+\bar{\gamma}_2'}}) \tag{7.16}$$

où $\bar{\gamma}_1'$ et $\bar{\gamma}_2'$ sont les valeurs moyennes de γ_1' et γ_2', avec $\bar{\gamma}_1' = \frac{\sigma_1^2 P_{T1}}{N_0 B}$ et $\bar{\gamma}_2' = \frac{\sigma_2^2 P_{T2}}{N_0 B}$. σ_1^2 et σ_2^2 sont respectivement les atténuations moyennes des canaux allant du nœud s_1 au nœud d et du nœud s_2 au nœud d.

Nous proposons une stratégie d'allocation de puissance qui minimise la puis-

sance totale transmise au nœud source et au nœud relais, pour les communications coopératives par relais, et aux deux nœuds émetteurs coopératifs pour les communications coopératives MISO virtuel, sous la contrainte d'une probabilité d'erreur prédéfinie P_{eThr}. Dans ce cas, le problème d'optimisation peut être formulé comme suit :

$$\min \quad f = P_i + P_j \tag{7.17}$$

$$\begin{aligned} & P_e = P_{eThr} \\ subject \quad to \quad & P_i \leq P_{\max} \\ & P_j \leq P_{\max} \end{aligned}$$

Dans un premier temps nous résolvons le problème sans tenir compte des contraintes inégalités. Pour la transmission coopérative par relais, les puissances optimales d'émission sont :

$$P_s = N_0 B \frac{\sqrt{\frac{3}{16 P_{eThr} \sigma_{sd}^2 \sigma_{rd}^2}} - \frac{1}{\sigma_{sd}^2} + \sqrt{(\sqrt{\frac{3}{16 P_{eThr} \sigma_{sd}^2 \sigma_{rd}^2}} - \frac{1}{\sigma_{sd}^2})^2 + \frac{3}{4 P_{eThr} \sigma_{sd}^2 \sigma_{sr}^2}}}{2} \tag{7.18}$$

$$P_r = N_0 B \sqrt{\frac{3}{16 P_{eThr} \sigma_{sd}^2 \sigma_{rd}^2}} \tag{7.19}$$

Pour la transmission coopérative MISO virtuel, nous obtenons :

$$P_{T1} = \frac{N_0 B}{\sigma_1^2} ((1 - (\frac{4 P_{eThr}}{3(1 - \sqrt{\sigma_2^2 P_{T2} / (N_0 B + \sigma_2^2 P_{T2})})})^{-2} - 1)^{-1} \tag{7.20}$$

$$P_{T2} \approx \frac{\sqrt{(N_0 B)^2 + 16 A_2} - 3 N_0 B}{4 \sigma_2^2} \tag{7.21}$$

Considérons maintenant les contraintes inégalités. Si les puissances optimales obtenues P_s et P_r respectent ces contraintes, la solution obtenue précédemment convient. Sinon, si P_s dépasse la contrainte maximale, la puissance d'émission allouée au nœud source doit être limitée à $P_{\max}$ (la contrainte inégalité est alors considérée comme active) et la puissance d'émission du nœud relais est déterminée

en résolvant l'équation de la probabilité d'erreur. Si la nouvelle valeur de P_r dépasse également la contrainte maximale, le taux d'erreur visé pour le système coopératif par relais ne peut pas être atteint.

Le raisonnement peut se faire de façon analogue pour le système coopératif par relais. Lorsque les puissances d'émission P_{T1} et P_{T2} obtenues sans considérer les contraintes inégalités respectent les puissances d'émission maximales alors la solution obtenue convient. Dans le cas contraire on suppose que la contrainte non vérifiée est active et la puissance correspondante est saturée à la valeur maximale. La puissance d'émission de l'autre nœud est déterminée par l'équation de la probabilité d'erreur. Si elle ne peut pas satisfaire la contrainte sur la puissance d'émission maximale, les performances visées pour le système coopératif MISO virtuel ne peuvent pas être atteintes.

B.4.3 Stratégies coopératives

Considérons une topologie de réseau constituée de quatre nœuds où un ou deux nœuds relais pourraient participer à la transmission coopérative entre le nœud source et le nœud de destination. Nous supposons que chaque nœud connaît l'atténuation moyenne du canal de chaque lien de cette topologie. Nous nous plaçons dans l'hypothèse où le lien direct entre le nœud source et le nœud de destination est indisponible, ce qui correspond, par exemple, à la situation où la distance entre la source et la destination est importante et que la puissance d'émission est limitée. Cette situation exclue l'implémentation directe du système coopératif par relais.

Deux stratégies coopératives seront étudiées.

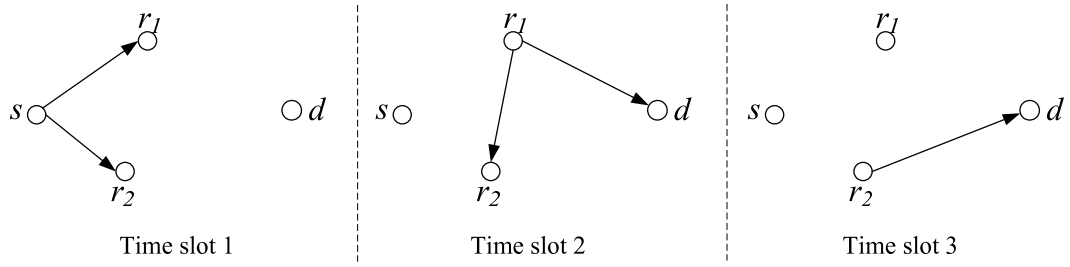

FIGURE 7.3 – Etapes constituant la première stratégie

Pour la première stratégie, illustrée à la figure 7.3, un système coopératif par relais est implémenté entre les quatre nœuds. Durant le premier intervalle de temps, l'information est diffusée par le nœud source s. Pour la réalisation, nous supposons

qu'un des deux nœuds relais, par exemple r_1, fonctionne en mode AF (amplification et retransmission). Il amplifie et retransmet le signal reçu vers l'autre nœud relais r_2 et le nœud de destination d lors d'un second intervalle de temps. A la réception du signal provenant du nœud source s et du nœud relais r_1, une combinaison de type MRC et une décision sont exécutés par le nœud relais r_2. Puis, durant un troisième intervalle de temps, l'information décodée est retransmise vers le nœud de destination. A la réception, le décodage et la décision sont effectués grâce à une combinaison de type MRC des signaux provenant du nœud relais r_1 reçu durant le deuxième intervalle de temps et provenant du nœud r_2 reçu durant le troisième intervalle de temps. Ainsi, dans la première stratégie, les règles appliquées au deux nœuds relais sont différentes. L'un effectuera une opération d'amplification et de retransmission alors que l'autre effectuera une opération de décodage et de retransmission.

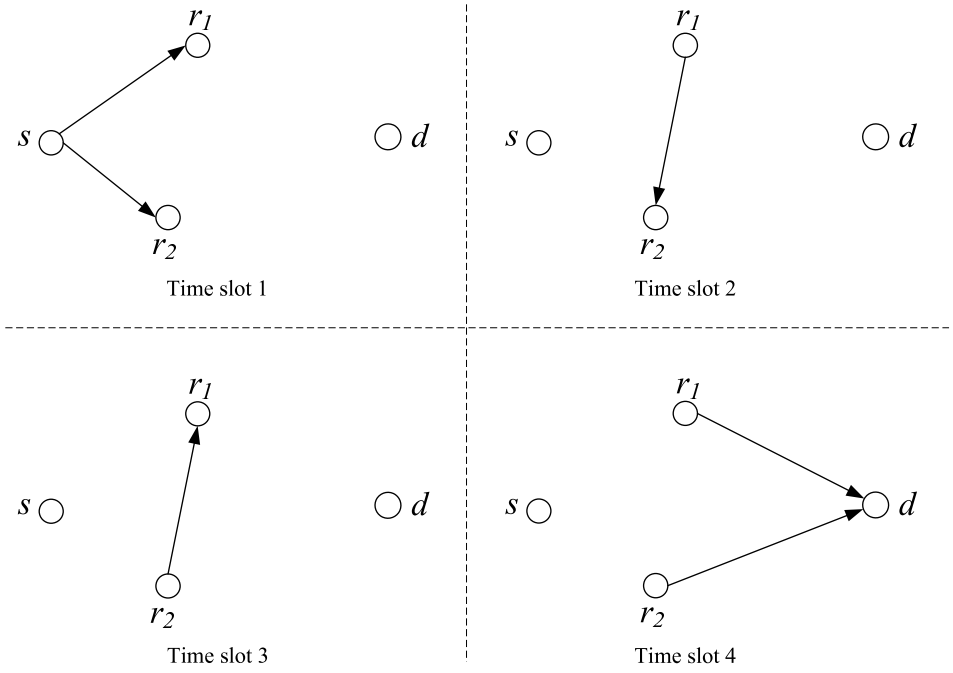

FIGURE 7.4 – Etapes constituant la seconde stratégie

La seconde stratégie proposée, illustrée à la figure 7.4, associe un système coopératif par relais à un système coopératif MISO virtuel. L'information est tout d'abord diffusée par le nœud source s durant le premier intervalle de temps. Ensuite, durant le second et le troisième intervalles de temps, les nœuds relais r_1 et r_2 amplifient et se retransmettent le signal. Une combinaison MRC et un décodage

d'information sont effectués au nœuds relais r_1 et r_2. Ainsi, les deux nœuds relais reçoivent le signal d'information source par l'intermédiaire d'un système coopératif par relais. Ensuite, un système coopératif MISO virtuel est réalisé entre les deux nœuds relais et le nœud de destination durant le quatrième intervalle de temps.

Dans la partie précédente, nous avons obtenu l'allocation de puissance optimale pour le système coopératif par relais (basé sur le principe « amplification et retransmission ») et le système coopératif MISO virtuel. Pour utiliser ces résultats il est nécessaire de déterminer la probabilité d'erreur requise durant chacune des étapes des stratégies proposées.

Pour la première stratégie, si nous fixons un taux d'erreur global égal à $P_e^{(1)}$, les choix de P_{e1} et P_{e2} pour les deux systèmes coopératifs par relais doivent satisfaire la condition suivante :

$$\begin{aligned} P_e^{(1)} &\leq (1 - P_{e1})P_{e2} + P_{e1} \\ &\leq P_{e1} + P_{e2} \end{aligned} \tag{7.22}$$

Pour la seconde stratégie, les taux d'erreur requis (P'_{e1}, P'_{e2} et P'_{e3}) des différentes étapes peuvent être approximés, par :

$$P_e^{(2)} \leq P'_{e3} + (P'_{e1} + P'_{e2})Prob_1 \tag{7.23}$$

où $P_e^{(2)}$ est la probabilité d'erreur requise pour la communication complète.

B.4.4 Analyse des performances et discussion

Notons tout d'abord la bonne concordance entre les simulations et les résultats numériques basés sur les expressions du paragraphe précédent.

La puissance totale émise optimale pour le système coopératif MISO virtuel décroît au fur et à mesure que le nœud coopératif se rapproche du nœud de destination. Ce résultat est dû au fait que les deux nœuds s_1 et s_2 ont déjà connaissance du signal d'information. Alors que pour le système coopératif par relais, seul le nœud s connaît le message d'information. Nous remarquons que, lorsque le nœud relais coopératif est localisé dans une région proche du nœud de destination, le système coopératif par relais nécessite une puissance totale émise optimale plus

faible. Le minimum de puissance est obtenu lorsque le rapport entre les distances approche 0,6 et le système coopératif par relais obtient alors la meilleure efficacité énergétique.

Pour comparer les deux stratégies coopératives, nous considérons deux configurations de placement des nœuds, décrites à la figure 7.5 : une topologie symétrique horizontale et une topologie symétrique diagonale.

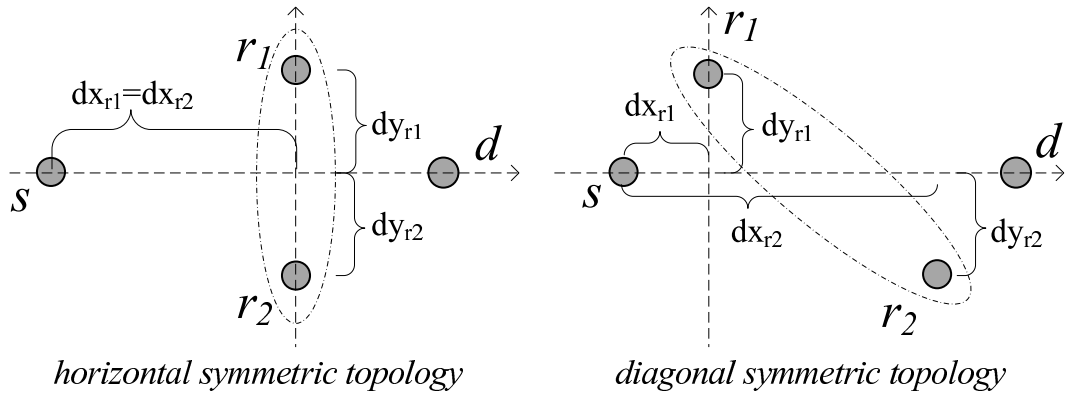

FIGURE 7.5 – Deux configurations de placement des nœuds

En comparant l'allocation de puissance entre le nœud source et les nœuds coopératifs, nous proposons une démarche heuristique pour sélectionner les nœuds coopératifs et choisir les stratégies coopératives appropriées pour les réseaux de capteurs sans fil.

Dans la structure topologique symétrique horizontale, les nœuds coopératifs devraient être situé dans la région proche du milieu du trajet source destination. D'autre part, quand les deux nœuds coopératifs sont proches l'un de l'autre, la seconde stratégie coopérative est la meilleure. Par contre, la première stratégie coopérative est plus économe en énergie.

Dans la structure topologique symétrique diagonale, l'ensemble des deux stratégies coopératives proposées donnent de bonnes performances au niveau de la consommation d'énergie lorsque les deux nœuds coopératifs sont proches du nœud source et du nœud de destination.

5.4.5 Conclusion

Dans ce chapitre, nous avons proposé une stratégie d'allocation de puissance optimale pour les communications coopératives dans les réseaux de capteurs sans fil.

Pour une contrainte de probabilité d'erreur, elle contribue à réduire la puissance de transmission totale pour le système coopératif par relais (basé sur le principe « amplification et retransmission ») et le système coopératif MISO virtuel dans le cas d'un canal de Rayleigh.

En outre, en l'absence de lien direct entre les nœuds source et de destination, nous avons proposé deux stratégies coopératives efficaces en énergie où une allocation de puissance optimale est appliquée aux différentes étapes. Nous avons comparé les performances des deux structures topologiques et développé une démarche heuristique pour sélectionner les nœuds coopératifs et choisir la communication coopérative appropriée.

B.5 Efficacité énergétique dans les réseaux de capteurs sans fil

B.5.1 Introduction

Dans les réseaux de capteurs sans fil, les données d'information sont généralement sensibles aux erreurs de transmission. Des systèmes de contrôle d'erreur, tels que les codes de contrôle d'erreur (ECC pour Error Control Codes) et les demandes de répétition automatique (ARQ pour Automatic Repeat reQuest), peuvent être utilisés pour obtenir des communications sans fil fiables. Comme les systèmes de contrôle d'erreur introduisent de la redondance au niveau des données d'information ou réduisent l'efficacité spectrale, ceux-ci entraînent une surconsommation d'énergie. Lorsque nous considérons leur mise en place dans les réseaux de capteurs sans fil, nous devons impérativement nous interroger sur leur efficacité énergétique.

Dans ce chapitre, nous considérons trois types de protocoles de contrôle d'erreur : le ARQ basique, le ARQ hybride-I et le ARQ hybride-II. Ils seront intégrés dans les systèmes SISO et MISO coopératifs. Pour tous ces protocoles, une séquence de contrôle de redondance cyclique (CRC) est utilisée afin de détecter les erreurs de transmission sur les données d'information. Dans le cas des protocoles ARQ hybride-I et ARQ hybride-II, des codes correcteurs d'erreurs sont également employés, le traitement de correction d'erreurs étant effectuée avant la détection d'erreurs par CRC. De plus, dans le ARQ hybride-II, la redondance du code correcteur d'erreurs est transmise uniquement lorsque cela est nécessaire.

Comme les codes robustes fournissent plus de gain de codage, mais ajoutent

plus de redondance dans le mot codé et plus de complexité dans le processus de codage/décodage, le choix des codes correcteurs d'erreurs ont une influence sur l'efficacité énergétique des protocoles de contrôle d'erreur.

Pour analyser cette efficacité énergétique, nous considérons que la consommation totale d'énergie inclut l'énergie émise ainsi que, l'énergie consommée par les traitements numériques et les différents circuits analogiques concernés.

L'évaluation complète de l'efficacité énergétique devrait nous amener à obtenir un compromis entre la consommation d'énergie d'émission et la qualité de la transmission.

Dans ce chapitre, selon les différentes conditions du canal, nous étudions l'utilité des codes correcteurs d'erreurs et l'impact de leur mise en place sur l'efficacité énergétique dans les protocoles de contrôle d'erreur.

B.5.2 Les protocoles de contrôle d'erreur

Le protocole de contrôle d'erreur qui combine CRC (Cyclic Redundancy Check) et ARQ est spécifié dans la norme IEEE 802.15.4 au niveau de la sous-couche MAC. Dans ce protocole, l'émetteur envoit un paquet avec une demande d'acquittement sur la réussite de la réception. En vérifiant la clé calculée du CRC, le récepteur renvoie une trame d'acquittement à l'émetteur si le paquet est correctement reçu. Lorsque cette trame d'acquittement est reçue dans un délai prédéfini, la transmission est considérée comme réussie. Par contre, si le paquet n'est pas correctement reçu, aucune trame d'acquittement ne sera renvoyée à l'émetteur et celui-ci conclut que la tentative d'émission précédente a échoué. Si le nombre maximum de tentatives pour la retransmission n'est pas atteint, le paquet d'origine sera retransmis à nouveau. Sinon, l'émetteur suppose que la transmission a échouée.

Sans considérer les limites sur le nombre de tentatives de retransmission, le nombre de retransmissions moyen τ_0 nécessaire pour une réception réussie dans ce protocole ARQ basique est le suivant :

$$\begin{aligned}
&\tau_0 = (1 - P_{epkt}) + 2P_{epkt}(1 - P_{epkt}) + \cdots + nP_{epkt}^{n-1}(1 - P_{epkt}) + \cdots \\
&= 1 + P_{epkt} + P_{epkt}^2 + P_{epkt}^3 + \cdots + P_{epkt}^n + \cdots \qquad (7.24) \\
&= \tfrac{1}{1-P_{epkt}}
\end{aligned}$$

où P_{epkt} est la probabilité d'erreur sur les paquets. En plus du code de détection d'erreurs, des codes correcteurs d'erreurs sont également utilisés dans les systèmes ARQ Hybrides (ARQH). Les systèmes ARQH exploitent simultanément les avantages de l'ARQ et des codes correcteurs d'erreurs pour fournir une communication fiable. En utilisant la redondance du code correcteur d'erreur, la séquence de réception peut être corrigée, dans la limite des capacités de correction du code, avant le traitement d'intégrité des paquets par le CRC. Dans nos travaux, nous considérons deux systèmes ARQ hybrides que nous détaillons dans la suite.

ARQH-I : La différence entre le protocole ARQH-I et le protocole ARQ basique est que les paquets sont codés à l'aide de codes correcteurs d'erreurs dans le protocole ARQH-I. Par conséquent, le nombre de retransmissions moyen τ_1 nécessaire pour une communication réussie est donné par :

$$\tau_1 = \frac{1}{1 - P_{epkt}^{(c)}} \tag{7.25}$$

où $P_{epkt}^{(c)}$ est le taux d'erreurs paquet pour les paquets codées.

ARQH-II : Dans le cas de codes systématiques et par exemple pour un code Hamming ou de Reed-Solomon, la redondance peut être facilement séparée de l'information. Le système ARQH-II exploite cette propriété en ne retransmettant que la redondance. Dans le cas d'un canal BBAG, comme les performances sont identiques pour chaque retransmission de la redondance, la combinaison de la première séquence d'information émise avec la dernière retransmission de la redondance peut être considérée comme équivalente à une émission codée une nouvelle fois. Alors, le taux d'erreur paquet $P_{epkt}^{(c)}$ pour chaque combinaison codée est supposé identique. Par conséquent, le nombre de retransmissions moyen pour le protocole ARQH-II dans le cas d'un canal BBAG peut être exprimé par :

$$\begin{aligned}
\tau_2 &= (1 - P_{epkt}) + 2P_{epkt}(1 - P_{epkt}^{(c)}) + \cdots + nP_{epkt}(P_{epkt}^{(c)})^{n-2}(1 - P_{epkt}^{(c)}) + \cdots \\
&= 1 + P_{epkt} + P_{epkt}P_{epkt}^{(c)} + P_{epkt}(P_{epkt}^{(c)})^2 + \cdots + P_{epkt}(P_{epkt}^{(c)})^n + \cdots \\
&= 1 + P_{epkt}\frac{1}{1-P_{epkt}^{(c)}} = \frac{1+P_{epkt}-P_{epkt}^{(c)}}{1-P_{epkt}^{(c)}}
\end{aligned} \tag{7.26}$$

B.5.3 Analyse des performances

B.5.3.1 Comparaison des consommations d'énergie

Dans ce paragraphe, nous comparons la consommation d'énergie totale pour les communications SISO et MISO coopérative basée sur le codage d'Alamouti. Le système MISO coopératif n'étant intéressant qu'en présences d'évanouissements, nous ne l'étudierons que dans le cas de canaux de Rayleigh.

Les résultats montrent que le système MISO coopératif consomme moins d'énergie que le système SISO lorsque la distance entre l'émetteur et le récepteur est supérieure à un seuil dans le cas d'un canal de Rayleigh. En outre, nous remarquons que, pour le système MISO, l'augmentation de la consommation d'énergie totale évolue assez lentement au fur et à mesure que la distance augmente. Le même phénomène peut aussi être observé pour le système SISO dans le cas d'un canal à bruit blanc additif gaussien. La raison de cela peut s'expliquer si l'on considère le rapport entre la consommation d'énergie Eb_T et la consommation d'énergie totale.

Nous montrons que, pour un système SISO en présence d'un canal BBAG et un système MISO en présence d'un canal de Rayleigh, l'énergie d'émission requise augmente lentement et représente un rapport faible (inférieur à 0,1) dans la consommation d'énergie totale pour une distance inférieure à 20 mètres. Dans ces conditions, la consommation d'énergie au niveau des circuits est prépondérante dans la consommation d'énergie totale.

D'autre part, lorsque la distance de communication augmente, l'énergie d'émission requise devient plus grande et le rapport entre l'énergie d'émission et l'énergie totale augmente plus rapidement pour le système SISO dans le cas du canal à évanouissements de Rayleigh. Ce rapport se rapproche de un lorsque la distance devient supérieure à 50 mètres. Par conséquent, dans le cas d'un canal à évanouissements de Rayleigh, le système SISO consomme beaucoup plus d'énergie d'émission que le système MISO coopératif basé sur le codage d'Alamouti. Le système MISO coopératif est plus efficace en énergie lorsque la consommation de l'énergie d'émission dépasse la consommation d'énergie des circuits.

B.5.3.2 Système SISO dans le cas d'un canal BBAG

Pour les communications courte distance, le canal BBAG entre les nœuds est un modèle pratique et le système SISO est le plus approprié. Dans ce cas, nous étudions la consommation d'énergie totale par bit et le nombre de transmissions moyen

pour le protocole de base ARQ. Nous considérons plusieurs distances de séparation d=[5m, 10m, 20m]. Les points de consommation d'énergie minimum apparaissent pour une puissance d'émission autour de -5dBm, 5dBm, et 15dBm. A ces puissances d'émission, le nombre de transmissions moyen est proche de 1. Ces résultats montrent qu'un nombre faible de retransmission est préférable pour obtenir une consommation d'énergie minimale. La raison est que la consommation d'énergie sur les circuits analogiques domine la consommation d'énergie totale dans ces cas. Pour une distance de séparation inférieure à 20m, le rapport optimal entre la puissance d'émission et la consommation totale est inférieure à 0,1 en considérant que le protocole de base ARQ est appliquée. Par conséquent, lors de l'étude des protocoles de contrôle d'erreurs dans le cas d'un système SISO avec un canal BBAG, nous devrions accorder plus d'importance à la réduction de la consommation d'énergie des circuits analogiques et réduire le nombre moyen de retransmissions.

B.5.3.3 Système coopératif dans le cas d'un canal de Rayleigh

Considérons le cas d'un canal à évanouissements de Rayleigh, nous interprétons la probabilité de coupure de la transmission à une certaine efficacité spectrale Φ comme le taux d'erreur paquet. Alors, pour le protocole ARQ basique, le nombre de transmission moyen dans le cas d'un canal de Rayleigh est donné par :

$$\tau_0 = \frac{1}{1 - P_{epkt}} = \frac{1}{1 - P_{out}(\Phi)} \tag{7.27}$$

où $P_{out}(\Phi)$ représente la probabilité de coupure de la transmission pour un système coopératif MISO basé sur le codage d'Alamouti. Les résultats de simulation montrent que le nombre de transmission moyen optimal pour obtenir la consommation d'énergie minimale approche de 2 lorsque le rapport signal à bruit est autour de 6dB pour des paquets de longueur de 100 bits et lorsqu'il est autour de 8dB pour des paquets de longueur de 1000 bits.

En appliquant le protocole ARQ basique, la consommation d'énergie d'émission surpasse la consommation d'énergie des circuits pour une distance de séparation supérieure à 50 mètres. Dans le cas extrême de $\beta_{M_T,M_R} \approx 1/(1+\alpha)$ le nombre de transmission moyen optimal est déterminé par :

$$\tau_{opt} = \frac{1}{(1+2\frac{2^{\Phi}-1}{(\bar{E}_b/N_0)_{opt}})e^{-2\frac{2^{\Phi}-1}{(\bar{E}_b/N_0)_{opt}}}} = \frac{1}{(1+\frac{2}{\sqrt{5}-1})e^{-2\frac{2}{\sqrt{5}-1}}} \approx 1.93 \qquad (7.28)$$

On choisit donc ici de réduire la puissance d'émission au prix d'un taux de retransmission des paquets plus élevé. Cet optimum est justifié par le fait que, comme la consommation d'énergie d'émission domine la consommation d'énergie totale dans ce scénario, diminuer la puissance d'émission est raisonnable pour améliorer l'efficacité énergétique.

B.5.3.4 Efficacité énergétique des protocoles ARQ Hybrides

Dans les protocoles ARQ hybride, des codes correcteurs d'erreur sont appliqués. Ils apportent un gain de codage, mais au prix d'une efficacité spectrale réduite. Par conséquent, une plus grande consommation d'énergie sur les circuits analogiques est nécessaire pour transmettre un débit binaire identique. L'efficacité énergétique lors de l'utilisation des protocoles ARQ hybrides doit donc être étudiée.

Nous observons que le nombre moyen de retransmission pour la consommation d'énergie optimale approche la valeur de un dans le cas d'un système SISO avec un canal BBAG. Les codes correcteurs d'erreur servent donc ici essentiellement à réduire le nombre de retransmissions. D'autre part, la consommation d'énergie des circuits analogiques domine la consommation d'énergie totale dans ce scénario, ainsi la mise en œuvre de l'efficacité énergétique des codes de contrôle d'erreur doit vérifier que la réduction de l'énergie d'émission permet de compenser la surconsommation d'énergie occasionnée par la séquence redondante et le codage/décodage.

Dans le cas d'un système MISO avec canal de Rayleigh, l'application des codes de contrôle d'erreur doit également satisfaire la condition que, la réduction de l'énergie d'émission pour obtenir la même probabilité de coupure optimale peut compenser la surconsommation d'énergie amenée par la séquence redondante et le codage/décodage. Comme l'énergie d'émission domine l'énergie totale dans ce scénario, l'utilisation des codes pourrait être très intéressante pour améliorer l'efficacité énergétique. Dans ce cas, le protocole ARQH-I, qui peut réduire la puissance d'émission nécessaire, est préférable. C'est la raison pour laquelle nous considérons uniquement le protocole ARQH-I dans le cas d'un système MISO avec canal à évanouissements de Rayleigh.

Les conditions générales pour que les protocoles soient plus efficaces en énergie que le protocole ARQ basique sont :

ARQH-I :

$$\begin{aligned} g(r) &> \frac{(1+\alpha)\beta_{i,j}}{(1+\alpha)r\beta_{i,j}+(1-r)-\beta_{i,j}\Psi(r)R/P_T^u} \approx \frac{(1+\alpha)\beta_{i,j}}{(1+\alpha)r\beta_{i,j}+(1-r)} \\ with \quad & (1+\alpha)r\beta_{i,j}+(1-r)-\beta_{i,j}\Psi(r)R/P_T^u > 0 \end{aligned} \tag{7.29}$$

ARQH-II :

$$\begin{aligned} g(r) &> \frac{r(1-r)(1+\alpha)\beta_{i,j}}{r(1-r)(1+\alpha)\beta_{i,j}+r^2-r\beta_{i,j}\Psi(r)R/P_T^u} \approx \frac{(1+\alpha)\beta_{i,j}}{(1+\alpha)\beta_{i,j}+r/(1-r)} \\ with \quad & r(1-r)(1+\alpha)\beta_{i,j}+r^2-r\beta_{i,j}\Psi(r)R/P_T^u > 0 \end{aligned} \tag{7.30}$$

Ces deux équations fournissent les conditions nécessaires sur le taux de codage pour rendre le code de contrôle d'erreur employé efficace en énergie.

B.5.4 Conclusion

Dans ce chapitre, nous considérons l'efficacité énergétique de trois protocoles de contrôle d'erreur dans les réseaux de capteurs sans fil, dans le cas d'un système SISO avec canal BBAG pour les communications courte distance et d'un système MISO avec canal de Rayleigh pour les communications longue distance.

Dans le cas du système SISO avec canal BBAG, comme la consommation d'énergie des circuits analogiques domine la consommation d'énergie totale, un taux faible de retransmission est préférable. Comme le protocole ARQH-II ne transmet la redondance que si elle est nécessaire, il semble être plus facilement efficace en énergie que les autres.

Dans le cas du système MISO avec canal de Rayleigh, à cause des évanouissements du canal et de la distance de séparation relativement longue, une plus grande puissance d'émission est nécessaire. Le protocole ARQH-I permet de réaliser un compromis entre une augmentation de la puissance d'émission et un accroissement du taux de retransmission. En fonction du taux de code, nous proposons des seuils sur le gain de codage permettant de rendre le protocole ARQH-1 plus efficace en énergie.

B.6 Conclusion et perspectives

Grâce aux avantages des systèmes multi-antennes virtuels, les systèmes coopératifs de communications fournissent de bonnes performances au niveau de l'efficacité énergétique dans des conditions hostiles de propagation caractérisant un canal à évanouissements. L'objectif de cette thèse est d'étudier la mise en œuvre à faible complexité et l'efficacité énergétique de systèmes coopératifs dans les réseaux de capteurs sans fil.

Afin de mettre en avant les avantages des systèmes multi-antennes virtuels, nous avons évalué la capacité d'un canal à évanouissement de Rayleigh pour les systèmes MIMO dans le chapitre 1. L'augmentation du nombre d'antennes de réception améliore fortement les performances du système, mais ne semble pas envisageable dans le cas des réseaux de capteurs car elle augmente la complexité de l'ensemble émetteur-récepteur.

Compte tenu de l'exigence sur le déploiement simple et flexible, nous nous sommes intéressés, dans cette thèse, aux systèmes multi-antennes d'émission virtuels. Dans le chapitre 2, plusieurs systèmes coopératifs sont décrits. Durant notre travail, nous avons principalement porté notre attention sur la couche physique. Nous avons étudié le problème de la synchronisation temporelle distribuée, le principe d'allocation de puissance et les protocoles de contrôle d'erreurs dans l'application de ces systèmes coopératifs. L'objectif principal de ces travaux est la mise en oeuvre des communications coopératives avec la meilleure efficacité énergétique.

Contributions de la thèse

- Nous avons analysé la nécessité de la synchronisation dans les systèmes coopératifs de communications MISO virtuel, basé sur le codage d'Alamouti. Bien que la synchronisation temporelle d'arrivée du signal est nécessaire pour ces systèmes coopératifs, une erreur de synchronisation légère a peu d'effet sur les performances en réception. Connaissant l'effet de l'erreur de synchronisation, nous avons proposé un schéma de synchronisation au niveau de la couche physique pour les transmissions coopératives MISO virtuel dans les réseaux de capteurs sans fil. Une méthode basée sur le principe du maximum de vraisemblance a été proposée pour l'estimation de l'erreur de synchronisation à la réception des données. Elle offre de bonnes performances, même avec une séquence de synchronisation courte. La matrice de décision peut

être pré-calculée et réutilisée dans le processus d'estimation de l'erreur de synchronisation avant le décodage d'Alamouti. Nous avons également étudié et comparé deux stratégies après l'estimation de l'erreur de synchronisation.

- Nous avons proposé une stratégie d'allocation de puissance optimale pour un système coopératif par relais (basé sur le principe « amplification et retransmission ») et pour un système coopératif MISO virtuel dans les réseaux de capteurs sans fil. Avec une contrainte sur le taux d'erreur, elles permettent de minimiser la puissance totale d'émission dans le cas d'un canal à évanouissements de Rayleigh. Moyennant certaines approximations, validées par simulation, l'allocation de puissance de chaque nœud peut être calculée de manière analytique. En outre, en l'absence de lien direct entre les nœuds source et destination, nous avons proposé deux solutions efficaces en énergie pouvant exploiter le système coopératif par relais et le système coopératif MISO virtuel. Les stratégies d'allocation de puissance optimales peuvent être appliquées aux différentes étapes de ces schémas de transmission. Nous avons comparé leurs performances pour deux topologies représentatives des nœuds, ce qui nous a permis de proposer une démarche heuristique pour sélectionner les nœuds coopératifs et choisir la solution coopérative la plus appropriée.

- Nous avons analysé l'efficacité énergétique de trois protocoles de contrôle d'erreur utilisés dans les réseaux de capteurs sans fil. Deux scénarios : système SISO avec canal BBAG pour les communications à courte distance et système MISO avec canal de Rayleigh pour les communications à longue distance ont été pris en considération.

  Pour un système SISO avec canal BBAG, comme la consommation d'énergie des circuits analogiques domine la consommation d'énergie totale, un faible taux de retransmission est préférable. Comme le protocole ARQH-II ne transmet la redondance que lorsque cela est nécessaire, il se révèle le mieux adapté à ce scénario.

  Pour un système MISO avec canal de Rayleigh, à cause des évanouissements du canal et de la distance de séparation relativement longue, une plus grande puissance d'émission est nécessaire. Un compromis entre la puissance d'émission moindre et le nombre de retransmission peut être réalisé en utilisant le protocole ARQH-I. En fonction du taux de code, nous proposons des seuils

sur le gain de codage permettant de rendre le protocole ARQH-1 plus efficace en énergie.

Perspectives

Dans les travaux de cette thèse, nous avons proposé des solutions pour la mise en œuvre pratique et efficace en énergie des communications coopératives dans les réseaux de capteurs sans fil. Il reste encore dans ce domaine de nombreuses perspectives de recherche :

- Combinaison avec le codage de réseau : Dans cette thèse, nous nous sommes concentrés sur les communications coopératives au niveau de la couche physique et avons étudié leur efficacité énergétique. Pourtant, nous avons montré que le système coopératif peut être mis en œuvre au niveau de la couche réseau (codage de réseau). Il paraît donc intéressant d'aller plus loin dans la comparaison de ces deux approches ou d'étudier un fonctionnement conjoint entre la couche physique et la couche réseau.

- Communication coopérative basée sur l'OFDM : Nous avons montré que des communications coopératives peuvent être simplement réalisées en OFDM avec l'avantage de réduire l'exigence de synchronisation temporelle. Le problème de synchronisation fréquentielle reste toutefois important et peut accroître la complexité du traitement du signal. Bien que des recherches aient été faites sur ce problème, la mise en œuvre efficace en énergie reste un sujet ouvert. Par ailleurs, le problème de dynamique des signaux OFDM, qui pourrait introduire une faible efficacité énergétique dans les communications coopératives, est intéressant à étudier.

- Prise en compte de la couche MAC : Les systèmes de communications coopératifs exigent une importante coordination entre les nœuds concernés. Un système strict AMRF (Accès Multiple par Répartition de Fréquence) pourrait affecter le rendement énergétique et le débit. D'autre part, les protocoles probabilistes MAC, tel que le protocole CSMA (Carrier Sense Multiple Access), ne peuvent pas garantir la participation de tous les nœuds coopératifs nécessaires. Par conséquent, un protocole MAC spécifique pour les systèmes de communications coopératifs est intéressant à étudier.

- Mise en œuvre matérielle : Un certain nombre de travaux de recherche ont montré, de manière théorique, les avantages des communications coopératives. Mais peu de prototypes ont été mis en œuvre avec des supports concrets pour les systèmes coopératifs. La plupart des nœuds actuels supportent le standard IEEE-802.15.4, norme qui ne prévoit pas les communications coopératives. Nos travaux ont proposé un système de synchronisation temporelle adapté aux communications coopératives, mais la mise en œuvre d'un banc de test pourrait révéler des problèmes pratiques auxquels nous n'avons pas pensé.

Publications

Journal Papers

1. Haitao Wan, Jean-François Diouris, and Guillaume Andrieux, *Time Synchronization for Cooperative Communication in Wireless Sensor Networks*, Springer Wireless Personal Communications, on revision.

2. Haitao Wan, Jean-François Diouris, and Guillaume Andrieux, *Power Allocation and Cooperative Strategy in Wireless Sensor Networks*, EURASIP Journal on Wireless Communications and Networking, on revision.

Conference Papers

1. Haitao Wan, Jean-François Diouris, and Guillaume Andrieux, *Power Allocation for Virtual MISO Cooperative Communication in Wireless Sensor Networks*, European Microwave Week, Paris, France, 2010.

2. Haitao Wan, Jean-François Diouris, and Guillaume Andrieux, *Effect of Synchronization Errors on Alamouti Coding in Wireless Sensor Networks*, IEEE Wireless Communication and Networking Conference (WCNC), Budapest, Hungary, 2009.

3. Haitao Wan, Max Agueh, and Jean-François Diouris, *Energy Efficient Protection of Data in the Wireless Sensor Networks*, 5th European Workshop on Wireless Sensor Networks (EWSN)-Poster Session, Bologna, Italy, 2008.

Bibliography

[1] S. Cui, A. Goldsmith, and A. Bahai, "Energy-efficiency of mimo and cooperative mimo techniques in sensor networks," *IEEE Journal on Selected Areas in Communications*, vol. 22, no. 6, pp. 1089–1098, aug. 2004.

[2] A. Mainwaring, D. Culler, J. Polastre, R. Szewczyk, and J. Anderson, "Wireless sensor networks for habitat monitoring," in *Proceedings of the 1st ACM international workshop on Wireless sensor networks and applications*, 2002, pp. 88–97.

[3] E. Basha and D. Rus, "Design of early warning flood detection systems for developing countries," in *International Conference on Information and Communication Technologies and Development*, dec. 2007, pp. 1–10.

[4] L. Mo, Y. He, Y. Liu, J. Zhao, S.-J. Tang, X.-Y. Li, and G. Dai, "Canopy closure estimates with greenorbs: sustainable sensing in the forest," in *Proceedings of the 7th ACM Conference on Embedded Networked Sensor Systems*, 2009, pp. 99–112.

[5] *IEEE 802.15.4-Wireless Medium Access Control (MAC) and Physical Layer (PHY) Specifications for Low-Rate Wireless Personal Area Networks (WPANs)*, 2006.

[6] I. Akyildiz, W. Su, Y. Sankarasubramaniam, and E. Cayirci, "A survey on sensor networks," *IEEE Communications Magazine*, vol. 40, no. 8, pp. 102–114, aug. 2002.

[7] J. G. Proakis, *Digital Communications*, 4th ed. McGraw-Hill Science, 2000.

[8] A. Paulraj, R. Nabar, and D. Gore, *Introduction to Space-Time Wireless Communications*. Cambridge University Press, 2003.

[9] B. Sklar, "Rayleigh fading channels in mobile digital communication systems: I.characterization," *Communications Magazine, IEEE*, vol. 35, no. 9, pp. 136–146, sep. 1997.

[10] I. E. Telatar, "Capacity of multi-antenna gaussian channels," *European Transactions on Telecommunications*, vol. 10, pp. 585–595, 1999.

[11] A. Edelman, "Eigenvalues and condition numbers of random matrices," Ph.D. dissertation, Department of Mathematics, MIT, Cambridge, MA, 1989.

[12] M. Dohler, "Virtual antenna arrays," Ph.D. dissertation, Department of Electrical and Electronic Engineering, King's College London, University of London, 2003.

[13] L. Zheng and D. Tse, "Diversity and multiplexing: a fundamental tradeoff in multiple-antenna channels," *IEEE Transactions on Information Theory*, vol. 49, no. 5, pp. 1073–1096, may. 2003.

[14] J.-F. Lemieux, M. El-Tanany, and H. Hafez, "Experimental evaluation of space/frequency/polarization diversity in the indoor wireless channel," *IEEE Transactions on Vehicular Technology*, vol. 40, no. 3, pp. 569–574, aug. 1991.

[15] R. Ahlswede, N. Cai, S.-Y. Li, and R. Yeung, "Network information flow," *IEEE Transactions on Information Theory*, vol. 46, no. 4, pp. 1204–1216, jul. 2000.

[16] S. Zhang, S. C. Liew, and P. P. Lam, "Hot topic: physical-layer network coding," in *Proceedings of the 12th annual international conference on mobile computing and networking*, 2006, pp. 358–365.

[17] S. Katti, S. Gollakota, and D. Katabi, "Embracing wireless interference: analog network coding," in *Proceedings of the 2007 conference on applications, technologies, architectures, and protocols for computer communications*, 2007, pp. 397–408.

[18] J. Laneman, D. Tse, and G. Wornell, "Cooperative diversity in wireless networks: efficient protocols and outage behavior," *IEEE Transactions on Information Theory*, vol. 50, no. 12, pp. 3062–3080, dec. 2004.

[19] J. Laneman and G. Wornell, "Energy-efficient antenna sharing and relaying for wireless networks," in *Proceedings of IEEE Wireless Commmmunications and Networking Conference*, vol. 1, sep. 2000, pp. 7–12.

[20] ——, "Distributed space-time-coded protocols for exploiting cooperative diversity in wireless networks," *IEEE Transactions on Information Theory*, vol. 49, no. 10, pp. 2415–2425, oct. 2003.

[21] S. Jayaweera, "Energy efficient virtual mimo-based cooperative communications for wireless sensor networks," in *Proceedings of 2005 International Conference on Intelligent Sensing and Information Processing*, jan. 2005, pp. 1–6.

[22] A. Coso, S. Savazzi, U. Spagnolini, and C. Ibars, "Virtual mimo channels in cooperative multi-hop wireless sensor networks," in *40th Annual Conference on Information Sciences and Systems*, mar. 2006, pp. 75–80.

[23] D. Woldegebreal and H. Karl, "Network-coding-based cooperative transmission in wireless sensor networks: diversity-multiplexing tradeoff and coverage area extension," in *Wireless Sensor Networks*, ser. Lecture Notes in Computer Science. Springer Berlin / Heidelberg, 2008, vol. 4913, pp. 141–155.

[24] A. Nosratinia, T. Hunter, and A. Hedayat, "Cooperative communication in wireless networks," *IEEE Communications Magazine*, vol. 42, no. 10, pp. 74–80, oct. 2004.

[25] A. Bletsas, A. Khisti, D. Reed, and A. Lippman, "A simple cooperative diversity method based on network path selection," *IEEE Journal on Selected Areas in Communications*, vol. 24, no. 3, pp. 659–672, mar. 2006.

[26] V. Tarokh, H. Jafarkhani, and A. Calderbank, "Space-time block codes from orthogonal designs," *IEEE Transactions on Information Theory*, vol. 45, no. 5, pp. 1456–1467, jul. 1999.

[27] M. Dohler, Y. Li, B. Vucetic, A. Aghvami, M. Arndt, and D. Barthel, "Performance analysis of distributed space-time block-encoded sensor networks," *IEEE Transactions on Vehicular Technology*, vol. 55, no. 6, pp. 1776–1789, nov. 2006.

[28] S. Alamouti, "A simple transmit diversity technique for wireless communications," *IEEE Journal on Selected Areas in Communications*, vol. 16, no. 8, pp. 1451–1458, oct. 1998.

[29] V. Tarokh, H. Jafarkhani, and A. Calderbank, "Space-time block coding for wireless communications: performance results," *IEEE Journal on Selected Areas in Communications*, vol. 17, no. 3, pp. 451–460, mar. 1999.

[30] M.-K. Oh, X. Ma, G. Giannakis, and D.-J. Park, "Cooperative synchronization and channel estimation in wireless sensor networks," in *Conference Record of the Thirty-Seventh Asilomar Conference on Signals, Systems and Computers*, vol. 1, nov. 2003, pp. 238–242.

[31] S. Jagannathan, H. Aghajan, and A. Goldsmith, "The effect of time synchronization errors on the performance of cooperative miso systems," in *Proceedings of IEEE Global Telecommunications Conference Workshops*, nov. 2004, pp. 102–107.

[32] Y. Mei, Y. Hua, A. Swami, and B. Daneshrad, "Combating synchronization errors in cooperative relays," in *Proceedings of IEEE International Conference on Acoustics, Speech, and Signal Processing*, vol. 3, mar. 2005, pp. 369–372.

[33] D. L. Mills, "A brief history of ntp time: memoirs of an internet timekeeper," *ACM SIGCOMM Computer Communication Review*, vol. 33, no. 2, pp. 9–21, 2003.

[34] C. Intanagonwiwat, R. Govindan, and D. Estrin, "Directed diffusion: a scalable and robust communication paradigm for sensor networks," in *Proceedings of the 6th annual international conference on mobile computing and networking*, aug. 2000, pp. 56–67.

[35] W. Heinzelman, A. Chandrakasan, and H. Balakrishnan, "Energy-efficient communication protocol for wireless microsensor networks," in *Proceedings of the 33rd Annual Hawaii International Conference on System Sciences*, vol. 2, jan. 2000, p. 10.

[36] O. Younis and S. Fahmy, "Heed: A hybrid, energy-efficient, distributed clustering approach for ad hoc sensor networks," *IEEE Transactions on Mobile Computing*, vol. 3, pp. 366–379, 2004.

[37] O. Younis, M. Krunz, and S. Ramasubramanian, "Node clustering in wireless sensor networks: recent developments and deployment challenges," *IEEE Network*, vol. 20, no. 3, pp. 20–25, may. 2006.

[38] J. Elson, L. Girod, and D. Estrin, "Fine-grained network time synchronization using reference broadcasts," *ACM SIGOPS Operating Systems Review*, vol. 36, no. SI, pp. 147–163, 2002.

[39] S. Ganeriwal, R. Kumar, and M. Srivastava, "Timing-sync protocol for sensor networks," in *Proceedings of the 1st international conference on embedded networked sensor systems*, 2003, pp. 138–149.

[40] M. Sichitiu and C. Veerarittiphan, "Simple, accurate time synchronization for wireless sensor networks," in *Proceedings of IEEE Wireless Communications and Networking Conference*, vol. 2, mar. 2003, pp. 1266–1273.

[41] W. Su and I. F. Akyildiz, "Time-diffusion synchronization protocol for wireless sensor networks," *IEEE/ACM Transactions on Networking*, vol. 13, no. 2, pp. 384–397, 2005.

[42] Q. Li and D. Rus, "Global clock synchronization in sensor networks," *IEEE Transactions on Computers*, vol. 55, no. 2, pp. 214–226, 2006.

[43] J. E. Elson, "Time synchronization in wireless sensor networks," Ph.D. dissertation, University of California, Los Angeles, 2003.

[44] F. Sivrikaya and B. Yener, "Time synchronization in sensor networks: a survey," *IEEE Network*, vol. 18, no. 4, pp. 45–50, jul. 2004.

[45] B. Sundararaman, U. Buy, and A. Kshemkalyani, "Clock synchronization for wireless sensor networks: A survey," *Ad Hoc Networks (Elsevier)*, vol. 3, pp. 281–323, 2005.

[46] G. Barriac, R. Mudumbai, and U. Madhow, "Distributed beamforming for information transfer in sensor networks," in *Third International Symposium on Information Processing in Sensor Networks*, apr. 2004, pp. 81–88.

[47] A. Scaglione and Y.-W. Hong, "Opportunistic large arrays: cooperative transmission in wireless multihop ad hoc networks to reach far distances," *IEEE Transactions on Signal Processing*, vol. 51, no. 8, pp. 2082–2092, aug. 2003.

[48] A. D. Coso, U. Spagnolini, and C. Ibars, "Cooperative distributed mimo channels in wireless sensor networks," *IEEE Journal on Selected Areas in Communications*, vol. 25, no. 2, pp. 402–414, feb. 2007.

[49] T.-D. Nguyen, O. Berder, and O. Sentieys, "Cooperative mimo schemes optimal selection for wireless sensor networks," in *Proceedings of IEEE Vehicular Technology Conference, VTC2007-Spring*, apr. 2007, pp. 85–89.

[50] M. Siam, M. Krunz, and O. Younis, "Energy-efficient clustering/routing for cooperative mimo operation in sensor networks," in *IEEE INFOCOM*, apr. 2009, pp. 621–629.

[51] T.-D. Nguyen, O. Berder, and O. Sentieys, "Efficient space time combination technique for unsynchronized cooperative miso transmission," in *Proceedings of IEEE Vehicular Technology Conference, VTC2008-Spring*, may. 2008, pp. 629–633.

[52] M. K. Simon and M.-S. Alouini, *Digital Communication over Fading Channels: A Unified Approach to Performance Analysis*. Wiley-Interscience, 2000.

[53] K. Rajawat and A. Chaturvedi, "A low complexity symbol timing estimator for mimo systems using two samples per symbol," *IEEE Communications Letters*, vol. 10, no. 7, pp. 525–527, jul. 2006.

[54] X. Li, Y.-C. Wu, and E. Serpedin, "Timing synchronization in decode-and-forward cooperative communication systems," *IEEE Transactions on Signal Processing*, vol. 57, no. 4, pp. 1444–1455, apr. 2009.

[55] P. Dmochowski and P. Mclane, "Timing error detector design and analysis for orthogonal space-time block code receivers," *IEEE Transactions on Communications*, vol. 56, no. 11, pp. 1939–1949, nov. 2008.

[56] S. Wei, D. Goeckel, and M. Valenti, "Asynchronous cooperative diversity," *IEEE Transactions on Wireless Communications*, vol. 5, no. 6, pp. 1547–1557, jun. 2006.

[57] Y. Li and X.-G. Xia, "A family of distributed space-time trellis codes with asynchronous cooperative diversity," *IEEE Transactions on Communications*, vol. 55, no. 4, pp. 790–800, apr. 2007.

[58] X. Li, "Energy efficient wireless sensor networks with transmission diversity," *Electronics Letters*, vol. 39, no. 24, pp. 1753–1755, nov. 2003.

[59] R. van Nee and R. Prasad, *OFDM for Wireless Multimedia Communicaitons*, 1st ed. Artech Publishers, 2000.

[60] D. Agrawal, V. Tarokh, A. Naguib, and N. Seshadri, "Space-time coded ofdm for high data-rate wireless communication over wideband channels," in *Proceedings of IEEE Vehicular Technology Conference*, vol. 3, may. 1998, pp. 2232–2236.

[61] K. Lee and D. Williams, "A space-time coded transmitter diversity technique for frequency selective fading channels," in *Proceedings of IEEE Sensor Array and Multichannel Signal Processing Workshop*, 2000, pp. 149–152.

[62] ——, "A space-frequency transmitter diversity technique for ofdm systems," in *Proceedings of IEEE Global Telecommunications Conference*, vol. 3, 2000, pp. 1473–1477.

[63] Z. Li and X.-G. Xia, "An alamouti coded ofdm transmission for cooperative systems robust to both timing errors and frequency offsets," *IEEE Transactions on Wireless Communications*, vol. 7, no. 5, pp. 1839–1844, may. 2008.

[64] H. Wang, X.-G. Xia, and Q. Yin, "Distributed space-frequency codes for cooperative communication systems with multiple carrier frequency offsets," *IEEE Transactions on Wireless Communications*, vol. 8, no. 2, pp. 1045–1055, feb. 2009.

[65] Z. Zhou, S. Zhou, J.-H. Cui, and S. Cui, "Energy-efficient cooperative communication based on power control and selective single-relay in wireless sensor networks," *IEEE Transactions on Wireless Communications*, vol. 7, no. 8, pp. 3066–3078, aug. 2008.

[66] M. Hasna and M.-S. Alouini, "Optimal power allocation for relayed transmissions over rayleigh-fading channels," *IEEE Transactions on Wireless Communications*, vol. 3, no. 6, pp. 1999–2004, nov. 2004.

[67] R. Annavajjala, P. C. Cosman, and L. B. Milstein, "Statistical channel knowledge-based optimum power allocation for relaying protocols in the high

snr regime," *IEEE Journal on Selected Areas in Communications*, vol. 25, no. 2, pp. 292–305, feb. 2007.

[68] J. Luo, R. Blum, L. Cimini, L. Greenstein, and A. Haimovich, "Power allocation in a transmit diversity system with mean channel gain information," *IEEE Communications Letters*, vol. 9, no. 7, pp. 616–618, jul. 2005.

[69] X. Zhang and Y. Gong, "Joint power allocation and relay positioning in multi-relay cooperative systems," *IET Communications*, vol. 3, no. 10, pp. 1683–1692, oct. 2009.

[70] X. Deng and A. Haimovich, "Power allocation for cooperative relaying in wireless networks," *IEEE Communications Letters*, vol. 9, no. 11, pp. 994–996, nov. 2005.

[71] Y. Li, B. Vucetic, Z. Zhou, and M. Dohler, "Distributed adaptive power allocation for wireless relay networks," *IEEE Transactions on Wireless Communications*, vol. 6, no. 3, pp. 948–958, mar. 2007.

[72] M. Seo and S. W. Kim, "Power adaptation in space-time block code," in *Proceedings of IEEE Global Telecommunications Conference*, vol. 5, nov. 2001, pp. 3188–3193.

[73] L. Xian and H. Liu, "An adaptive power allocation scheme for space-time block coded mimo systems," in *Proceedings of IEEE Wireless Communications and Networking Conference*, vol. 1, mar. 2005, pp. 504–508.

[74] D. Michalopoulos, A. Lioumpas, and G. Karagiannidis, "Increasing power efficiency in transmitter diversity systems under error performance constraints," *IEEE Transactions on Communications*, vol. 56, no. 12, pp. 2025–2029, dec. 2008.

[75] G. Jakllari, S. V. Krishnamurthy, M. Faloutsos, P. V. Krishnamurthy, and O. Ercetin, "A framework for distributed spatio-temporal communications in mobile ad hoc networks," in *IEEE INFOCOM 2006*, apr. 2006, pp. 1–13.

[76] M. Siam, M. Krunz, and O. Younis, "Energy-efficient clustering/routing for cooperative mimo operation in sensor networks," in *IEEE INFOCOM 2009*, apr. 2009, pp. 621–629.

[77] T.-D. Nguyen, O. Berder, and O. Sentieys, "Cooperative mimo schemes optimal selection for wireless sensor networks," in *Proceedings of IEEE Vehicular Technology Conference*, apr. 2007, pp. 85–89.

[78] P. Anghel and M. Kaveh, "Exact symbol error probability of a cooperative network in a rayleigh-fading environment," *IEEE Transactions on Wireless Communications*, vol. 3, no. 5, pp. 1416–1421, sept. 2004.

[79] H. Wan, J.-F. Diouris, and G. Andrieux, "Power allocation for virtual miso cooperative communication in wireless sensor networks," in *Proceedings of European Conference on Wireless Technology*, sept. 2010.

[80] S. Lin and D. J. Constello, *Error Control Coding: Fundamentals and Applications*. Prentice Hall, 1983.

[81] A. S. Tanenbaum, *Computer Networks*, 4th ed. Prentice Hall, 2002.

[82] M. Goe and N. Shanbhag, "Low-power channel coding via dynamic reconfiguration," in *Proceedings of IEEE International Conference on Acoustics, Speech, and Signal Processing*, 1999, pp. 1893–1896.

[83] S. Howard, C. Schlegel, and K. Iniewski, "Error control coding in low-power wireless sensor networks: when is ecc energy efficient," *EURASIP Journal on Wireless Communications and Networking*, vol. 2, pp. 1–14, 2006.

[84] S. Cui, A. Goldsmith, and A. Bahai, "Energy-constrained modulation optimization," *IEEE Transactions on Wireless Communications*, vol. 4, no. 5, pp. 2349–2360, sep. 2005.

[85] R. Nabar, H. Bolcskei, and F. Kneubuhler, "Fading relay channels: performance limits and space-time signal design," *IEEE Journal on Selected Areas in Communications*, vol. 22, no. 6, pp. 1099–1109, aug. 2004.